University of Alberta

Effect of surface conditions on electrochemical and mechanical properties of pipeline steels in near-neutral pH environment

by

Daxiong HE 

A thesis submitted to the Faculty of Graduate Studies and Research in partial fulfillment of the requirements for the degree of *Master of Science*

in

Materials Engineering

Department of Chemical and Materials Engineering

Edmonton, Alberta

Spring, 2002

University of Alberta

Library Release Form

Name of Author: Daxiong HE

Title of Thesis: Effect of surface conditions on electrochemical and mechanical properties of pipeline steels in near-neutral pH environment

Degree: Master of Science

Year this Degree Granted: 2002

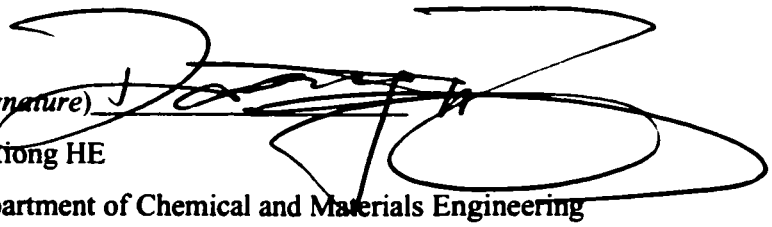

(*Signature*)

Daxiong HE

Department of Chemical and Materials Engineering

University of Alberta

Edmonton, AB, Canada, T6G 2G6

University of Alberta

Faculty of Graduate Studies and Research

The undersigned certify that they have read, and recommend to the Faculty of Graduate Studies and Research for acceptance, a thesis entitled ***Effect of surface conditions on electrochemical and mechanical properties of pipeline steels in near-neutral pH environment*** submitted by ***Daxiong HE*** in partial fulfillment of the requirements for the degree of ***Master of Science*** in Materials Engineering.

(*Signature*) Reg Eadie

Dr. Reginald. L. Eadie, Committee Chair

(*Signature*)

Dr. Weixing CHEN, supervisor

(*Signature*) J.A Luo

Dr. Jingli LUO, co-Supervisor

(*Signature*) G. Grondin

Dr. G. Y. Grondin, Committee member

(*Date*): Jan. 10th, 2002

Abstract

This research focused on the effect of surface conditions on electrochemical and mechanical properties of pipeline steels in near-neutral pH soil environment. These conditions included surface roughness, surface scratch orientation, and surface deposits arisen from the reaction between cathodic current and soil electrolytes. The electrochemical response of steels in various surface conditions was investigated by using the traditional electrochemical technologies. Davanathan electrochemical hydrogen charging system was used to study the hydrogen permeation behaviors of pipeline steel under the influence of surface variables. LECO Hydrogen Determinator was used to measure the total hydrogen content in the samples exposed to various chemical and electrochemical conditions. The standard slow strain rate tensile testing was conducted to understand the combined effect of corrosion and hydrogen on the mechanical properties of the pipeline steel. The mechanisms governing the synergistic interactions among near-neutral pH environment, dynamic loading and material variables at the surface were also discussed.

Acknowledgement

I am earnestly grateful to Dr. Weixing CHEN and Dr. Jingli LUO for their supervision, guidance and encouragement through the whole course of this research project. I am deeply impressed by their profound knowledge, strict attitude to do research and scientific teaching methods, which will definitely influence my working and studying in the future.

I wish to thank Drs. T. R. Jackson and F. King of NOVA Research & Technology Corporation, Drs. A. Glover and D. Dorling of TransCanada Pipelines Limited for providing additional guidance to my research, Dr. Reginald L. Eadie and Dr. Gilbert Y. Grondin for their valuable advice and suggestions on my thesis, and Ms. Christine Stewart for her helps with the English language corrections and improvement.

Appreciation is extended to Ms. Tina Barker, Mr. Bob Scott, Bob Konzuk and Walter Boddez for their technical supports and advice during the progress of this work. Helpful discussion with Dr. Shenghui WANG is also gratefully acknowledged.

Thanks are also due to TransCanada Pipelines Limited and NSERC for providing financial support to my research.

Daxiong HE

December 14, 2001

Contents

List of tables

List of Figures or illustrations

LIST OF SYMBOLS, NOMENCLATURE, OR ABBREVIATIONS

a	Thickness of sample
A	Exposed area of specimen in charging and detection call
b	Radius of oxidation side
C	Concentration of hydrogen in the steel, mol/cm^3
C_H	Hydrogen content determined by the LECO hydrogen analyzer, ppm
C_h^m	Subsurface hydrogen concentration, mol/cm^3
C_0	Concentration of hydrogen on the charging surface, mol/cm^3
d	Radius of charging side, sometimes which equals to or less than b
D	Diffusion coefficient, the hydrogen volume passing in one-second through a surface
D_L	Lattice diffusivity
E	Activity energy of hydrogen to diffusion, J
E_0	Heat of diffusion, J/mol
E_B	Bonding energy between hydrogen and trps
E_s	Heat of solution of hydrogen in iron
F	Faraday constant, 96500 coulombs/mol
i	Measured hydrogen permeation current density
ISO	International Standard Organization
I_0	Passivating current on oxidation side (detection side) before start of charging
$I_{(t)}$	Time dependant hydrogen permeation current, less I_0
I_{ss}	Steady state hydrogen permeation current, less I_0
J_0	Initial hydrogen flux.
$J_{(t)}$	Time dependant atomic hydrogen flux measured on the oxidation side, which equals to $I_{(t)}/AF$
J_{ss}	Atomic hydrogen permeation flux at steady state measured on the oxidation side, which equals to I_{ss}/AF
$J_{(t)}/J_{ss}$	Normalized flux of atomic hydrogen
k	Boltzman's constant
K	Kelven constant
L	Specimen thickness
n	Integer

n1	Concentration of hydrogen atoms in diffusion sites
n2	Concentrations of hydrogen atoms in sites of reversible sites traps
n3	Concentrations of hydrogen atoms in sites of irreversible saturable traps
n_e	Number of electrons involved in the oxidation, equals to one
N_L	Densities of normal lattice site
N_r	Number of reversible trap sites per unit volume
N_T	Densities of traps
N_x	Number density of hydrogen in steels
p	Partial pressure of hydrogen, mmHg
R	Gas constant
SCE	Saturated Calomel Electrode
t	Time from start of hydrogen charging
t_l	Time lag for lattice diffusion
t_b	Time measured by extrapolating the linear portion of the rising permeation current transit to J0, which is the intersection of the extension of linear pick-up portion to the time axes
t_{lag}	Time to achieve a value of $J_{(t)}/J_{ss}=0.63$
t_t	Time lag for diffusion in the presence of traps
τ	Normalized time (Dt/L^2)
T	Temperature in °C
V	Thickness loss of materils, μm/year
x	Distance into the specimen, cm
ρ	Density of materials, g/cm^2

1 INTRODUCTION

Stress corrosion cracking (SCC) of pipeline steels is a synergistic interaction between applied stress and susceptible steels in a corrosive environment. The development of SCC proceeds from initiation through a continuum of events that may lead to final failure. A prerequisite for SCC on a pipeline is that an appropriate electrolyte comes into contact with exposed steel. This can occur where protective coatings applied to the outside of a pipeline fail due to damage or degradation in service in such a way as to allow groundwater to access the underlying pipe surface. Not all locations where vulnerable steel surfaces are exposed to the soil environment develop SCC.

There are two types of SCC occurring in pipeline steels: high pH SCC and near neutral pH SCC. The former has been extensively studied since the mid-1960's, and is related to intergranular fracture in concentrated carbonate-bicarbonate solutions with pH in the range of 9.5 to 12.5. The latter was first observed in 1985, and has been responsible for an increasing number of pipeline failures in recent years. In contrast to high pH SCC, neutral pH SCC is characterised by transgranular fracture in the dilute carbonate-bicarbonate solutions with a pH in the range from 5.5 to 8.5.

Although both types of SCC are frequently encountered, the near-neutral pH SCC has been primarily responsible for the pipeline ruptures in Alberta and other regions of Canada. This research was initiated to understand some fundamental aspects of synergistic interactions of pipeline steels with near-neutral pH soil environment. In particular, attention was paid to various surface factors that may change the electrochemical and mechanical behaviours of the pipeline steels exposed to the near-neutral pH soil environments.

The surface factors investigated in this study included the surface physical conditions of the line pipe steels and the altered surface conditions arisen from the electrochemical reactions between the steel surface and the near-neutral pH soil environment under the influence of cathodic current.

These surface variables were studied in terms of their influence on the corrosion behaviour of the steel and the hydrogen permeation through the steel. The generation of hydrogen in the near-neutral pH corrosion system is due to the reduction of H^+ by free electrons either from the dissolution of Fe and/or from the cathodic current present in the system. Hydrogen is important since it could induce micro-cracks in the steel and change the eternal load response of the steel. The combined effect of the surface variables on the susceptibility of the steel to near-neutral pH SCC was further evaluated using slow strain rate testing.

This thesis is presented with a comprehensive literature review at the beginning, followed by Materials and Experimental Methods in Chapter 3, Results in Chapter 4, Discussion in Chapter 5, and Summaries and Suggestions at the end. Because of the potential importance of hydrogen in the development of near-neutral pH SCC in the pipeline steels, various aspects of hydrogen interactions with metallic materials was also included in the literature review, in addition to the review on the current understanding of the near-neutral pH SCC in pipeline steels.

2 Literature review

The mechanisms related to the high-pH Stress Corrosion Cracking (SCC) have been studied extensively in the past (*Parkins, 1994; Wilmott and Diakow, 1996*) and therefore will not be included in the current literature review. In contrast, mechanisms on near-neutral pH SCC remain unidentified, although much research has been conducted in the past decade. The influence of hydrogen is believed to be a key factor in the development of SCC in the pipeline steels exposed to near-neutral pH environments. This section reviews various aspects of hydrogen-metal interactions such as hydrogen permeation, hydrogen diffusion modeling, hydrogen detection and monitoring, as well as its role in near neutral pH SCC. This is followed by a review of current understanding of near-neutral pH SCC in pipeline steels.

2.1 HYDROGEN DIFFUSION, PERMEATION AND TRAPPING

2.1.1 Diffusion and permeation of hydrogen

The importance of hydrogen as a factor in the behavior of metals, its effect on metal properties, and its many uses in metal processing are well established *(Galaktionowa, 1981)*. "Diffusion" is defined as the transport of matter caused by random thermal motion of molecules, atoms, ions, or other particles in gases, liquids or solids. According to Einstein, the diffusion coefficient may be, statistically, a function of a unit act of particle motion and the time needed for such unit motion *(Arkid, 1994; Beck, 1966)*. Hydrogen diffusion is always preceded by activated adsorption, i.e., chemical adsorption of the hydrogen on the metal surface established *(Galaktionowa, 1981)*. The diffusion rate of hydrogen in a given metal is a definite constant (for a given set of parameters-composition and structure of the metal, temperature, etc.) and is always higher than the diffusion rate of any other atom under the same conditions. The diffusion coefficients of hydrogen in Alpha-Fe at 800°C and Gamma-Fe at 1100°C are 2.7×10^{-4} and 1.9×10^{-4} (cm^2/s), respectively (*Galaktionowa, 1981*). In the hydrogen/iron system, the measured quantity of the hydrogen diffusion coefficient is not diffusion alone but a combination of adsorption, diffusion, dissolution and desorption processes that are more properly

described as "permeation" *(Krasnikov Izvestiya, 1946; Darken and Gurry, 1953; Belash et al., 1979).*

Hydrogen diffuses in metals in an atomic or protonated state and its paths have been studied in detail. Many authors have shown that the diffusion rate is independent of the grain size of the metal, i.e., grain boundaries either play no role in the diffusion process or diffusion along grain boundaries is slower than transgranular diffusion. This is illustrated by the data in Table 2-1 *(Galaktionowa, 1981).*

Table 2-1 Diffusion rates of hydrogen in iron at various temperatures

Temperature, °C	Pressure, mmHg	D, (cm^2.sec)	
		Fine grains	Single crystal
245	140	2.4×10^{-6}	1.2×10^{-6}
413	140	17.6×10^{-6}	17.1×10^{-6}
621	140	92.8×10^{-6}	89.5×10^{-6}
779	140	203.0×10^{-6}	205.0×10^{-6}

The diffusion rate of hydrogen in metals is very sensitive to the nature and concentration of defects in the metal. Dislocations, internal stresses causing a disruption of mosaic structures, and other imperfections may act as "traps" and slow-down the diffusion of the proton *(Beck, 1966; HU, 1998; Benson and Edyvean, 1998).* Precipitation of fine new phases, or changes in the state of inclusions (e.g., formation of platelike carbide from spheroidal carbides) have a similar effect. Data on the effect of alloying on the diffusion rate of hydrogen in iron are controversial, but, in all cases, the diffusion rate increases with increasing temperature and partial pressure of hydrogen. At low temperature, the structure of steels affected the diffusion rate of hydrogen, but at elevated temperatures, the diffusion rate did not depend on the structure. On the subject of the mode of transport of hydrogen in iron, most authors agree that the transport is transcrystalline, and that grain boundaries have little effect. Electrochemical hydrogen permeation measurements are sensitive to many types of equipment and operating parameters *(Shaw, 1998).* This will be discussed in detail later.

2.1.2 Surface deposits, oxide and coatings

A collaborative study to examine the standard International Standard Organization (ISO) method for the determination of diffusible hydrogen in ferritic arc weld metals noted that the accuracy and reproducibility of the results depended, in part, upon the surface condition of the sample. Parker and Jenkins (*1987*) studied effects of surface cleaning methods on the analysis of hydrogen samples, and grit or blasting was the best recommendation. HU *et al.* (*1998*) studied the influence of cathodic protection conditions on the hydrogen absorption by underground steel pipes for natural gas transport in media containing thiosulfate. Their results confirmed the catalytic effect of the thiosulphate on the hydrogen absorption. The catalytic effect of thiosulphate on hydrogen absorption decreased and almost disappeared at very high cathodic potential. In the presence of thiosuphate, formation of a calcium-magnesium deposit clearly reduced the permeation current.

Benson and Edyvean (*1998*) measured cathodically protected and unprotected BS 4360, grade 50D steel with various surface finishes and coatings in open seawater and marine mud. Cathodically protected, uncoated steel showed the greatest hydrogen permeation, and coated steels showed the least. The antifouling coating gave the lowest hydrogen permeation in both environments.

C. Kato and his co-workers (*1984*) determined cathodic and anodic polarization curves and hydrogen permeation for Fe, Fe-0.5Cu and Fe-3.4Cu in sulfuric acid. A black layer, consisting of metallic Cu and Fe-oxides or –hydroxides, is formed on the surface of the alloys by preferential dissolution of Fe. The black layer acts as a barrier and a catalyst for H_2 evolution. The layer reduces the permeation rate by a factor of two when compared to pure iron; in the presence of H_2S, the reduction is by a factor of six. Addition of H_2S and/or an increase in pH can shift the cathodic polarization curve to more negative potentials where the scale is not stable. Under such conditions, the permeation rate is faster on the alloys than on Fe.

Yen (*1999*) investigated the retarding effect of thermally grown oxide films on hydrogen embrittlement and entry. The permeation test has indicated that the subsurface hydrogen concentration C_h^m (8.0×10^{-5} mol/cm^3) has been reduced to $C_h^{m'}$ (1.3×10^{-5}mol/cm^3) by the

oxide film. The explanation for this reduction is that the hydrogen permeation rate is much lower in the oxide film than in the metal itself.

Kim *et al.* (*1998*) investigated the role of the electroplated nickel layer on hydrogen permeation through AISI 4340 steel. The permeation test, composed of three steps, was conducted to measure the hydrogen diffusivity and surface hydrogen concentration. The nickel-coated layer contributed to a decrease in the hydrogen permeability of Ni coated AISI 4340 steel specimens. This is due to the fact that the surface hydrogen concentration and hydrogen diffusivity in the Ni coated layer was lower than those of AISI 4340 steel substrate. It is proposed that the thin Ni layer on AISI 4340 steel acts as a barrier for hydrogen permeation through AISI 4340 steel.

Zakroczymski and co-workers (*1997*) measured the hydrogen permeation through plasma nitrided, nitrocarburized, sulphur-oxy-nitrided and oxy-nitrocarburized iron membranes by the electrochemical technique. In the alkaline solution, the permeation rate of hydrogen through plasma-treated membranes was by two or three orders of magnitude lower than that through an unmodified membrane. Contributions to the reduced hydrogen absorption were evaluated for the hindrance of the hydrogen entry into the compound layers, and for the hindrance of hydrogen transport through the compound and diffusion layers. In the acid solution, all the applied nitridings also reduced hydrogen permeation; however, this effect was obscured by corrosion of the nitride layer.

Polarization and permeation experiments showed that a thin layer of electroplated bismuth (1μm to 2μm) inhibited the evolution and penetration of hydrogen through nickel-chromium alloy 718 and type 4340 steel (*Popov, 1995*). Inhibition effects were due to the kinetic limitations of the hydrogen reduction reaction and to the suppression of hydrogen adsorption on the deposited layers. The hydrogen evolution reactions on alloy 718 and type 4340 steel were inhibited by 28% and 85%, respectively. The hydrogen permeation rates through these alloys were reduced by 76% and 65%, respectively.

In another experiment done by Manohar and co-workers (*1995*), Fe-Pd, Fe-Pt, and Fe-Au surface alloys were produced using a technique consisting of electrodeposition of the respective noble metal on quenched and tempered AISI 4135 steel followed by laser surface melting using a CO_2 laser at three power levels. Hydrogen permeation testing

carried out on the surface-alloyed specimens showed reduced hydrogen absorption compared with the untreated and the surface-melted-only conditions, with the Pt-alloyed specimens showing the greatest reduction. Attempts made to determine the effect of the laser surface treatment on the hydrogen surface coverage as well as the other parameters of the hydrogen evolution reaction using the I-P-Z model were inconclusive, since several parameters were found to be simultaneously affected by the surface treatment.

2.1.3 Trapping: interaction of hydrogen and defects

2.1.3.1 Definition and classification

Hydrogen trapping typically becomes appreciable below ~150°C, and below this temperature the activation energy for diffusion effectively becomes the sum of that for lattice diffusion (about 2 kcal/mole for H in α-Fe) and that for releasing H from traps (typically 5-10 kcal/mole in Fe). A number of sites interact significantly enough with hydrogen in ferrous alloys to act as traps under circumstances in which the material exhibits hydrogen-induced loss of ductility *(Parker, 1987; Chew, 1971; Asano, et al. 1974; Sakamoto and Mantani, 1976; Asaoko, Dagbert, Aucouturier and Galland, 1977).* These sites include point defects, dislocations, and volume defects *(Chaudhari and Radhakrishnan, 1993).*

Quantitative estimates of number densities, binding energies and saturabilities of defects can be used to imply probable susceptibilities to hydrogen embrittlement *(Charitidou, et al., 1999).* It is well established that hydrogen embrittlement of steel is closely correlted to hydrogen-defect interaction processes. A defect trap for hydrogen is well characterized if its binding energy, E_B, its number density, N_X, and its specific saturability (proportional to the number of hydrogen atoms trapped per defect site) are known. Research has resulted in a significant increase in knowledge of the hydrogen trapping ability of various imperfections in steels. Hirth and Gibala *(Hirth, 1980; Gibala, 1977)* have summarized most of the literature available at that time. Table 2-2 gives the value of E_B and N_X for a number of traps, along with a few other recent results not included in their compilations. Most traps can be classified into one of three categories relative to E_S, the heat of the solution of hydrogen in iron, which is ~29 kJ/mole: weak traps with $E_B<E_S$, moderate traps with $E_B \sim E_S$, and strong traps with $E_B>E_S$. Strong traps behave irreversibly in the

sense that the rate of escape of hydrogen is relatively small. Pressouye and Bernstein *(Pressouyre and Bernstein, 1978, 1979; Pressouyre, 1979; Pressouyre, 1980)* have argued that E_B>=60 kJ/mole dictates irreversibility in hydrogen embrittlement situations. The nature of the crack path in hydrogen embrittlement should be determined by the extent to which strong traps present in adequate numbers can collect hydrogen from external source or reversible traps. Table 2-3 *(Pressouyre and Bernstein, 1979)* summarizes this statement in a general way.

Table 2-2 Hydrogen-trap interactions

Trap	E_B (kJ/mol)	N_X (no/m^3)
Interstitial solutes (N,C)	~3-15	10^{25}
Si atom	>20	10^{27}
Ti atom	26	10^{27}
Vacancy	46	$<10^{23}$
Y-vacancy	126	$\sim10^{23}$
_Elastic stress field	20	10^{19}-10^{26}
⊥Core (screw)	20-30	10^{19}-10^{26}
⊥Core (mixed)	59	10^{19}-10^{26}
$1/2H_2$ (vapor/void)	29	--
Grain boundary	~59	10^{19}-10^{23}
Free surface	70-95	10^{21}
AlN interface	65	10^{24}-10^{25}
Fe_3C interface	84	10^{24}-10^{25}
TiC interface	96	10^{24}-10^{25}

Table 2-3 Trap classification for hydrogen-assistant cracking

Principle microstructural traps	Nature of trap	HAC susceptibility
Solute atoms Microvoids Low anle boundaries Dislocations Coherent precipitates	Weak/moderate Reversible E_B=<60 kJ/mole	Cracking along well-defined interfaces in not favored.
Microcracks (pre-existing, propagation) High angle boundaries Incoherent (precipitates, interfaces)	Strong Irreversible E_B>=60 kJ/mole	Cracking along interfaces that are irreversible traps is favored.

2.1.3.2 Relationship between microstructure, traps and hydrogen-assisted Cracking

(1) Alloying elements

Based on the definition and classification above, the traps always correlated to certain microstructure of steels. Recently, Chan *(1999)* studied the effects of microstructure on the hydrogen trapping ability and effective diffusivity in steels with different carbon content. The results showed that the hydrogen pick-up was generally increased with the amount of grain boundary area in the steel.

The presence of traps for hydrogen atoms influences the diffusivity and solubility of hydrogen itself in steels. Valentini *et al. (1996)* studied the influence of titanium and carbon content on the hydrogen trapping of micro-alloyed steels. The number per unit volume of irreversible traps was correlated to calculated volume fraction of Ti(C,N) precipitates. These results, combined with microstructural investigations by transmission electron microscopy (TEM), showed that the largest number of irreversible traps was associated with steels having the largest volume fraction of fine and coherent Ti(C,N) precipitates. The reversible traps were associated with free Ti atoms, dislocations, and ferritic grain boundaries.

Jung and Lee *(1996)* found that cross rolling is better in reducing the embrittlement than unidirectional rolling because the cross rolling develops stable dislocation cellular structures acting as a hydrogen trapping sites. Stephens and Berstein (*1989*) correlated the susceptibility of a Ti microalloyed HSLA steel to internal hydrogen induced cracking with the hydrogen trapping character of the microstructure. Their results showed that both of these properties are influenced by aging reactions that determine the type and extent of carbide precipitation as well as metalloid segregation to grain boundaries.

Johnson and WU (*1987*) electrochemically determined the coefficient of hydrogen permeation and diffusion at constant current for commercially pure iron, annealed 1010, 1035, 1050, 1090 and heat treated 1050 steel between 273 and 303°C. Their results indicated that coefficient of hydrogen permeation and diffusion in annealed steel decrease with an increase in iron carbide volume fraction in the order iron, 1010, 1035 and 1090 steel. Coefficients of hydrogen permeation and diffusion decrease with heat treatments that refine the iron carbide distribution in the order speroidized, annealed, normalized,

austempered, and quench/tempered. Correspondingly, apparent solubility increases and lattice solubility decreases as the carbon content and iron carbide fineness increase.

(2) Heat treatment and microstructure

D. S. DeMiglio *et al.* (*1996*) studied the effect of hydrogen on 4340 steels tempered at various temperatures. Hydrogen charging was done cathodically in 4% H_2SO_4 at 30A/m^2 for 300s with no catalytic poison and was followed immediately by cadmium plating. The charged materials exhibited a reduction in area in tensile tests and a larger dimple size than their counterparts. Study results also indicate a simple generalization: materials tempered at the higher temperatures tend to have an abundance of reversible types of traps, whereas materials tempered at the lower temperatures tend to have an abundance of irreversible traps. After investigation on alloy K-500 with different heat treatment, Pound (*1999; 1998; 1997*) pointed out that an increase in trapping capacity produced by annealing leads to an increase in HE susceptibility. The laboratory tests pointed to annealing, rather than hardness, as the critical factor in the irreversible trapping behavior and HE susceptibility of aged alloy K-500 (*Chaudhari and Radhakrishnan, 1993*).

A review done by Kushida *et al.* (*1997*) covers the basic understanding of hydrogen embrittlement, the role of tempering in quenched and tempered steel, the role of baking after electroplating and behaviors of hydrogen in other heat treatments. It is emphasized that there is a close relationship between delayed fracture and the heat treatment, and that its relation could be explained by concentration and existing states of hydrogen in steels. Pound (*1999; 1998; 1997*) also introduced an irreversible trapping constant (K) to evaluate the capacity of hydrogen trapping in high strength steels, and their theoretical results showed a consistency with the experimental results. Luppo and Ovejero-Garcia (*1991*) studied the effect of the microstructure on the hydrogen embrittlement susceptibility, hydrogen mobility and hydrogen distribution in a low carbon steel. The hydrogen diffusivity attains a minimum value in a fresh martensite and diffusivity increases with increasing tempering temperature. There is a direct relationship between hydrogen embrittlement susceptibility and the quantity of desorped hydrogen, as well as between the hydrogen segregation and crack location.

(3) Pre-deformation

Brass, *et al.* (*1999*) and *Garet et al. (1998)* investigated the mechanisms of hydrogen interactions with dislocations and voids in a large deformation range in three Cr-Mo steels using the electrochemical permeation technique. Brass and Chene (*1998*) reviewed some experimental data about the influence of deformation on the hydrogen behavior in iron and nickel alloys. Experimental data on hydrogen, deuterium and tritium diffusion and trapping show: (a) a strain dependent hydrogen ingress in bcc alloys through natural or passive films; (b) strain induced hydrogen trapping; (c) an accelerated transport of hydrogen in pre-strained samples or during dynamic straining; (d) a hydrogen enhanced localized plasticity; and (e) a deformation enhanced embrittlement.

Beck *et al. (1966)* investigated the effect of plastic deformation on hydrogen permeation in 4340. Their hydrogen diffusivity and solubility results show that only a very small amount of plastic strain is sufficient to produce a two-fold increase in hydrogen concentration. Mailer and co-workers (*1991*) studied the effect of the dislocation arrangement on hydrogen permeation in spheroidized low alloy steel using the electrochemical permeation technique. The dislocation cell structure formed during fatigue reduces the apparent diffusion coefficient as the trap density is increased. On the other hand, the steady state hydrogen permeation flux is increased as dislocation cores act as short diffusion paths.

Kumnick and Johnson (*1974*) studied the effect of deformation and annealing on hydrogen transport through Armco Iron H.P. membranes. Two types of hydrogen traps were indicated by transient measurements on membranes with different processing histories. These traps may be caused by deformation and are not readily explained in terms of the stress field of a single dislocation and are probably associated with some feature of the dislocation cell structure caused by deformation.

2.2 MODELING AND CALCULATION ISSUES

2.2.1 Diffusible hydrogen in metals

2.2.1.1 General steps for solving the apparent diffusivity

The boundary conditions are established for solution of Fick's second law *(DeLuccia and Berman, 1981; Cailletet, 1864; Mcbreen, et al., 1966; Devanathan and Stachurski, 1962;*

Frank, 1958; Pumphrey, 1980; Zakcroczymaki and Szklarska-Smialowska, 1985; Ryun and Oriani, 1989; Song, et al., 1990; Bruzzoni and Garavaglia, 1992;Chaudhari and Radhakrishnan, 1990)

$$\frac{\partial^2 C}{\partial x^2} - \frac{1}{D}\frac{\partial C}{\partial t} = 0 \quad \text{.....2-1}$$

The boundary conditions for this equation:

$$\begin{cases} \text{On the charging surface: } x=0,\ C=C_0; \\ \text{On the exit surface: } x=L,\ C=0. \end{cases}$$

Using those boundary conditions and a Laplace transform method, a solution can be arrived at:

$$C(x,t) = C_0 - C_0\sum_{n=0}^{\infty}(-1)^n erfc\frac{(2n+1)L-x}{2(Dt)^{1/2}} - C_0\sum_{n=0}^{\infty}(-1)^n erfc\frac{(2n+1)L+x}{2(Dt)^{1/2}} \quad \text{.....2-2}$$

From Fick's first law,

$$\frac{J_t}{zF} = -D\left(\frac{\partial C}{\partial x}\right)_{x=L} \quad \text{.....2-3}$$

From these two equations,

$$\frac{J_t}{zF} = C_0\left(\frac{D}{\pi t}\right)^{1/2}[1 - e^{-L^2/Dt} + e^{-4L^2/Dt} + ...] \quad \text{.....2-4}$$

If $L^2/Dt \geq 4$, all exponential terms could be dropped to use a first-term solution,

$$t_{max} = \frac{L^2}{4D} \quad \text{.....2-5}$$

The first-term solution is,

$$\frac{J_t}{zF} = C_0\left(\frac{D}{\pi t}\right)^{1/2} \quad \text{.....2-6}$$

From $t = \frac{L^2}{4D}$, and z=1, C_0 could be calculated.

$$C_0 = \frac{\pi^{1/2}}{2}\cdot\frac{J_t L}{DF} \quad \text{.....2-7}$$

If the experimental extraction current density-time transient fits the theoretical curves plotted from the above equation, and if the diffusivity of hydrogen through the given steel is known, a measurement of J at any given extraction time will give the hydrogen content

C_0. If D is unknown, the value $D^{1/2}C_0$ can be determined; that is, the current (or current density) at a given time is proportional to the hydrogen concentration. t_b is the time measured by extrapolating the linear portion of the rising permeation current transit to J_0, which is the intersection of the extension of linear pick-up portion to the time axis. The elapsed time at which the H flux equals 0.63 times the steady-state flux is the time lag (t_{lag}) from which the apparent diffusion coefficient D of H in the metals films may be calculated.

The time to breakthrough expression is

$$D = L^2 / 15.3 t_b \quad \text{2-8}$$

The time-lag method employs

$$D = L^2 / 6 t_{lag} \quad \text{2-9}$$

There are two methods to get the value of D.

<1> Fourier method for D:

$$J / J_{ss} = 1 - 2\exp(-\pi D t / L^2) \quad \text{2-10}$$

D can be derived from the slope of a plot of $\ln(1-J/J_{ss})$ against t.

<2>The Laplace method uses:

$$J / J_{ss} = [2L / (\pi D t)^{0.5}]\exp(-L^2 / 4Dt) \quad \text{2-11}$$

Which can be rearranged to,

$$\ln(Jt^{0.5}) = const.(-L^2 / 4Dt) \quad \text{2-12}$$

where the constant is $\ln(2LJ_{ss}/(\pi D)^{0.5}$, so that D can be obtained from the slope of a plot of $\ln(Jt^{0.5})$ against t^{-1} or from the intercept. Additionally, the apparent diffusion coefficient may be determined from the current transit at two short times (t_1 and t_2) as:

$$\frac{Lt_1}{Lt_2} = \left(\frac{t_2}{t_1}\right)^{1/2} \exp\left[-\frac{L^2}{4D}\left(\frac{1}{t_1} - \frac{1}{t_2}\right)\right] \quad \text{2-13}$$

In steels, H is subject to trapping in reversible and irreversible traps. In the presence of reversible traps of binding energy (Eb) with low occupancy, Johnson and Lin (*1980*) reported,

$$D = D_L\left[1 + \frac{N_T}{N_L}\exp(E_b / RT)\right] \quad \text{2-14}$$

This equation shows D is independent of C_0 at low occupancy of the traps and decreases with increases in N_T and E_b. H trapped in irreversible traps is known as non-diffusible H, whereas H in interstitial sites and reversible traps is called diffusible H. Assuming the activity coefficient of H in the steel is unity, the elapsed time $t_{1\%}$ at which C_0 is 0.01 times the constant C is related to D as:

$$D = L^2 / 16.4 t_{1\%} \quad \text{.....2-15}$$

2.2.1.2 Hydrogen diffusion with and without trapping

2.2.1.2.1 Diffusion without traps

Diffusion of hydrogen atoms in steel occurs through interstitial sites with the octahedral site being preferentially occupied at high temperatures and tetrahedral sites at low temperatures *(Kiuchi and Mclelan, 1983)*. For an ideal homogeneous material the depth of the potential wells and energy barriers between adjacent tetrahedral sites will be uniform and the distribution of hydrogen atoms in the steel can be derived from the solution of Fick's second law (*Crank, 1956*). If the concentration of hydrogen atoms at the input side of a membrane is constant at all times (i.e. equilibrium between the surface coverage and sub-surface hydrogen atom concentration is established instantaneously) and the concentration is zero at the output side the permeation transients can be described by

$$\frac{J_\tau}{J_\infty} = 1 + \sum_{n=1}^{\infty} (-1)^n \exp(-n^2 \pi^2 \tau) \quad \text{.....2-16}$$

and by

$$\frac{J_\tau}{J_\infty} = \frac{2}{(\pi\tau)_{1/2}} \sum_{n=1}^{\infty} \exp\left(-\frac{(2n+1)^2}{4\pi}\right) \quad \text{.....2-17}$$

where J_τ is the time dependant flux and J_∞ is the steady state value. The dimensionless time parameter τ is Dt/L^2. The first equation for the normalized flux is the Fourier solution, and the second one represents the Laplace solution. Both give equivalent results provided enough steps in the summation are used. If the boundary condition on the input side of the membrane is a constant flux (i.e. the desorption step is very slow) then the normalized flux is given by *(Boes and Zuchner, 1976)*

$$\frac{J_\tau}{J_\infty} = 1 - \frac{4}{\pi}\sum_{n=0}^{\infty}\frac{(-1)^n}{(2n+1)}\exp\left(-\frac{(2n+1)^2\pi^2\tau}{4}\right) \quad \text{2-18}$$

Pumphrey *(1980)* has examined the applicability of these different boundary conditions for palladium and for iron. The constant flux condition is most appropriate for palladium, but for iron the situation is less clear. The assumption of equilibrium at the interface (and hence constant concentration) may be inexact at short times and conceivably could affect the permeation transient. Pumphrey suggested that this effect could be isolated by assessing the effect of thickness on the current transient.

The decay of the permeation current from the steady state value (after eliminating the charging current) has been solved for two limiting conditions. The subsurface concentration on the input side immediately goes to zero (to give fast decay) and the normalized flux is then given by

$$\frac{J_\tau}{J_\infty} = 1 - \frac{2}{\pi^{1/2}}\cdot\frac{1}{\tau^{1/2}}\sum_{n=0}^{\infty}\exp\left(\frac{-(2n+1)^2}{4\tau}\right) \quad \text{2-19}$$

The flux across the input boundary is reduced to zero as soon as the charging current is switched off. In this case, the decay is slower and only occurs through the anodic side of the membrane. The normalized flux is then given by

$$\frac{J_\tau}{J_\infty} = 1 - 2\sum_{n=0}^{\infty}(-1)^n \, erfc\frac{2n+1}{2\tau^{1/2}} \quad \text{2-20}$$

Analysis of the decay curves has not been undertaken at this stage of the work and these two equations are included only for reference.

2.2.1.2.2 Diffusion with traps

The consequence of trapping is a decrease in the rate of transport of hydrogen atoms because there is finite probability of the hydrogen atoms jumping into trap sites and because the residence time in the site will be longer than in a normal diffusion site *(Kiuchi and Mclelan, 1983),* since these trapping sites essentially act as sources or sinks for hydrogen atoms. Fick's second law for conservation of species is no longer valid and a more comprehensive treatment is required. Ideally, this treatment would embrace a complete description of all types of traps requiring a definition of the different types of

sites, the number of such sites per unit volume, and the average time of transfer between sites for each type of site.

The most comprehensive approach to this problem was developed by Leblond and Dubois *(1983)* based on a statistical approach to diffusion. A more tractable set of equations was obtained by making the assumption that the probability of capture was the same for each type of site; i.e. the height of the potential barrier is not dependant on the nature of the site, and thus there are no specifically attracting sites or repelling sites. A further important assumption was to describe the metal as containing only three types of site: diffusion sites, reversible sites, and irreversible saturable traps. Thus, there is no specific metallurgical distinction between the sites at this stage, and all sites are considered collectively in the three categories with average times of transfer for each type of sites.

If the diffusion coefficient and the solubility are assumed uniform throughout the material (the latter assumption will be invalid if a stress gradient is present), the transport equations from the Leblond and Dubois model can be simplified to:

$$\frac{\partial n_1}{\partial t} = D_1 \frac{\partial^2 n_1}{\partial x^2} + p_2 \frac{n_2}{\tau_2} - p_2 \frac{n_1}{\tau_1}[1 - \frac{n_2}{n_2^s}] - p_3 \frac{n_1}{\tau_1}[1 - \frac{n_3}{n_3^s}] \quad \text{2-21}$$

$$\frac{\partial n_2}{\partial t} = \frac{n_1}{\tau_1}[1 - \frac{n_2}{n_2^s}] - \frac{n_2}{\tau_2} \quad \text{2-22}$$

$$\frac{\partial n_3}{\partial t} = \frac{n_1}{\tau_1}[1 - \frac{n_3}{n_3^s}] \quad \text{2-23}$$

Under steady state conditions the time derivatives are zero and equation reduces to

$$\frac{\partial^2 n_1}{\partial x^2} = 0 \quad \text{2-24}$$

which is Laplace's equation, the solution of which yields a linear relationship between n1 and x. An analytical solution of the last three equations is not possible, particularly in view of the non-linearity of equation 2-24, but a numerical treatment of these equations is being pursued.

2.2.1.3 Concentration-dependent hydrogen diffusivity

Mostly, Lyer *(1989, 1988, 1990)* and Pickering *(1989, 1990)* have identified the embrittlement process as diffusion controlled, and not much attention has been paid to the actual value of the hydrogen diffusion coefficient and the material variables affecting this value. The reported values of diffusivity of hydrogen in α-iron and ferritic steels, for example, vary over four orders of magnitude at low temperature. Such a lack of agreement in diffusivity values is a hindrance to the evaluation and prediction of hydrogen embrittlement characteristics of commercial structural materials.

Room temperature diffusivity values under various charging conditions were determined and were correlated with the hydrogen concentration within the material, indicating a positive concentration dependence of hydrogen diffusivity in Armco iron. From Fick's first law, the flux of hydrogen at the anodic side of a membrane of thickness L is given by

$$Flux = -D(\frac{\partial C}{\partial x})_{x=L} \quad \text{2-25}$$

From this equation, the permeation current density, J, is derived as

$$J = -nFD(\frac{\partial C}{\partial x})_{x=L} \quad \text{2-26}$$

In order to evaluate the concentration gradient at x=L, McBreen *et al. (1966)* solved the diffusion equation for the gradient of concentration as a function of time

$$\frac{\partial^2 C}{\partial^2 x} - \frac{1}{D}\frac{\partial C}{\partial t} = 0 \quad \text{2-27}$$

and developed a mathematical basis for the permeation technique. Recently, Nanis and Namboodhiri (*1972*) modified and extended the results of MCBreen *et al.* (*McBreen, et l., 1966; Bolton and Shreir, 1963; Wach, 1971).* Important relationships used in the present calculations are given below. The normalized permeation build-up current is expressed as

$$\frac{J_r}{J_\infty} = \frac{2}{\pi^{1/2}}\frac{1}{\tau^{1/2}}\sum_{n=0}^{\infty} e^{-(2n+1)^2/4\tau} \quad \text{2-28}$$

The expression in this equation can be plotted against *log*r to obtain the theoretical build-up curve in a convenient form. The procedure adopted here to obtain diffusivity values is as follows: the experimental build-up currents are normalized and the J/J_∞ values are plotted against *log*t. These curves are then compared with the theory to obtain a best fit,

and the t value (in seconds) corresponding to some fixed value of τ is noted. Then D can be calculated. The concentration of hydrogen at the charging side of the membrane may be calculated using the relationship

$$C_0 = \frac{J_\infty L}{DF} \quad \text{2-29}$$

which is essentially the steady-state version of equation 2-27. The decay of the permeation current from the steady state was recently examined by Nanis and NamBoodhiri (*1972*). The experimental results showed that hydrogen diffusivity in Armco iron is dependent on the hydrogen concentration within the metal, and that the data could be approximated by the linear equation given by $D = D_0(1+1.09Z)$ ($D_0=4.05\times10^{-5}cm^2sec^{-1}$, $Z=(C_{average}/C_{avergae\text{-}max})$). When the diffusion coefficient D is concentration-dependent, the conclusion could be drawn that D is not a constant. At this time, the most general form of Fick's second law should be used as

$$\frac{\partial}{\partial x}(D\frac{\partial C}{\partial x}) - \frac{\partial C}{\partial t} = 0 \quad \text{2-30}$$

There are no general techniques that can be used to solve this equation when D is a function of C. Only a limited number of formal exact solutions have been obtained for the problem of concentration-dependent diffusion *(Nais and NamBoodhiri, 1972)*. The semi-infinite solution of equation 2-30 for C could be assumed to apply for the finite sheet within the range $0<\tau\leq0.04$. For later times, equation 2-30 was solved by a finite difference method. For convenience, a new variable, S, was introduced such that

$$S = \int_0^C D'dC \Big/ \int_0^1 D'dC \quad \text{2-31}$$

In terms of S, X, and τ, equation 2-31 becomes

$$\frac{\partial^2 S}{\partial X^2} - \frac{1}{D'}\frac{\partial S}{\partial \tau} = 0 \quad \text{2-32}$$

A modified Schmidt method was used to solve this equation. Using Crank's finite difference notations for the differentials, it yields the solution

$$S_m^+ = S_m + (\frac{D_m^+ + D_m}{2})\frac{\delta\tau}{(\delta X)^2}\times\{S_{m+1} - 2S_m + S_{M-1}\} \quad \text{2-33}$$

The steady state profile was independently calculated using Barrer's solution for a plane sheet, expressed as

$$X = \frac{C_0 + F(C_0) - C - F(C)}{C_0 + F(C_0)} \quad \text{2-34}$$

Where

$$F(C) = \int_0^C \left(\frac{D(C)}{D_0} - 1\right) dC \quad \text{2-35}$$

The permeation current J is directly proportional to $\partial C/\partial x|_{x=L}$. Since the concentration at x=L is always maintained at zero, D is always maintained as D_0. Hence, by noting the build-up of $\partial C/\partial x|_{x=L}$ we could obtain the build-up of permeation current. The slope at X=1 of the concentration profiles was calculated using the five point interpolation formula recommended by Hildebrand as

$$\frac{\partial C}{\partial X}\Big|_{X=1} = \frac{3C_{0.6} - 16C_{0.7} + 36C_{0.8} - 48C_{0.9} + 25C_{1.0}}{12\delta X} \quad \text{2-36}$$

The slopes were then normalized on the basis of the steady state slope. The permeation current increases at a faster rate than for the constant D case. The computed shift and distortion away from the constant D permeation curve is in conformity with the experimental data. Based on the agreement between the experimental results and the mathematical analysis, it is proposed that hydrogen diffusivity in annealed Armco iron increases with the increase in the concentration of hydrogen in the metal.

2.2.2 Quantitative analysis of hydrogen trapping

2.2.2.1 Quantitative analysis

Since 1949 hydrogen trapping has been well substantiated, both experimentally and theoretically. In the presence of traps, diffusivity values estimated from a simple breakthrough time will be different from the true diffusivity. It is also conceivable that the permeation build-up and decay curves may be affected by the presence of traps in the metal. The experimental value of diffusivity D is related to the true lattice diffusivity D_L by the relationship

$$\frac{D_L}{D} = (1 + 3\frac{Nx}{C_L^0}) \quad \text{2-37}$$

where N_x is volume of traps in cm^3 per unit volume of metal, and C^0_L is the true lattice solubility of hydrogen in units of cm^3 of hydrogen per cm^3 of iron. The experimental diffusivity D is always less than the true lattice diffusivity when trapping is involved. The true lattice diffusivity for iron may be estimated by the following expression (*Nanis and Namboodhiri, 1972; McBreen, et al., 1966; Bolton and Shreir, 1963; Wach, 1971)* as

$$D_L = 0.78 \times 10^{-3} \exp(-1900/RT) \quad \text{2-38}$$

The effect of hydrogen trapping on permeation built-up and decay transits can be evaluated only by solving non-linear differential equations of the type proposed by McNabb and Foster (*1963*). The presence of traps can only retard the movement of hydrogen atoms through the metal. According to the trapping formalism of McNabb and Foster, the number of atoms captured by pre-existing active traps is directly proportional to the local concentration of diffusing atoms. During a permeation build-up, the local hydrogen concentration in the metal increases. As permeation continues, the number of trapped atoms increases until the steady state is reached.

The measured or apparent H diffusivity (D_a) obtained by permeation methods is generally lower than the lattice diffusivity (D_L) because of trapping at lattice defects, such as vacancies and dislocations. A general model for hydrogen diffusivity with reversible trapping was developed by McNabb and Foster, who showed that the time lag evaluated from the permeation curves is given by

$$\frac{t_t}{t_l} - 1 = \frac{3\alpha}{\beta} + \frac{6\alpha}{\beta^2} - \frac{6\alpha}{\beta^3}(1+\beta)\ln(1+\beta) \quad \text{2-39}$$

where α and β are parameters characterizing the trap site. α can be expressed in terms of the binding energy (E_b) of the trap:

$$\alpha = \frac{N_r}{N_L}\exp\frac{E_b}{RT} \quad \text{2-40}$$

For traps with a low occupancy, equation 2-39 reduces to the following expression

$$\frac{t_t}{t_l} - 1 = \alpha \quad \text{2-41}$$

And, when the traps are near saturation, the following equation could be obtained (*McNabb and Foster, 1963; Johnson, 1988*).

$$\frac{t_t}{t_l} - 1 = \frac{3N_r}{C_0} \quad \text{2-42}$$

The graphic method of data analysis described by Johnson and Lin (*1981*) was used to obtain values of N_r and E_b. In this method, the normalized time t_t/t_l-1 is plotted against the reciprocal square root of hydrogen pressure, which allows N_r to be determined in the saturation region at high hydrogen pressures and then E_b to be determined from a single parameter fit in the low occupancy region (*Uhlemann and Pound, 1987*).

As previously discussed, any analysis of irreversible trapping in an alloy should be undertaken on the first polarization transient, where traps are in the process of being irreversibly filled. However, since reversible trapping is simultaneously operating, the analysis must use a compound variable accounting for both types of trapping.

2.2.2.2 Trapping of hydrogen at impurities

Budin and co-workers have measured the isochronal annealing of hydrogen in copper wires containing about 100ppm of impurities of unknown species (, *et al., 1964)*. The results of two samples loaded with about 20ppm of hydrogen show the large irreversible recovery stage occurring around room temperature which we also observed and which we could attribute to the formation of bubbles. When the sample was cooled quickly the increase was present, but when it was cooled slowly the increase did not occur. We attribute this annealing stage to the trapping of hydrogen at impurities and de-trapping at higher temperature. If E_b is the binding energy of the hydrogen at impurities with concentration C_t, and if $v=D/a^2$ (a lattice parameter) is the jump rate of hydrogen, then the rate equation for the atomic fraction c of un-trapped hydrogen is

$$\frac{dC}{dt} = 8(C_H - c)v\exp(\frac{-E_b}{kT}) - 48vC_t c \quad \text{2-43}$$

The first term of the right hand side describes detrapping and the second the trapping. The solution of this equation reads

$$C = (C_H - C_\infty)\exp(-\lambda t) + C_\infty \quad \text{2-44}$$

$$\lambda = 48\nu C_t + 8\nu \exp(\frac{-E_b}{kT}) \quad \text{2-45}$$

$$C_\infty = \frac{C_H}{1 + 6C_t \exp(\frac{E_b)}{kT}} \quad \text{2-46}$$

The atom fraction c of untrapped hydrogen is the superposition of two contributions. The first is the diffusion limited trapping term which is strongly temperature dependent through the diffusion coefficient D. The second is the untrapped fraction C_∞ in equilibrium.

2.3 MONITORING AND DETECTION OF HYDROGEN

Assuming that the hydrogen atoms are generated in a circular area on one side of the membrane and detected in a circular region on the other side, Hutchings *et al.* (*1993*) analyzed two-dimensional diffusion of hydrogen atoms in a membrane and calculated the average flux on the detection side as a function of membrane thickness and detection area. They suggested that the reasonable ratio of the charging surface to membrane thickness is larger than 10:1. All authors assumed that the appropriate boundary condition for the solution of Fick's diffusion equation was an instantaneous increase in surface concentration at the charged surface at the start of the experiment, and that this concentration remained constant thereafter. Recently, it has been argued that this boundary condition is applicable only to constant potential conditions *(Fullenwider, 1975; Early, 1978)*. Pumphrey *(1980, 1985)* discussed the experimental thickness dependencies of steady state permeation rates through potential-statically and galvanostatically charged iron membrane. The results showed that the boundary condition is one of constant surface coverage rather than constant surface concentration, and the flux entering the charged surface is limited by the finite rate constants for the transfer of hydrogen between the adsorbed and absorbed states. The flux decreases with time as the surface concentration increases to its steady state value.

2.3.1 Experimental set-ups for hydrogen permeation testing

Most used experimental set-ups include Devanathan cell (*Devanathan and Stachurski, 1962*), Barnacle Electrode *(Casanova and Crousier, 1996)*, Hay sensor (*Hay, 1983*),

Christensen sensor *(Christensen and Berman, 1981)*, and Morris-Fray sensor (*Morris_Fray and Scrosati, 1993*). The Devanathan cell was usually used in lab research and the Barnacles and Hay sensor were used for non-destructive monitoring in the field.

(1) Devanathan and Stachurski cell

Several papers deal with hydrogen permeation through steel using the Devanathan two-compartment cell, mostly with the aim of determining the hydrogen diffusion coefficient. The steel membrane was either palladium plated on both sides (*Zakcroczymaki and Szklarska-Smialowska, 1985; Ryun and Oriani, 1989; Song and Oriani, 1990; Bruzzoni and Garavaglia, 1992)*, or on the detection side (*Zakcroczymaki and Z. Szklarska-Smialowska, 1985; Chaudhari and Radhakrishnan, 1990; Flis and Zakroczymaki, 1992; Baez, Mendez and Vera, 2000)*, or on the input side *(Ryun and Oriani, 1989; Song, et al., 1990; Bruzzoni and Garavaglia, 1992)*, or without Pd coating *(Ryun and Oriani, 1989; Turnbull, et al., 1989; Razzini, et al., 1993; Turnbull, 1993)*, as well as with nickel plating on the exit side *(Carlos et al., 2000)*. In these latter cases, the effect of an iron oxide film on the exit side was also studied. A controversy arose about the possibility of using a membrane without a palladium coating on the exit side. From recent results it is known that kinetics of hydrogen oxidation is different with and without a palladium film

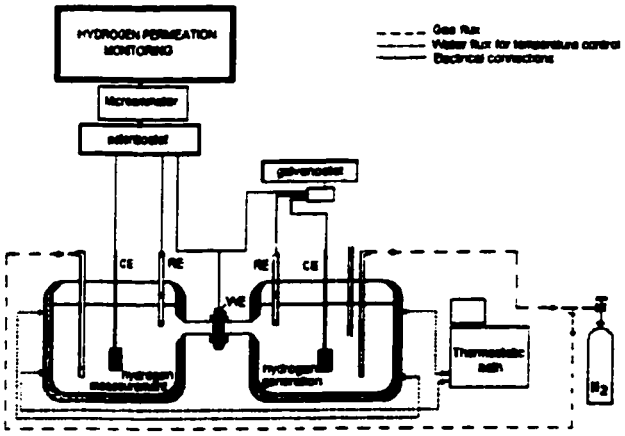

Fig.2-1 Schematic of conventional Davanathan-Srachurski cell *(Devanathan and Stachurski, 1962)*,

on the exit side, and that in the absence of palladium, an incomplete oxidation of hydrogen could occur which would falsify the results. Casanova and Crousier (*1996*) pointed out that an iron membrane without a palladium layer on the hydrogen exit side can be used, if the aim of the experiments is to detect the variation of the steady state hydrogen permeation current as a function of the experiments carried out in the input cell, running comparative experiments.

(2) Barnacle Electrode

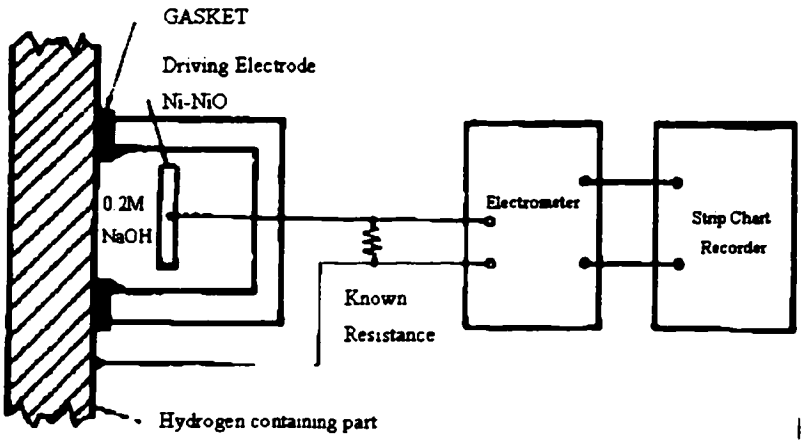

Fig.2-2 Schematic of barnacle electrode measuring apparatus
(Casanova and Crousier, 1996)

The barnacle electrode *(Casanova and Crousier, 1996)* was developed to measure the mobile hydrogen, and is being used to correlate hydrogen concentrations with delayed failure in high-strength steels. It consists of a steel specimen (anode), a nickel/nickel oxide electrode (cathodic), and a Teflon block that has a circular opening, and a silicone rubber gasket which, when clamped to the specimen, defines an exact area. The principle of this electrode is based on the electrochemical method of hydrogen permeation developed by Devanathan. A major simplification of this electrode over the electrochemical permeation technique is the use of nickel-nickel oxide electrode to replace the potentiostat and act as a stable nonplarizing power electrode (cathode) that maintains zero hydrogen concentration at the exit surface of the steel (anode) by oxidizing the emerging hydrogen atoms to water.

(3) Hay sensor

Fig.2-3 shows a schematic diagram of the hydrogen monitoring probe designed by Hay in 1983 (*Hay and Rider, 1999*). Hydrogen flux was measured in one-side charging experiments using pipe sections 150mm long filled with solution. The pipe sections were fitted with polycarbonate covers on the top and bottom. The top cover had openings for gas inlet and outlet, as well as for the temperature probe and heater.

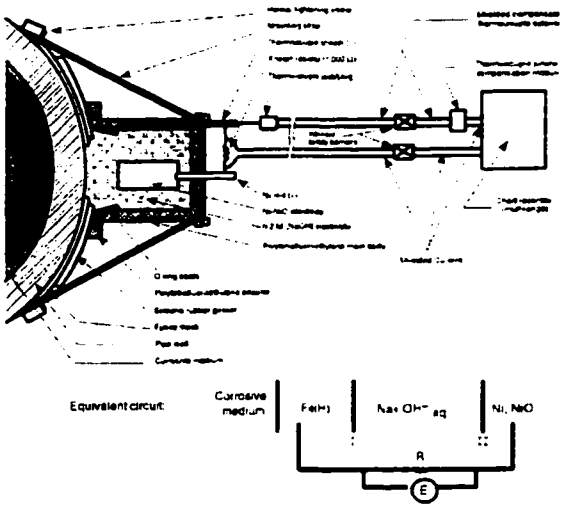

Fig.2-3 Sectional view and equivalent circuit of Hay sensor

(*Hay and Rider, 1999*)

2.3.2 Experimental technology on hydrogen trapping determination

Considerable efforts have been devoted to measuring the hydrogen distribution in metals in order to evaluate its effect on the stress corrosion cracking of high-strength steels. The experimental technique suggested to measure the hydrogen distribution in metals directly is tritium autoradiography. This is a non-destructive technique with very good resolution. It consists of charging a steel sample with tritium-enriched hydrogen and exposing to its β-ray emission a photographic emulsion that coats the metal surface. The images resulting from the exposure to the β radiation describe the hydrogen distribution pointing out defects, traps and plastic regions such as the stress field at the crack. Miyazawa *et al.* (*Miyazawa and Mori, 1998*) investigated the behavior of hydrogen accumulation in a long-term aged austenitic stainless steel SUS316 by tritium transmission electron microscopic (TEM) autoradiography using this method, Saito *et al.* (*Saito and Kasuya,*

1998; Saito, Mori and Ishida, 1996; Saito, et al, 1996; Saito and Kasuya, 1998; Saito, et al., 1995) observed the hydrogen sites in grain boundaries and grain boundary precipitates of an austenitic stainless steel.

Razzini *et al.* (*Razzini G., et al., 1997, 1999*) argued that there are drawbacks to the technique of tritium autoradiography. It is a time-consuming procedure because up to 40 days is necessary to get an image. It requires the handle of radioactive aqueous solutions, and spurious effects can result from the chemical interaction of a thin layer of the silver bromide left in contact for a long time with the metal surface. They developed a new experimental technique able to image hydrogen diffusion in iron with good resolution, scanning photo-electrochemical microscopy. The advantage of this technique is its capability to image hydrogen trapping and detrapping into blisters in real time, in situ and continuously, under hydrogen charging, which is so-called Scanning Photo-Electrochemical Microscopy (SPEM).

By the suggestion of Ross *et al.* (*Ross, Stefanopoulos and Kemali, 1999*), small angle neutron scattering (SANS) techniques have been used to investigate the trapping of hydrogen (H) and deuterium (D) on dislocations in palladium. Calculations of the expected form of this scattering are presented. It is shown that the different scattering lengths of H and D, respectively negative and positive, can be exploited to prove explicitly that the hydrogen is being trapped at the feature that is causing the SANS in the metal sample.

Nagumo *et al.* (*Nagumo, et al., 1999; Takai et al., 1998*) introduced the thermal desorption spectroscopy (TDS) to study the nature of hydrogen trapping in steels. Their results show that TDS using hydrogen as a tracer can be applied as a tool to investigate the various defects induced by plastic deformation. From transmission electron microscopy and TDS analysis, the lower temperature peak was attributed to hydrogen released from the trapping sites such as point defects, clustered defects, and dislocations in alpha-iron. The higher temperature peak was found to correspond to hydrogen released from the trapping sites, such as defects in Fe_3C, and/or the disordered interface between alpha-iron and Fe_3C. Smith and Scully (*2000, 1996*) identified the hydrogen trapping states in an Al-Li-Cu-Zr and correlated embrittlement trends with H trap sites using the TDS method. The propensity for high angle boundaries to trap H is a necessary but not

sufficient condition for H embrittlement. Abramov and Eliezer (*1996*) gave some advice on the major steps needed to obtain a reliable and quantitative analysis, and tried to demonstrate them by using TDS on hydrogen trapping mechanism and release behaviors. Moro *et al.* (*1998*) investigated the energetics of hydrogen atoms interacting with a cluster model of gamma-Fe, having a stacking fault by using the atom superposition and electron delocalization molecular orbital (ASED-MO) method to calculate the system energy. Szklarska-Smialowska and Xia (*1997*) evaluated the hydrogen trapping by cold-worked (CW) and non-cold-worked (NCW) X-52 steel through the use of the potentiostatic pulse method.

Trapping and release processes will strongly affect hydrogen isotopes inventories. In 1996, Valentini *et al.* (*1996*) developed a new computer-based code, THYDA, to calculate the concentrations of trapped and movable hydrogen atoms in metallic samples as well as hydrogen evolution rates during thermal desorption at elevated temperatures with variable heating rates. In these calculations, it is possible to take into account both the internal and external sources of hydrogen isotopes (i.e. generation in (n, p) nuclear reactions and by D-T ion implantation) and isolate reversible and irreversible hydrogen trapping in metals.

2.4 NEAR-NEUTRAL pH SCC OF PIPELINE STEELS

Stress corrosion cracking is the result of the combination and synergistic interaction of mechanical stress, environment, and materials. SCC of pipeline steels has two basic forms: high-pH SCC and near-neutral pH SCC (*Lambert, 1994*). The former has been studied extensively since the 1960's. Practical methods have been developed to reduce its damage (*Parkins, 1994*). This damage is related to intergranular fracture in concentrated (about 1mol/l) carbonate-bicarbonate solutions with pH in the range from 9.5 to 12.5. It is observed at potentials more positive than open circuit potential (OCP) and is more prevalent at higher temperatures.

Near-neutral pH SCC was first observed in 1985. It has caused an increasing number of pipeline failures recently. It is related to transgranular cracks with quasi-cleavage fracture. Colonies of longitudinal cracks form in response to the hoop stress resulting from the internal pressure. The electrolyte is mainly dilute (about 10^{-2} mol/l) carbonate-

bicarbonate solution containing a small amount of chloride and sulfate ions with a pH value of 5.5 to 8.5. Near-neutral pH SCC occurs at OCP or slightly cathodic potential (*Parkins R. N, 1997*). Because there is already a considerable body of literature talking about high-pH SCC, this section will focus on only near neutral pH SCC. A relatively thick white deposit of iron carbonate was observed on removing the coating from those regions where cracks were present. It is usually found under disbonded coatings, which shield the pipe surface from cathodic protection (CP). The difference between classic SCC and near-neutral pH SCC of pipeline steels is shown in Table 2-4, which implies different mechanisms of cracking.

Table 2-4 Differences between classic SCC and near-neutral pH SCC (*Wilmott and Diakow, 1996*)

	Classic SCC	Near-neutral pH SCC
bicarbonate-carbonate	High, about 1 mol/l	Low, about 0.01 mol/l
pH value	Around 9.5 (high pH), ≥9.3	around 6.5 (low pH), 5.5~7.5
Environmental characteristics	No correlation has been found between the incidence of SCC and soil characteristics close to cracked pipelines.	The CO_2 content in the vicinity of pipeline is important.
Temperature sensibility	Rate increases exponentially with temperature.	Without
Cathodic Potential	-0.60~-0.83 V_{SCE} or -0.52~-0.75 V_{SCE} more positive than E_{corr} more prevalent at higher temperature	At E_{corr} (-0.76~-0.79 V_{SCE} or -0.68~-0.71 V_{SCE}) or slightly cathodic (max. -0.05 V) under disbonded coating that shields CP
Association with welds	Without association	Tend to be concentrate near longitudinal welds
Associated reactions and products	Very small amount of iron carbonate is incorporated in the thin magnetite films.	Large amount of white iron carbonate is formed between the coating and pipe surface.
Cracks	Intergranular, narrow, spaced more widely and with no evidence for corrosion of crack wall. The films are strongly adhered to the crack sides and effectively prevent any lateral dissolution on the sides.	Transgranular, with very high density, with wide cracks filled with corrosion product. Significant lateral dissolution occurs, with appreciable amount of loosely adherent corrosion products forming in the crack enclaves.
Polarization curve	With active to passive transition	without passive zone

2.4.1 Materials and Mechanics aspects

Various grades of pipeline steels have been widely used. It is found that the steel structure (such as grain size) and micro-plastic deformation characteristics are important in determining the resistance to SCC (*Parkins, 1994*). The hot-rolled ferrite-pearlite structure steels have lower strength than the pearlite-reduced controlled-rolled steels (*Parkins, 1997*). The distribution of inclusions (such as manganese sulfide) is more important than the absolute values of specific elements in steels in terms of corrosion *(Willis, 1996)*. Service failures usually occurr when the hoop stressed in the pipe wall was greater than 60% of the specified minimum yield strength (SMYS) of the pipeline steel. Cyclic loading can markedly reduce the threshold stress of high pH SCC. Under cyclic loading conditions, which involves maximum stresses markedly below the yield stress, the material will suffer micro-plastic deformation. The magnitude of this deformation depends on the frequency, loading amplitude, and materials involved *(Parkins, et al., 1993)*. For near-neutral pH SCC, SCC intensity increases (*Gu et l., 1999; Yu et al., 1999; Parkins, 1974*) with a decrease of strain rate.

2.4.2 Effect of Environmental factors

2.4.2.1 Ionic aspects of the SCC sensitivity

The "chloride-induced brittle" is an important result of the investigation of the interaction of the electrochemical and mechanical effects, as well as the addition of 0.001 mol/l chloride ions which eliminate the passive region of a X-80 steel in 0.005 M HCO_3^- solution (*Liu et al., 1993)*. For passivated metals or alloys, the role of chloride was to reduce the stability of the passive film or break it down. However, there was no passive behavior for pipeline steels in a near-neutral pH environment. Therefore, changing the amount of chloride ion would not affect SCC intensity. It was demonstrated that SCC of pipeline steel is not dominated by film rupture (*Yu et al., 1999*). One example is the X-70 pipeline steels tested in two soil extracts. The chloride concentration in one is about 6 times higher than that in the other. However, their SCC susceptibility was quite similar. In addition, chloride ions showed no effect on the crack growth rate (*Jack and Boven, 1994*).

In the constant elongation rate testing of X-52 carbon steel in 0.1 N and 0.01 N $NaHCO_3$, both with pH of 8.3 at 50 °C, SCC susceptibility increased with increasing bicarbonate concentration at cathodic potentials (-1000mV to E_{corr}) *(Rebak et al., 1996)*. Both quantity and propagation speed increased with the increasing of bicarbonate concentration in near-neutral pH soil solutions *(Jack and Boven, 1994)*. That result suggests that bicarbonate species may play a role in the preferable corrosion of the active crack tips. In a $NaHCO_3$ solution with concentration as low as 0.005mol/l, the polarization curve gave a transition from active to passive, which is similar to the characteristics of classic SCC (*Gu et al., 1999*). When $NaHCO_3$ concentration was increased, the anodic current in the active regions increased.

The near-neutral pH SCC severity of pipelines increased with higher oxygen level (*Delanty and O'Beirne, 1992*) in the field. The results of X-80 pipeline steel tested in an NS-4 solution bubbling with different concentration of CO_2 gas at different potentials showed that the dependence of SCC intensity on potentials was different in NS-4 solution are bubbling with pure N_2 gas and bubbling with gas containing CO_2. Near E_{corr} (around -740 mV), SCC intensity was much less in solution with pure N_2 gas than that in solution with CO_2-containing mixture gas. The effect of CO_2 on SCC intensity was obvious not only near E_{corr}, but also at cathodic and anodic potentials. The local corrosion of the steel was facilitated and SCC intensity was increased (*Yu et al., 1999*).

Among those solutions associated with transgranular SCC, HCO_3^- and H_2CO_3 are the major chemical species; among those associated with intergranular SCC, the major chemical species are CO_3^{2-} and HCO_3^-. For a pH of about 6.5, which is most frequently associated with transgranular cracking, almost the same amounts of carbonic acid and bicarbonate ions are present. In classic SCC, in which the pH value of the solution is around 9.5 (≥9.3). The widely used solutions are 1 N sodium carbonate + 1 N sodium bicarbonate solution and 2 N ammonium carbonate solution (*Rebak et al., 1996; Pilkey et al., 1995; Parkins et al., 1993; Parkins and Singh, 1990*). The American Gas Association (AGA) first proposed 1N sodium carbonate+1N sodium bicarbonate solution and called it a "AGS electrolyte". Optimum conditions for cracking are at high temperature (70 °C) and narrow range of applied potential (-600 to -720 mV SCE). Cracks are intergranular and very narrow *(Lambert and Plumtree, 1994; Parkins, 1994)*. Pilkey *et al.* (*1995*)

developed an experimental system to reproduce high pH SCC of API X-60 pipeline steel in 1mol/l $NaCO_3$ + 1 mol/l Na_2CO_3 (pH = 10). Intergranular fracture developed in pre-cracked specimens under very low frequency (40 to 400 cycles /day) cyclic loading conditions with minimum to maximum stress ratio of 0.82, at 75 °C and -650 mV (SCE), which simulated actual pipeline conditions.

2.4.2.2 Contribution of hydrogen to SCC-Cathodic potential and pH value

Cathodic hydrogen could form either as a byproduct of anaerobic corrosion or as a direct result of effective cathodic protection. Entry of cathodic hydrogen into the steel as diffusible hydrogen could alter the properties of the material and play an important part in the growth of stress corrosion cracks (*Wilmott and Diakow, 1996; Delanty and Marr, 1992*). Due to the involvement of hydrogen in SCC, some specimens showed markedly reduced ductility to fracture but contained no secondary cracks; other specimens had internal secondary cracks, but none of them emanated from the outer surface where dissolution -related cracks would nucleate.

It was found that hydrogen concentration at the charging surface, C_0^H was related to cathodic potential and the type of electrolyte. For a certain electrolyte, C_0^H increased with more negative applied cathodic potential. For other electrolytes, C_0^H increased with more negative Open Circuit Potential (OCP). OCP was a linear function of logarithm of salinity. Therefore, the ability to generate diffusible hydrogen on steel surface depended on the salinity of the environment. However, the effect of potential on C_0^H and D_H was different in NS-4 from the results in soil extracts. For X-70 steel samples in NS-4 solution purging with 5% carbon dioxide balanced with nitrogen, C_0^H was the maximum at potentials close to and negative of E_{corr} (-900 to -1000 mV) and D_H was the minimum at potential of -950 mV. By contrast, for X-56 steel samples in NS-4 solution purging with 10% carbon dioxide balanced with nitrogen, the effect of potential on C_0^H was the same but the effect on D_H was different. D_H increased slightly with a decrease of potential in the range from OCP to -1100 mV.

When the applied cathodic potential was in the range from OCP to -900 mV (SCE), the apparent diffusivity of X-65 steel in NS4 solution was insensitive to cathodic potential.

When potential was below this insensitive range, diffusivity increased linearly with decrease of cathodic potential. Dependence of D_H on potential indicated the involvement a surface film, inhibiting hydrogen diffusion at more positive potential *(Parkins, 1997)*. A hollow tensile specimen was used to determine the effect of stress on D_H and C_0^H. It was shown that for stress larger than 80% yield stress, with the increase of elastic stress steady permeation current increased and C_0^H increased. But D_H was not a function of stress. The reason for increase in C_0^H was not clear (*Chen et al., 1999*). In general, hydrogen concentration at the charging surface C_0^H did not exceed 2.0×10^{-6} mol /cm^3. The minimum detected hydrogen current that could cause blistering was about 5.5×10^{-6} mol /cm^3. Therefore, the maximum hydrogen produced by the electrolytes in near-neutral pH conditions was less than that needed to produce visible hydrogen damage (blistering) on the steel surface.

Hydrogen causes grain boundaries to be more susceptible to corrosion *(Tomlison et al., 1981)*. When hydrogen was trapped in the defects in steels, the lattice was dilated and the interactive atomic cohesion was decreased. 1% hydrogen concentration could reduce the atomic bonding energy by 5 % for steels (*Hsiao and Chu, 1981*). In potentiodynamic polarization test of X-52 steel tested in NS-4 solution, the hydrogen pre-charged X-52 specimen has higher anodic current than that without hydrogen pre-charging, a difference which could result from the increase in the heterogeneity of the materials.

The pH value affects open circuit potentials (OCP) *(Linnet, 1970)*. When a specimen is immersed in soil electrolytes in equilibrium with 5% carbon dioxide balanced by nitrogen gas, OCP decreases linearly with the increase of pH. However, when a specimen is immersed in soil electrolytes in equilibrium with pure nitrogen, the relationship between OCP and pH is different. Since pH is a function of bicarbonate concentration, OCP is related to bicarbonate concentration, too.

In the SSRT testing of X-80 steels in NS-4 solution with different pH, the effect of pH on SCC susceptibility is different at different potentials. At cathodic potentials (-1000 mV), pH has no obvious effect on SCC susceptibility. At anodic potentials (-550 mV), SCC susceptibility increases with increasing pH *(Gu et al., 1999)*. At E_{corr}, SCC susceptibility decreases with increasing pH and, according to SEM observation, less cleavage area

appears with higher pH. Interestingly, SCC susceptibility of X-70 pipeline steel in soil electrolytes at OCP (measured in t_E/t_{air}) increased linearly with pH. SCC susceptibility of X-52 steel as a function of solution pH is determined using CERT. In 0.1 N Na_2SO_4 solutions with pH of 6 and 8, at anodic potential, SCC susceptibility increases with pH, which is consistent with the prior report. But at E_{corr}, SCC susceptibility of X-52 steel is the same , and at cathodic potential, SCC susceptibility decreased with pH.

It is generally believed that SCC occurs near the bottom of a holiday nearly free of cathodic current. If it were under adequate cathodic protection, excessive hydroxide ion would be generated, which would raise the pH of the environment to a non-neutral pH condition (*Jack et al., 1994*). Inadequate cathodic protection may help to maintain the near-neutral pH condition. When cathodic current density was kept at 0.04 mA/cm^2 for 10 days, no significant increase of pH was observed (*Charles, 1995; Parkins, 1995).*

It seems that the existence of CO_2 may reduce the hydroxide ion produced by CP. In SSRTs under CP, when 5 % CO_2 balanced by N_2 gas was supplied through tests, the initial near-neutral pH scarcely changed with time. It was shown that adequate CO_2 eliminated the effect of increasing pH by the hydroxide ion produced by CP.

A X-80 and X-52 pipeline steels in a NS-4 solution bubbled with 5 % CO_2 balanced with N_2 gas, in the range from -400 mV to -1000 mV, SCC intensity increased with decreasing potential till around E_{CORR}, then decreased and eventually increased again *(Yu et al., 1999)*. The effect of potentials could be explained as follows. At anodic potentials (till -600 mV), SCC intensity was lower due to the high general dissolution rate. Then when the potential decreased, uniform dissolution was restricted and local anodic dissolution predominated. As a result, SCC intensity increased sharply (around -750 mV). When the potential dropped to the cathodic region (-800 mV), local dissolution was restricted again as a result of cathodic protection and, consequently, SCC intensity decreased. Ductility decreased and SCC intensity increased when more negative potential applied. The same trend of SCC intensity changing with potential was reported in SSRT of X-65 steel in NS-1, NS-3 and NS-4 solutions not bubbling with CO_2, although the data were more scattered (*Parkins et al., 1994*).

In a NS-4 solution purging with 5% or 10% carbon dioxide balanced with nitrogen, at potentials more positive than E_{corr}, the surfaces of X-65 and X-70 pipeline steel samples dissolved uniformly. At potentials 100 to 200 mV more negative than E_{corr}, surfaces exhibited localized corrosion, where precipitated $CaCO_3$ was observed. At potentials greater than 300 mV and more negative than E_{corr}, the surface was uniformly covered by $CaCO_3$ (*King et al., Corrosion 2000*).

Potentials have an effect on the behavior of bacteria, too *(Delanty and O'Beirne, 1992)*. Sulfate reducing bacteria (SRB) can be stimulated by cathodic protection, since SRB counts increase with time under cathodic protection and decrease with time without cathodic protection (*Jack et al., 1994; Hardy, 1983*).

2.4.2.3 Effect of the environmental temperature and bacteria in soils

It was reported that over 90% of failures of high pH SCC were within 16 km downstream from a compressor station, where both the temperatures and stresses are higher than further down-stream. And the gas temperature was within the range of 10 to 60 °C, mostly above 35 °C, when service failures took place *(Parkins, 1997; Delanty and O'Beirne, 1992)*. Fessler obtained the following expression using quantifiable data for the effects of temperature on crack velocity and the width of the potential range for classic SCC (*Fessler, 1979*). The number of failures was reduced by about 55% for a 10°C drop in discharge temperature and about 80 % for a 20 °C drop. Lowering the temperature would reduce the probability of failure.

The cracking incidence of near-neutral pH SCC was unrelated to distance from compressor stations of gas transportation and, hence, unrelated to temperature. In addition, among the results of SSRTs of X-65 pipeline steel in NS-1, NS-2, NS-3 and NS-4 solutions at temperatures from 5 to 45 °C, there was no systematic trend in the effect of temperature (*Parkins et al., 1994*). It was indicated that near neutral pH SCC did not depend on temperature.

The severity of SCC increased with the presence of bacteria (*Delanty and O'Beirne, 1992*). Sulfate-reducing bacteria (SRB) could be stimulated by cathodic protection. And with decreasing sulfate concentration, the percentage of cracks showing growth

increased. The amount of sulfate ion in the final solution decreased with increasing initial SRB population (*Hardy, 1983*). Therefore, it was indicated that SRB played a role in setting up an environment suitable for the crack growing.

2.4.3 Mechanisms and its control

Typically, the crack propagation rate depends on the crack-tip stress intensity, and the crack propagation can be divided into three stages. SCC mechanisms are usually dependent on the crack stages. Crack initiation and stage I propagation can occur at existing flaws (such as fabrication defects and machining damages), surface inclusions, and corrosion pits. For crack initiation, the ratio of the depth to lateral length of the pits must be larger than 10; and for crack propagation, the ratio must be larger than 1000. Moreover, crack initiation and stage I propagation can take place during service or cleaning operations. It can result from breakdown of a protective film, intergranular corrosion, and slip planes, especially in low-stacking-fault-energy materials.

In stage II of the crack propagation, SCC mechanisms are basically based on dissolution models and mechanical fracture models. Dissolution models suggested that the crack propagates by preferential dissolution at its tip. Dissolution/oxidation of materials must be thermodynamically possible, and it is required that the crack tip is anodic compared with the crack walls. That is, a protective film must be thermodynamically stable. Film rupture mechanisms and active-path intergranular SCC is based on dissolution models. Film rupture mechanisms suppose that stress opens the crack and ruptures the protective film. The film rupture rate at the crack tip is larger than the re-passivation rate or the crack tip is re-passivated and periodically ruptured by the emergence of slip steps. The active-path intergranular SCC assumes that SCC occurs by an active-path process due to the difference in the microchemistry of the material at the grain or interface boundaries.

Some other models, the corrosion tunnel model, adsorption-enhanced plasticity model, tarnish-rupture model, film-induced cleavage model, stress-sorption brittle fracture model, and hydrogen embrittlement model are based on mechanical fracture models. The corrosion tunnel model assumes that cracks propagate by alternating tunnel growth and ductile fracture. A fine array of small corrosion tunnels forms at emerging slip steps. The

adsorption-enhanced plasticity model suggests that chemisorption of species in the environment (such as hydrogen and liquid metals) facilitates the nucleation of dislocations at the crack tip. The tarnish-rupture model assumes that crack propagates by alternating film growth and brittle film fracture. The film-induced cleavage model suggests that brittle crack initiates in a thin film formed on the surface. It crosses the film/matrix interface and continues to grow in the ductile matrix. The stress-sorption brittle fracture model assumes that the adsorption of species in the environment lowers the inter-atomic bond strength and the stress required for cleavage fracture. The hydrogen embrittlement model suggests that cathodic hydrogen is absorbed by the material and induces sub-critical cracks in the plastic zone ahead of the crack tip.

Near-neutral pH SCC is usually assumed to be dominated by the process of hydrogen-facilitated local anodic dissolution. Both dissolution and hydrogen ingress into the steel are involved (*Parkins, 1994; Parkins and Blanchard et al., 1994; Gu et al., 1999; Parkins, Blanchard , and Delanty, 1994*). Pitting plays an important role in the initiation of transgranular cracks. Localized acidification facilitates both the dissolution of the steel and hydrogen discharge from the solution. Therefore, it enhances the chances of crack initiation and growth. As indicated by attack on the crack sides and by corrosion products in the enclave, dissolution is involved in the crack growth. But a simple dissolution model is not sufficient to account for the crack growth. Polarization curves show the highest anodic current densities are unlikely greater than 10^{-3} A/cm^2, which corresponds to a crack growth of about 4×10^{-9} mm/s and is much smaller than that (10^{-6} mm/s) determined in SSRT experiments.

The fracture surface invariably displays areas of quasi-cleavage, as is often associated with hydrogen-induced cracking. A further indication of the entry of hydrogen into the steel is the secondary cracks that are not connected to the outer surface of the specimen and are nucleated on bands of pearlitic material. In the absence of significant cathodic protection current reaching the pipe surface, the pipe surface will be at open circuit and the discharge of hydrogen will require a balancing anodic reaction, indicated by dissolution on the crack sides. In addition, Yu *et al. (1999)*. assumes that the mechanism of near-neutral pH SCC is dominated possibly by anodic dissolution near E_{corr}. At

cathodic potentials, cracking is controlled by hydrogen-induced cracking It may be optimal for maximizing the safety of a pipeline and minimizing possible adverse effects. This test would rupture significantly smaller flaws than those which would fail at operation pressures and thereby ensures their integrity. Although hydrostatic testing was effective in removing near-critical flaws from the line, it could not permanently arrest the growth of all stress corrosion beyond a given threshold (*Delanty and O'Beirne, 1992*). Cathodic protection should aim at lowering the potential below about -0.85 V to avoid pitting and /or SCC, but not below -1.1 V. Otherwise, hydrogen will be produced to create a high pH environment that leads to formation of carbonate-bicarbonate (*Parkins, 1994*).

It was reported that grit blasting and shot peening could avoid or delay SCC in a variety of systems. When grit blasting was conducted for 10 seconds or longer, the threshold stress increased from 60 % SMYS, the specified minimum yield strengths, to 80% SMYS without grit blasting. However, the distorted surface layer may not extend far into the steel.

The incorporation of leachable inhibitors into primers may delay the incidence of cracking. Chromate-containing primers can inhibit intergranular SCC of pipeline steel. Minimizing pressure fluctuations and reducing the maximum pressures may be beneficial, too. It is hoped to control steel-making, rolling or fabrication procedures to achieve greater resistance to cracking through better understanding of why the existing pipeline steels differ in cracking susceptibilities. Other protection technologies used for high-pH SCC are also applicable for the near neutral pH SCC.

3 Materials and experimental details

3.1 MATERIALS

The material used in this study was X-65 line pipe steel, supplied by TransCanada PipeLine Limited and whose chemical compositions (wt%) are listed in Table 3-1. The steel consisted of mostly ferritic grains with some banded pearlite structures (Fig.3-1). This X-65 line pipe had been in service for about 20 years, and had experienced a rupture in February 1999 due to near-neutral pH stress corrosion cracking. The X-65 pipe section used in the present study was taken from near the rupture site but had not been mechanically damaged by the rupture. Coupons of the steel used for the hydrogen permeation testing were fully annealed after machining to reduce the residual stress arising from machining.

Table 3-1 Chemical composition of X-65 steel used in this study (wt%)

Element	X-65
Aluminum	0.010
Boron	<0.002
Calcium	<0.002
Carbon	0.13
Chromium	0.08
Cobalt	<0.002
Copper	<0.05
Manganese	1.55
Molybdenum	<0.01
Nickel	<0.05
Niobium	0.049
Nitrogen	0.010
Phosphorus	0.014
Silicon	0.30
Sulfur	<0.005
Tin	-0.010
Titanium	<0.002
Vanadium	<0.002
Iron	Balance

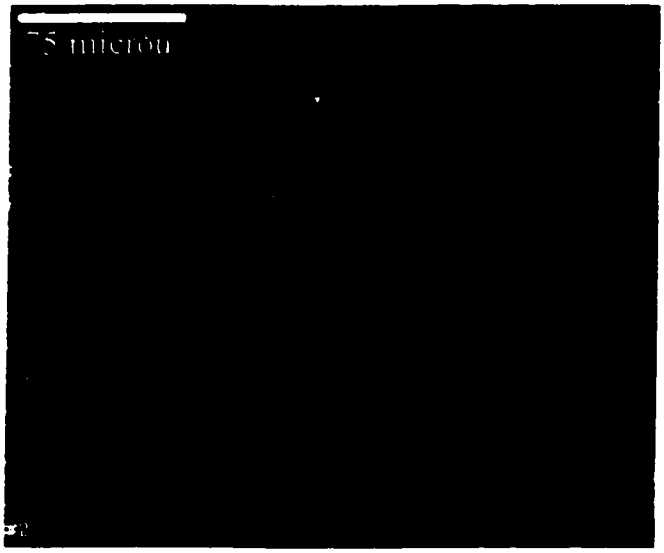

Fig.3-1 Microstructure of X-65 steel

3.2 SOIL ELECTROLYTES

The electrolytes used in corrosion tests included the NS4 synthetic soil solution, the treated NS4 solution as explained in the next paragraph, and an actual soil solution extracted from the soil (which is defined in the text following the next paragraph) saturated with distilled water. Their ionic concentrations, determined by Norwest Lab, Edmonton, are listed in Table 3-2.

The NS4 solution was a synthetic solution suggested by Parkins in the 1980s for the study of near neutral pH stress corrosion cracking (SCC) of pipeline steels (R. N. Parkins, 1988.). The treated NS4 solution was obtained by cathodically polarizing a steel specimen in NS4 solution at −1200 mV (saturated calomel electrode (SCE)) for 15 hours. This allowed a deposition of calcium carbonate on the surface of the steel sample. This treatment was designed to simulate the chemical redistribution process within a holiday on the line pipe steel in the field, as schematically illustrated in Fig.3-2. It is accepted that stress corrosion cracking in pipeline steels occurs near the bottom of the holiday where cathodic current is diminished due to the high resistivity of ground water. At the opening of the holiday, however, the cathodic current may alter the chemical composition of the soil solution due to the formation of corrosion deposition. It is believed that the

remaining electrolyte after the treatment might better represent the soil electrolyte responsible for near-neutral pH SCC in the pipeline steels.

Table 3-2 Ionic concentrations of electrolytes used in corrosion tests (mg/L)

Ions		Standard NS4[1]	NS4[2]	Treated NS4[2]	Soil solution[2]
Ca^{2+}		49.2	9.2	6.0	3.15
Mg^{2+}		12.8	11.7	9.11	1.06
Na^{+}		143	143	143	0.82
K^{+}		63.99	79.9	124	0.14
SO_4^{2-}		47.9	47.9	48.7	1.23
NO_3^{-}		-	0.109	0.138	0.02
Cl^{-}		148.8	174	223	0.16
NO_2^{-}		-	<0.002	<0.002	0.02
CO_3^{2-}		-	<6	<6	-
HCO_3^{-}		-	205	156	-
pH value	A[3]	-	7.4	-	7.4
	B[4]	-	7.0	6.8	6.8

Note: 1, Nominal composition of NS4 solution;

2, Analyzed by the Norwest Lab;

3, As-prepared solution;

4, after purging with 5%CO_2+N_2 mixture gas for 24 hours.

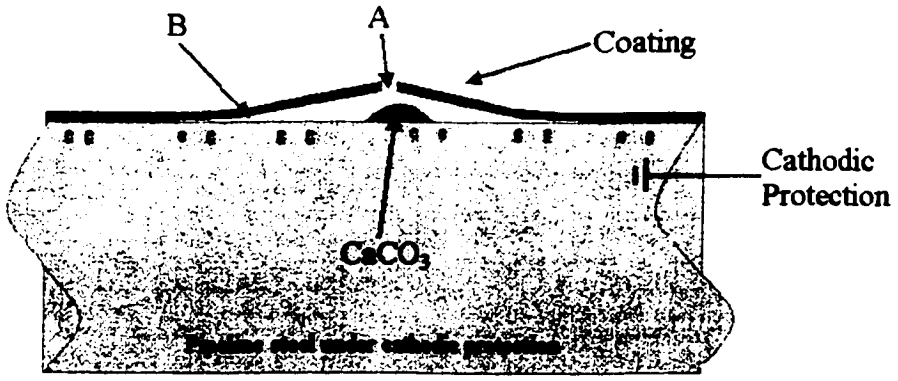

Fig. 3-2 Coating holidays on the cathodically protected pipeline steel

The soil solution was obtained by extracting water-saturated soil primarily composed of silt and clay, which was collected from a Marten Hill of Canada where near-neutral pH SCC was found. Minerals in this soil were quartz (90%), plagioclase (4%) and potassium feldspar (6%) by XRD. The soil extracts were prepared by mixing the soil with distilled water in a weight ratio of 20:5 until an equilibrium state between soil and water was achieved. The soil electrolyte was separated from the soil through centrifugal spinning at high speed.

In order to achieve a near-neutral pH condition, all the soil electrolytes were purged with 5% CO_2 + N_2 gas mixture for at least 24 hours before being introduced to the test cell. A supply of 5% CO_2 + N_2 gas mixture was also maintained during each of the tests in order to prevent an increase in the pH value, particularly due to the generation of excess OH^- when a cathodic potential is applied. The pH values of all the solutions used in the study are also listed in Table 3-2.

3.3 DETERMINATION OF HYDROGEN CONTENT

Steel coupons measuring 15 × 8 × 1.5 mm were used for the measurement of hydrogen content in the steel exposed to near-neutral pH soil environments. The coupons were also ground/polished to various roughnesses ranging from 240-, 400-, 600-grit, up to mirror finish (polished using 0.05μm Al_2O_3 paste) to study the effect of surface roughness on hydrogen generation.

The experimental set-up for hydrogen charging is shown in Fig.3-3. A platinum wire was used as the counter electrode. Hydrogen charging was done at various cathodic potentials ranging from open circuit potential (OCP) to −1500 mV (SCE).

The coupon after hydrogen charging was dried with compressed air in the lab and placed in the LECO RH-402 Hydrogen Analyzer (Fig.3-4) within 60 seconds for hydrogen determination. The flow chart of LECO RH-402 Hydrogen Analyzer is shown in Fig.3-5. The coupon was sealed in an induction heating furnace in the hydrogen analyzer, where the steel was heated up for hydrogen effusion. The hydrogen in the furnace was then

carried to the analyzing chamber by pure nitrogen gas. The hydrogen content was determined based on the change in the thermal conductivity of the flowing gas due to the presence of hydrogen. Impurities such as water vapor, oxygen, CO and CO_2 present in nitrogen were pre-eliminated to minimize their contribution to thermal conductivity. The oxygen was removed by flowing the gas through a heater filled with copper shavings heated to 650°C to form copper oxide, while water and CO_2 were absorbed by Anhydrone and Ascarite reagent, respectively.

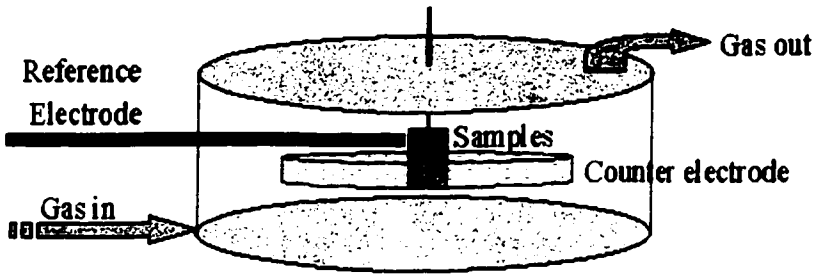

Fig.3-3 Experimental set-up used for the hydrogen charging in near-neutral pH soil electrolytes

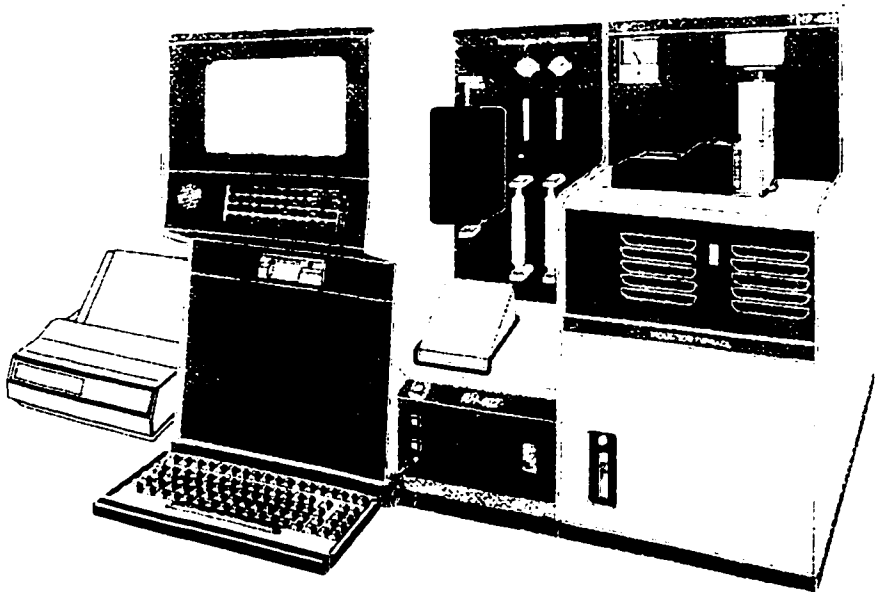

Fig.3-4 LECO RH-402 Hydrogen analyzer

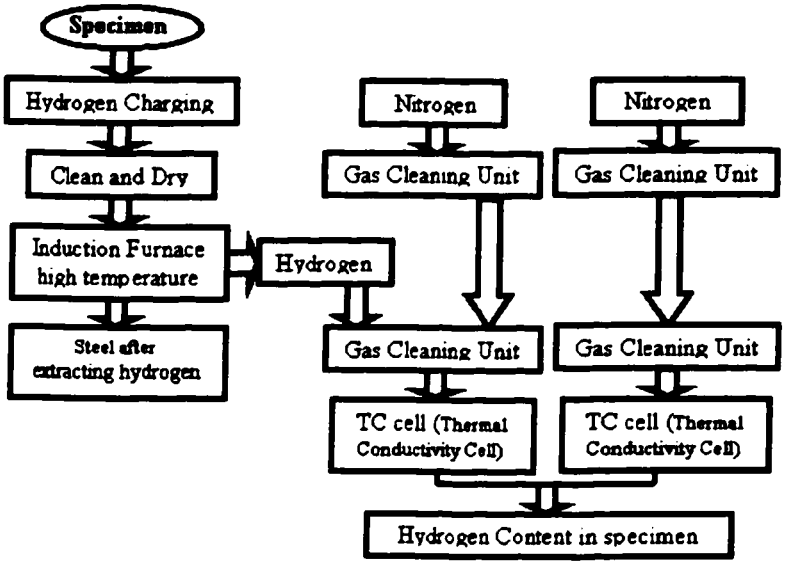

Fig 3-5 Flow chart of the process to determine hydrogen content in steels

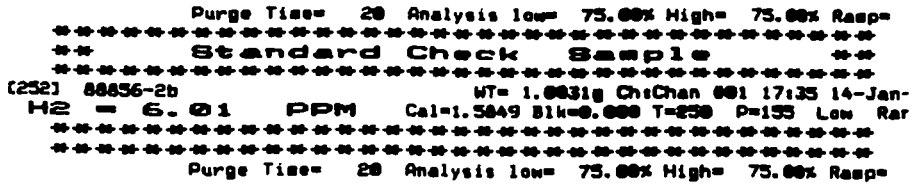

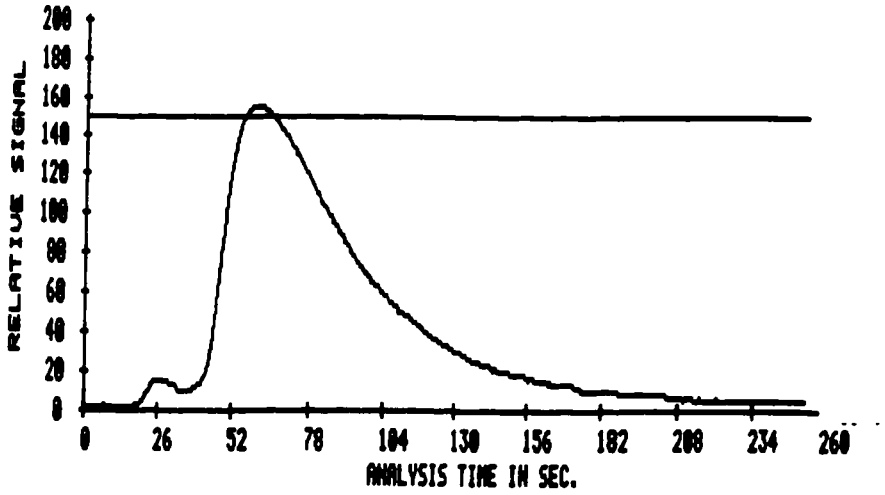

Fig.3-6 Hydrogen-time curve of a standard specimen

The system was usually calibrated using standard samples with known hydrogen content several (3-5) times before actual testing. Fig.3-6 is a typical hydrogen curve of a standard specimen in which the area under the curve represents the hydrogen concentration, and the two peaks in the figure were likely from the effused hydrogen with different trapping well depth in the standard material. Fig.3-7 is a typical curve of the steel coupon used in this study. There was only one peak observed on this curve, which may be due to the fact that hydrogen in the fully annealed steel is mostly diffusible.

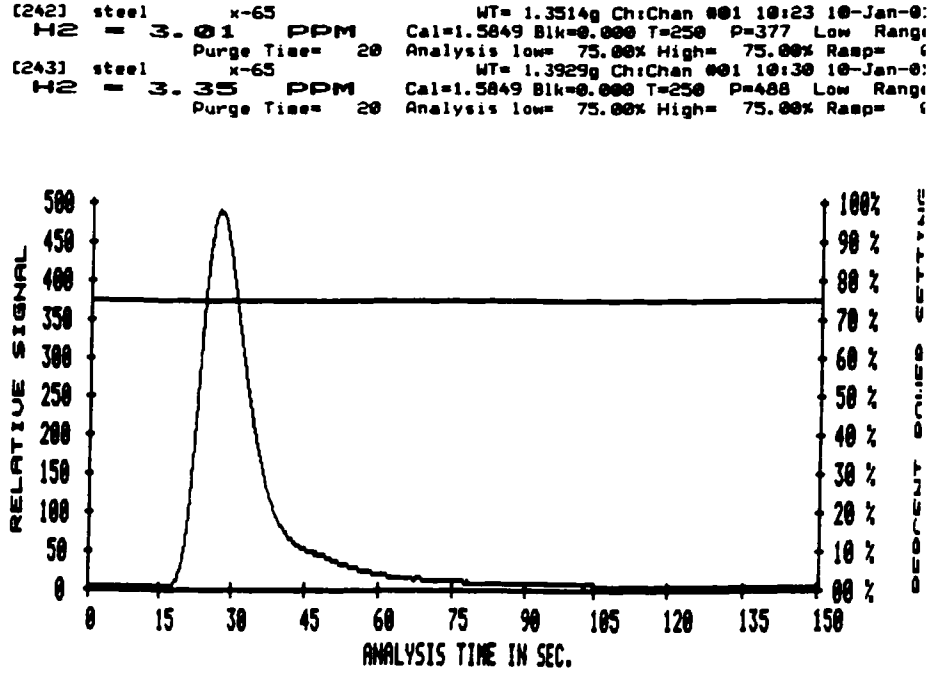

Fig.3-7 Hydrogen-time curve for the steel used in this study

3.4 HYDROGEN PERMEATION TESTING

Hydrogen permeation testing was carried out using a Devanathan-type of cell (*Devanathan and Stachurski, 1962; 1964*), which consists of a double-cell with the test coupon installed in between (see Fig.3-8). The charging cell was filled with synthetic ground water, while the "detection cell" contained 0.1M sodium hydroxide. In order to achieve a near neutral pH condition, the soil solution, prior to adding to the test cell, was

purged by bubbling a 5% CO_2 + N_2 mixture for at least 24 hours. The purging gas was also maintained throughout the entire test period. Various charging current densities and cathodic potentials were applied to the charging side of the coupon, as a way of producing varying amounts of hydrogen at the charging side. The detection side of the coupon was maintained at a constant potential of about +100 mV (SCE) for the purpose of hydrogen detection. This potential was applied well before the charging solution was added to the test cell so that the passivating current in the detection cell became very low (<0.1 $\mu A/cm^2$) and constant prior to the test. A carbon rod was used in both cells as the counter electrodes. The area of the steel coupon exposed to the test environment was about 707 mm^2 (30 mm in diameter). The current generated on the detection side by the oxidation of the emerging hydrogen was recorded on a strip chart recorder. The exit side/detection side of the specimen surface was coated with palladium (~1μm in thickness) to increase the efficiency of hydrogen effusion and the plating process will be described in Section 3.6.

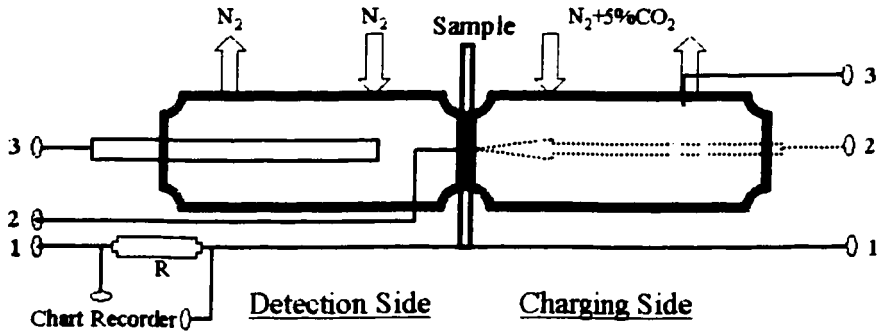

1-working electrode, 2-reference electrode, 3-counter electrode, R-resistor

Fig.3-8 Schematic of the hydrogen permeation testing setup

3.5 SLOW STRAIN RATE TESTING

ASTM standard flat tensile specimens, measuring 4 × 6 × 32 mm in gauge section (Fig. 3-9), were machined from the steel pipe using electrical discharging machining (EDM).

The length direction of the tensile specimen was parallel to the transverse direction of the pipe.

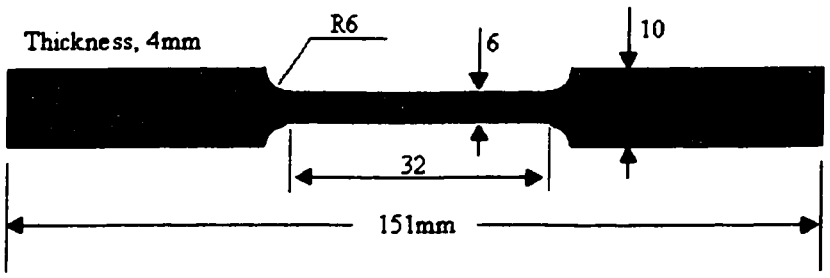

Fig.3-9 Draft of the standard ASTM flat specimen

In addition to the difference in roughness at the surface, the scratch orientation was also controlled to be either parallel, perpendicular, or about 45° inclined to the length direction of the tensile specimen. Each of the specimens was ultrasonically cleaned in acetone before testing.

The slow strain rate testing was conducted on an Instron hydraulic test frame (Model 8516) under a constant strain rate of 1×10^{-6} per second. The test specimen was sealed in a plastic container similar to that shown in Fig.3-3 for hydrogen charging. The test was conducted either at the open circuit potential (OCP) or at the applied cathodic potential ranging from -900 mV to -1500 mV (SCE).

3.6 OTHERS

Electroplating palladium on steel coupons

Before plating, the specimen was first polished to 0.05 μm Al_2O_3 finish and thoroughly degreased in acetone. This was followed by chemically activating in 10% hydrochloric acid and immediate rinsing with de-ionized water. The electroplating was conducted at lab temperature (22-25°C) and at 0.2-1.5 A/dm^2 in the solution bath containing $PdCl_2$ 10-

15g/L, $NH_3 \cdot H_2O$ (25%) 75-100ml/L, NH_4Cl 40-60g/L. The pH value of the electrolyte was conditioned to 7.5~9.0 by hydrochloride and ammonia hydroxide. The palladium film was controlled to a thickness of 0.5~1μm. This required a plating time of about 30-120 seconds, depending on the concentration of $PdCl_2$ (as $Pd(NH_3)_2Cl_2$ in solution state) in the solution. The concentration of palladium ions in the solution should be replenished after a few runs of plating.

Polarization curve

Polarization tests were conducted at a scan rate of 0.2 mV/second with EG&G Potentiostat / Gavanostat Model 273. Each test started 5 minutes after the specimen was immersed in the soil electrolyte. The corrosion rate in terms of thickness loss was determined from the polarization curve using the equation below:

$$V = K\frac{mi_{corr}}{n\rho} \quad \text{.....3-1}$$

where, V thickness loss, μm/year

m molar atomic weight of metals

i_{corr} corrosion current density (μA/cm^2), which was measured by extrapolation of the Tafel slopes

n 3, the number of electron lost in electrochemical reaction of materials

ρ Density of metals (g/cm^3)

K constant, which equals 3.27

The density of the X-65 steel used in the calculation is 7.9 g/cm^3, and the atomic weight is 57.3 g/mol.

Surface and microstructural characterization

The surface roughness was measured using the TENCOR Instrument at the MicroFab laboratory at the University of Alberta. The surface area increment due to the presence of scratches was calculated based on the surface roughness profiles and the density of scratches in an apparent area of 1000mm^2.

The microstructure of the steel and the surface morphology of the tested specimens were examined on a Hitachi S-2700 Scanning Electron Microscope Link EXL EDS System with light element detection capabilities in the Department of Chemical and Materials Engineering, University of Alberta.

4.1.2 Surface roughness profiles (Scanned images)

Typical profiles of various surface roughnesses (Ra), as determined by the surface morphology inspector (TENCOR Instruments), are shown in Fig.4-2. The calculated surface area increments based on the roughness profiles are compared in Fig.4-3 for samples with various surface roughnesses. The surface area increment refers to the difference of actual surface area (micro scale) and apparent surface area (macro scale).

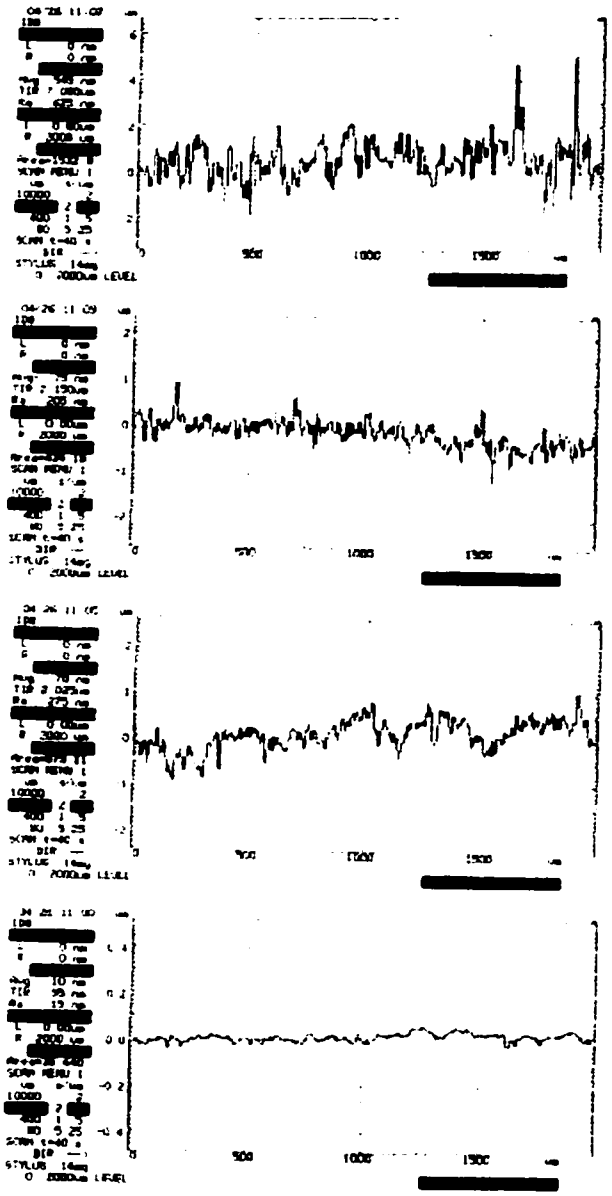

Fig.4-2 Surface roughness profiles of specimens

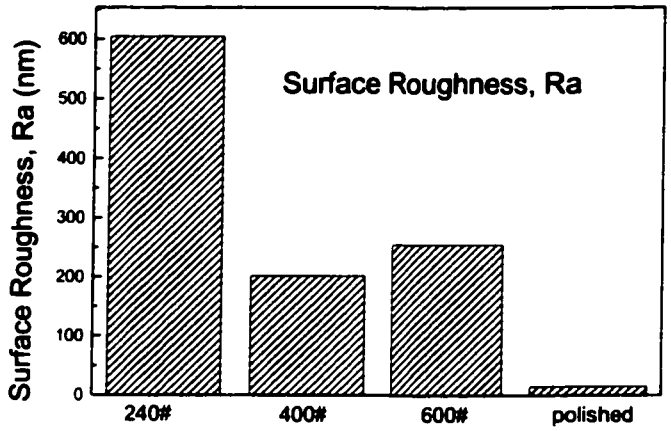

a. Surface roughness

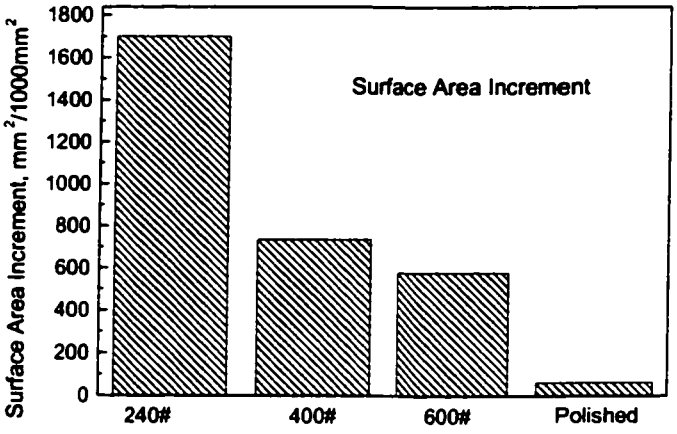

b. Surface areas increment

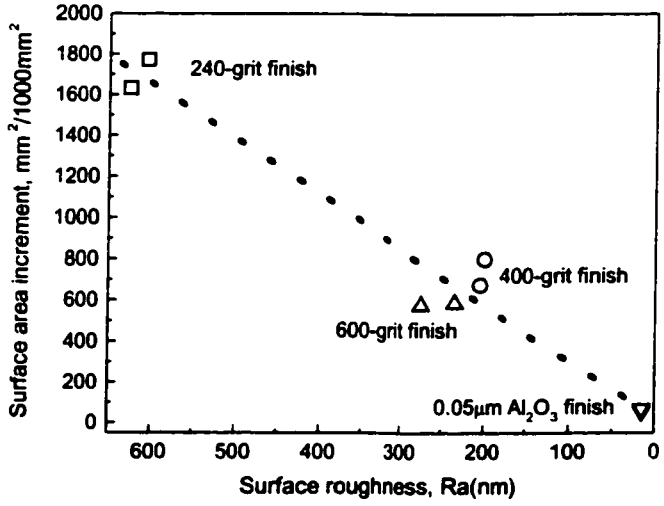

c. Surface roughness and surface area increment

Fig.4-3 Relationship between surface roughness and surface area increment

In general, the rougher surface has larger surface area increment, as shown in Fig.4-3. It appears that the difference in surface roughness/area increment between 400-grit and 600-grit finish is not significant. The surface with 600-grit finish is rougher but has less surface area increment than that with 400-grit finish. This is probably due to the fact that the surface roughness depends only on the average depth of the scratches while the surface area increment depends on both the depth of every single scratch and the density of scratches on the surface.

4.2 ELECTROCHEMICAL REACTION

4.2.1 Effect of surface roughness

Fig. 4-4 shows the polarization curves of the specimens with different surface roughnesses measured in NS4 solution. Consistent with what is reported in the literature, there was no passivation zone on the polarization curves for steels exposed to near-neutral pH soil solution.

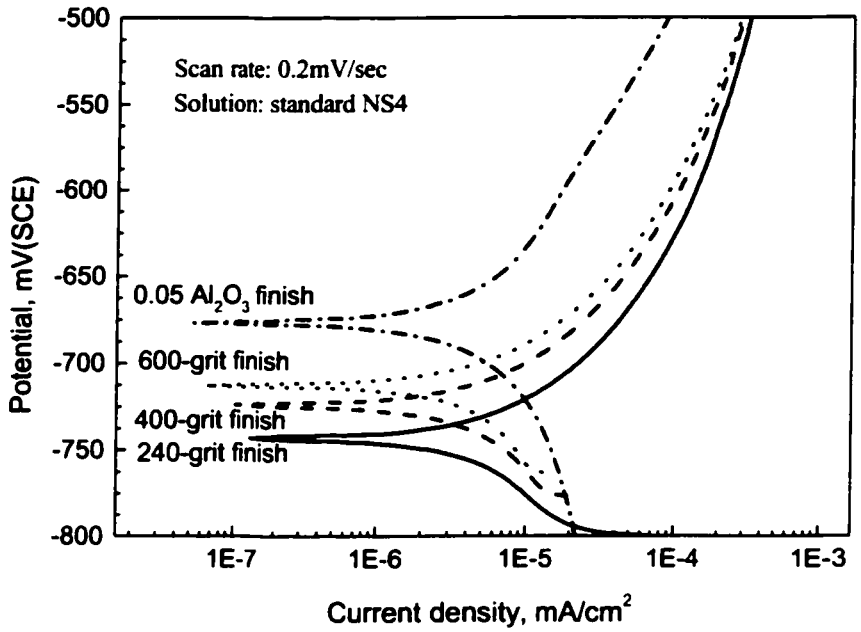

Fig.4-4 Polarization curves of specimens with various surface roughness in NS4 solution

The open circuit potential of the steel determined from the polarization curve is plotted against surface roughness and surface area increment, respectively, in Fig. 4-5 and Fig. 4-6. It is seen that the OCP appears quite sensitive to the surface roughness / surface area increment, and the specimen with the rougher surface or higher surface area increment has lower open circuit potential.

Similarly, the corrosion rates of specimens with various surface roughness, as determined using equation 3-1, were also plotted against surface roughness and surface area increment, respectively, in Figs. 4-5 and Fig. 4-6. The corrosion rate appears to increase with increasing surface roughness or surface area increment. This may be due to more electrochemically active areas present on the rougher surface for dissolution. Both the surface roughness and surface area increment are correlated well with the corrosion rate and the OCP. This is because of the linear relationship between the surface roughness and the surface area increment as shown in Fig. 4-3.

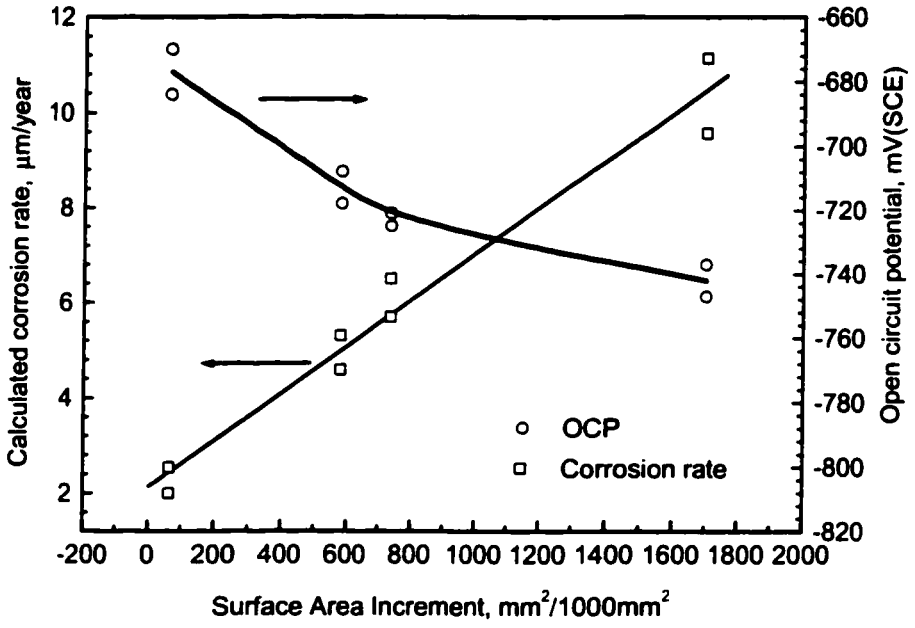

Fig.4-5 Relationship between corrosion rate, OCP and surface area increment of specimens in NS4 solution

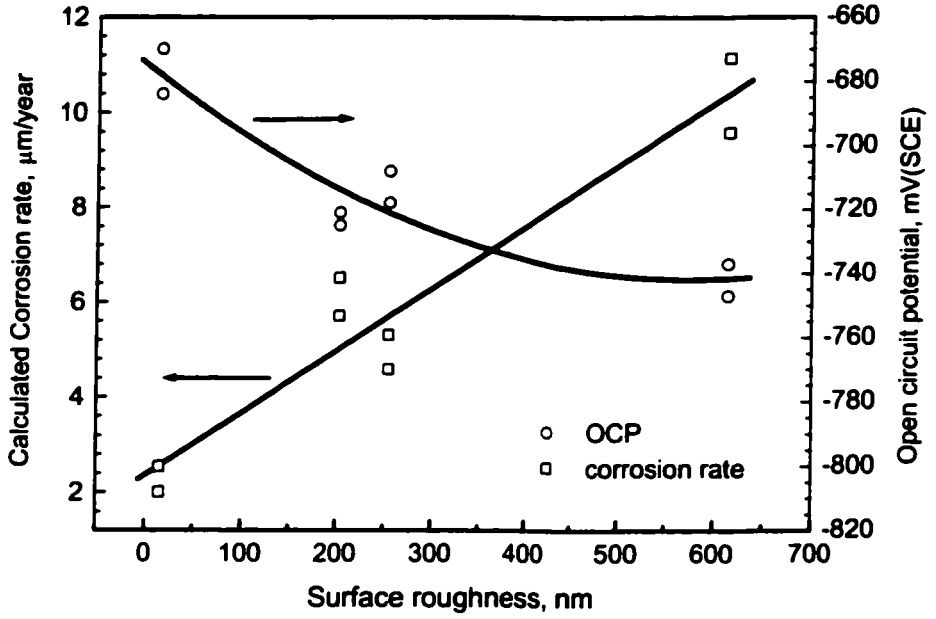

Fig.4-6 Relationship between corrosion rate, OCP and surface roughness of specimens in NS4 solution

4.2.2 Effect of solution chemistry

The polarization behaviour of the X-65 steel was also examined in the treated NS4 solution in which the concentration of Ca^{2+} ions was lower than that in the NS4 solution. These curves are summarized in Fig. 4-7 for the specimens with different surface roughness. A comparison of the polarization curve between the treated solution and the NS4 solution is shown in Fig.4-8 for the specimens with the same surface roughness. The polarization curves in both solutions were really identical except that the corrosion potentials were slightly higher in the treated solution than in the NS4 solution, as shown in Fig. 4-9a.

The dependence of corrosion potential and the corrosion rate on the surface area increment is also quite similar in both the solutions, that is, the rougher the surface, the higher the corrosion rate and the lower the open circuit potential. In particular, the difference in corrosion rate between the treated NS4 and NS4 solution increased with increasing roughness as shown in Fig.4-9b.

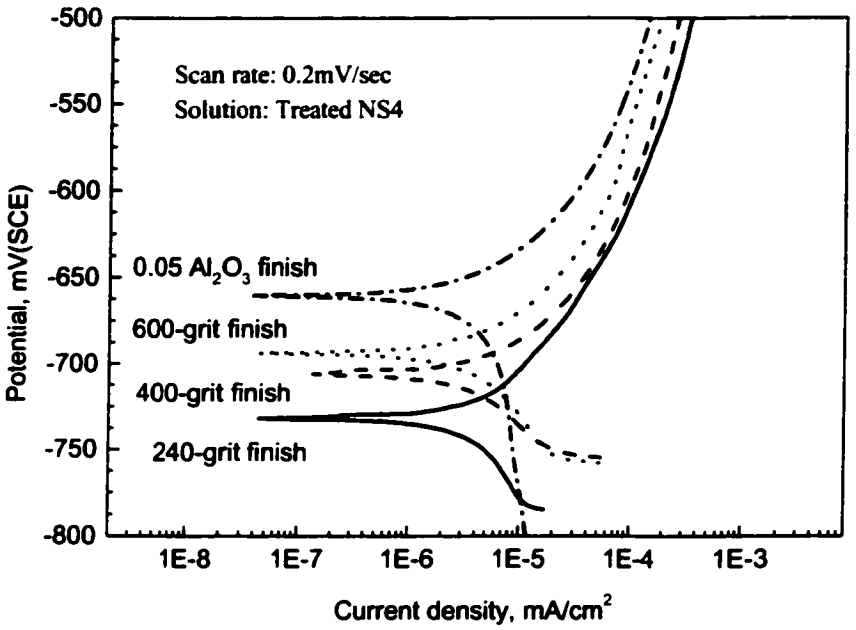

Fig.4-7 Polarization curves of the specimens with different surface roughness in the treated-NS4 solution

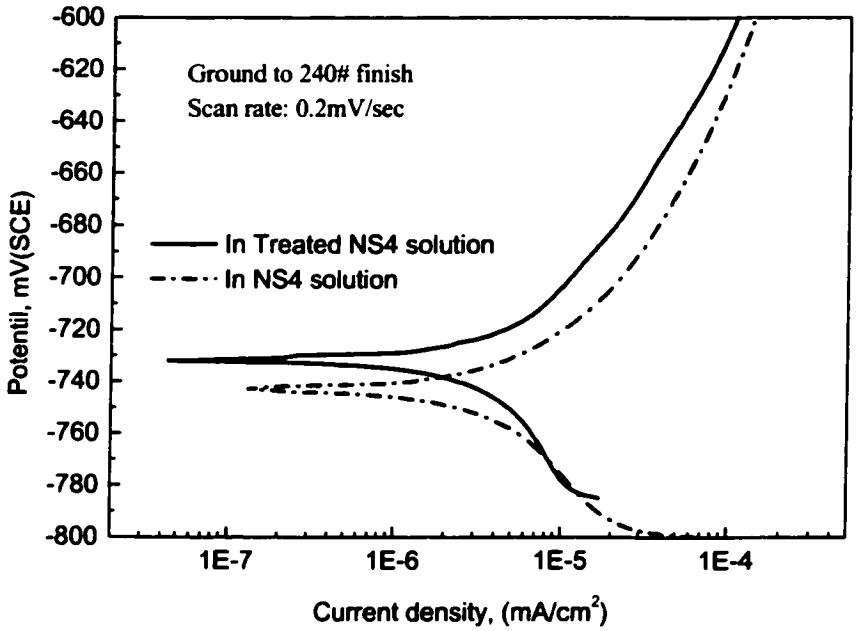

a. Specimen ground to 240# finish

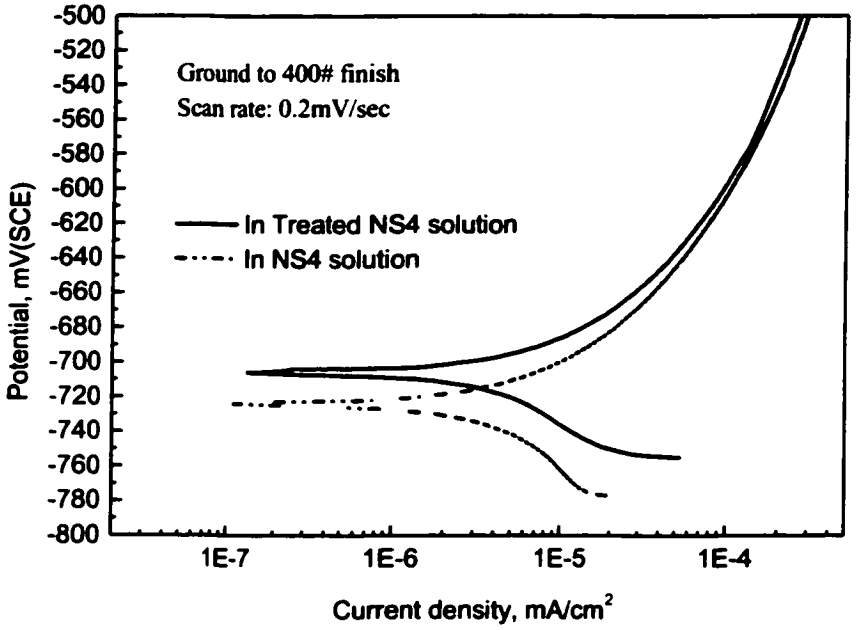

b. Specimen ground to 400# finish

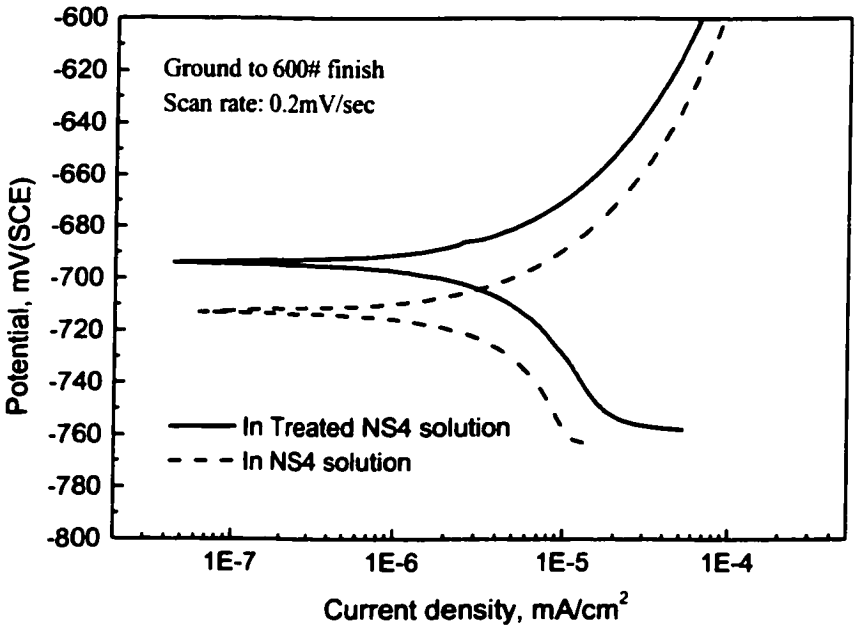

c. Specimen ground to 600# finish

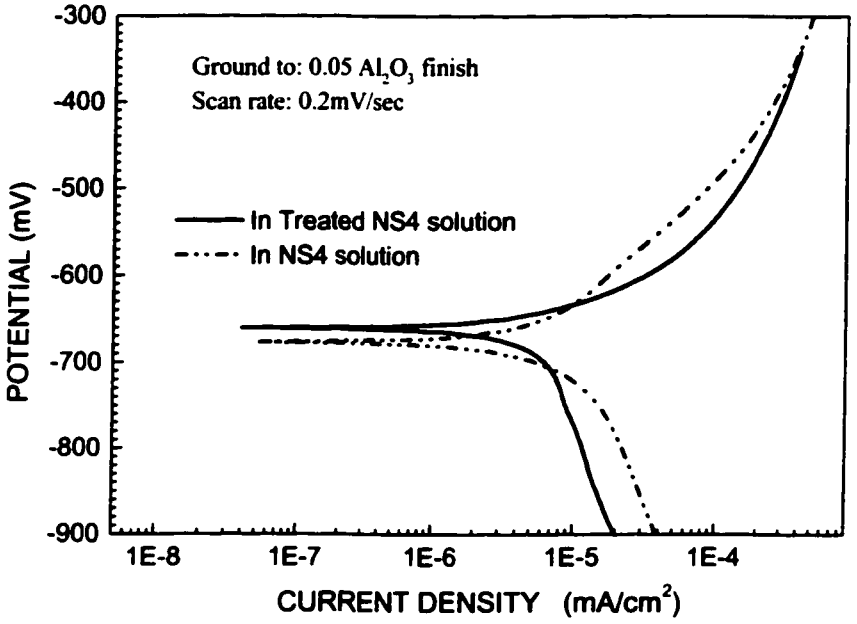

d. Specimen polished to 0.05μm Al_2O_3

Fig.4-8 Polarization curves in both NS4 and treated NS4 solutions

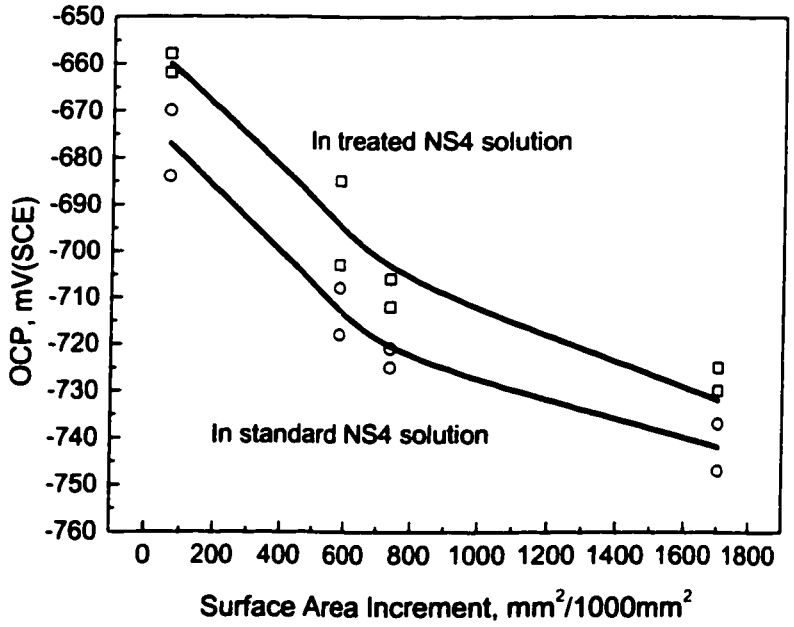

a. OCP, mV (SCE)

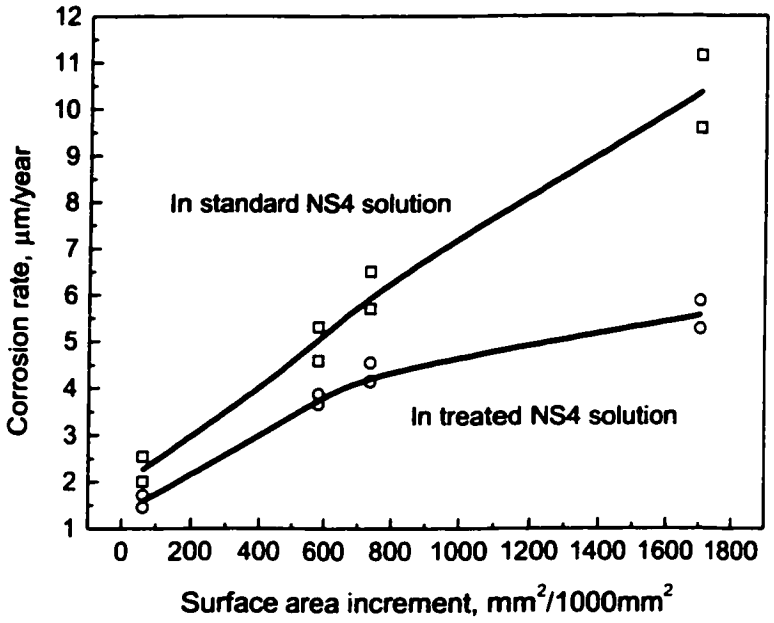

b. Corrosion rates

Fig.4-9 Corrosion rates and OCP of steels in both standard and treated NS4 solutions

4.3 HYDROGEN CHARGING PERFORMANCE

4.3.1 Time-dependent hydrogen charging and decaying behavior of steel

Fig.4-10 shows the hydrogen content in the steel as a function of charging time at -900mV in both NS4 and the treated NS4 solution. H content in both solutions was observed to increase almost linearly with charging time up to about 800 minutes and to reach a plateau at about 50 hours. The hydrogen content in the treated solution was lower than that in NS4. This difference, however, becomes less profound at an elongated charging time.

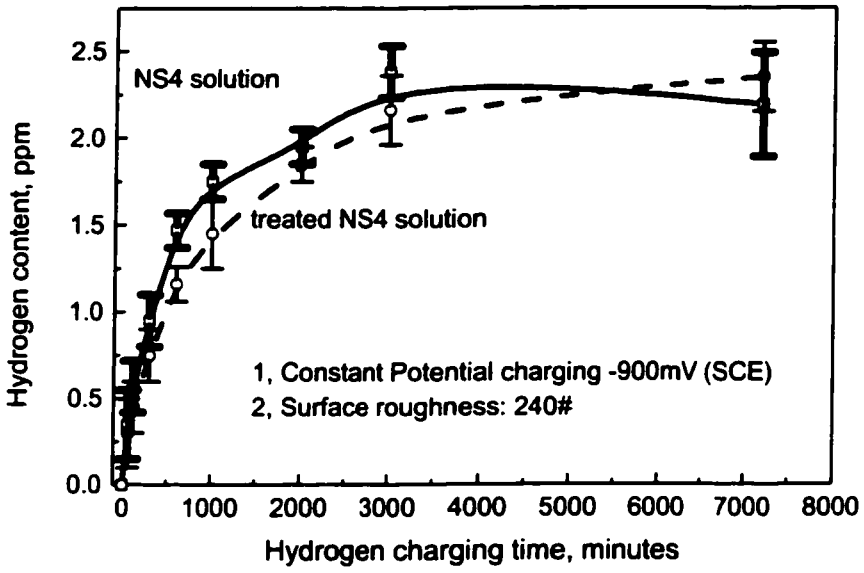

Fig.4-10 Variation of hydrogen content as a function of charging time in both NS4 and the treated NS4 solution

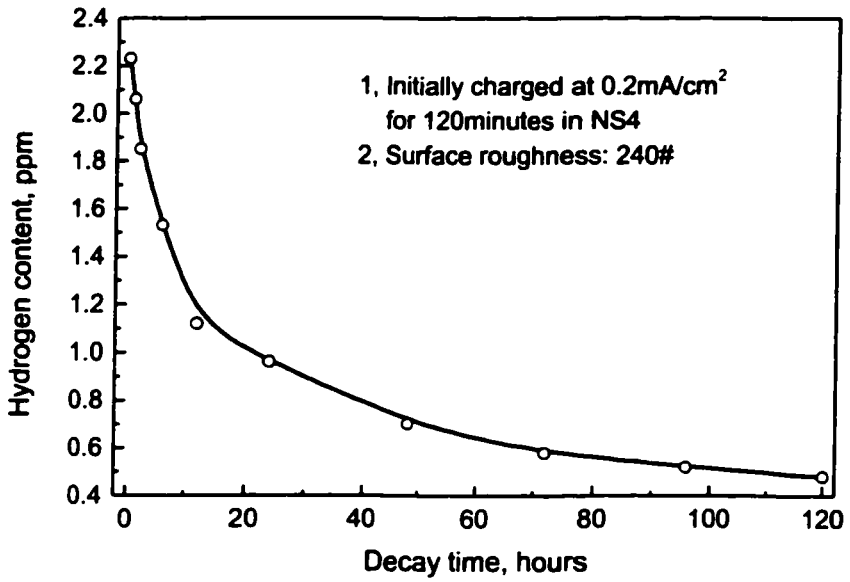

Fig.4-11 Decay curves for hydrogen in pipeline steels

To determine the influence of decay time on the hydrogen content in steels, the specimen after charging was kept at room temperature for various lengths of time before being tested in the Hydrogen Determinator. As is shown in Fig.4-11, hydrogen content decreased quickly in the first 24 hours; but became stabilized after 72 hours. The trapped hydrogen appeared quite low for the X-65 steel used, which composed about 20 % of total hydrogen in the steel.

4.3.2 Influence of potentials on hydrogen content

Fig.4-12 shows the hydrogen content of the X-65 steel coupons of different surface roughness charged at various cathodic potentials in the NS4 solution. It appears that hydrogen content is not very sensitive to cathodic potential at short charging times (60 minutes). For a longer charging time (15 hours), however, a strong dependence of hydrogen content in steel on charging potentials is observed. Regardless of surface roughness, the hydrogen content in the steel increases almost linearly with the potential from OCP up to −900 mV. At potential lower than -900mV, the hydrogen content

decreases at first with decreasing potential, and then increases again with a minimum hydrogen content at around −1200 mV. Besides the potential effect, the hydrogen content is also influenced by surface roughness but to a lesser extent. Rougher surfaces are typically higher in hydrogen contents.

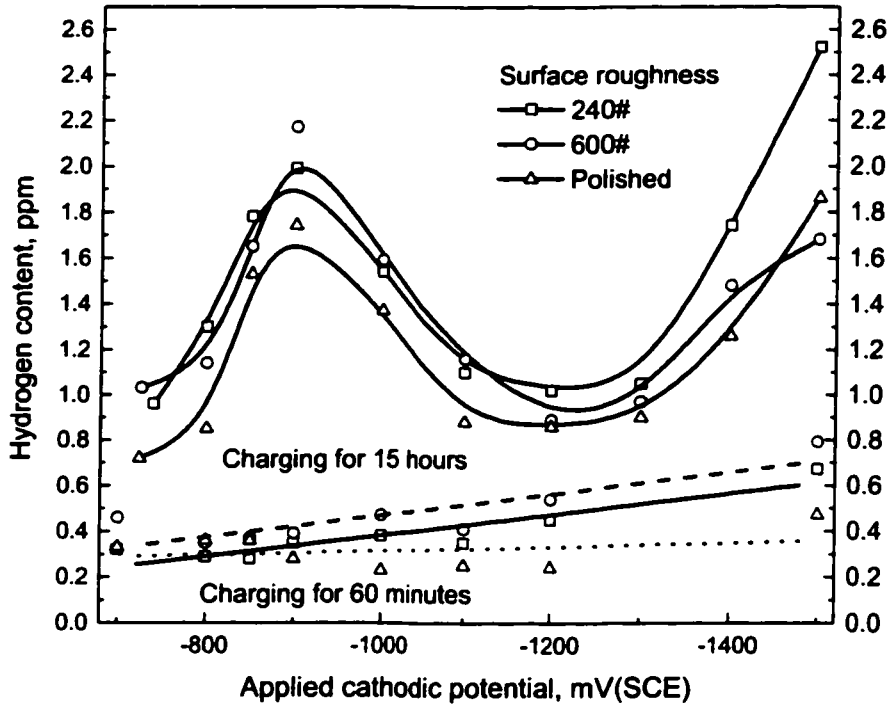

Fig.4-12 Hydrogen content as a function of applied cathodic potentials in NS4 solution

In order to understand the varied dependence of hydrogen content on cathodic potential, the sample surface was examined in the SEM after hydrogen charging at various potentials. As is shown in Fig. 4-13, grain boundaries were clearly observed on the surface charged at OCP because of uniform corrosion. At −900 mV, the original scratched surface was observed because of ample cathodic protection. Below −900 mV, white particles were seen on the specimen surface, which increased in population and size at decreased cathodic potentials. The surface area covered with the particles was maximized at −1200 mV. Below −1200 mV, the particles were so large that the film of particles became quite porous, while above −1200 mV, the surface showed reduced coverage. In addition, the film of particles was quite fragile at low cathodic potential, and

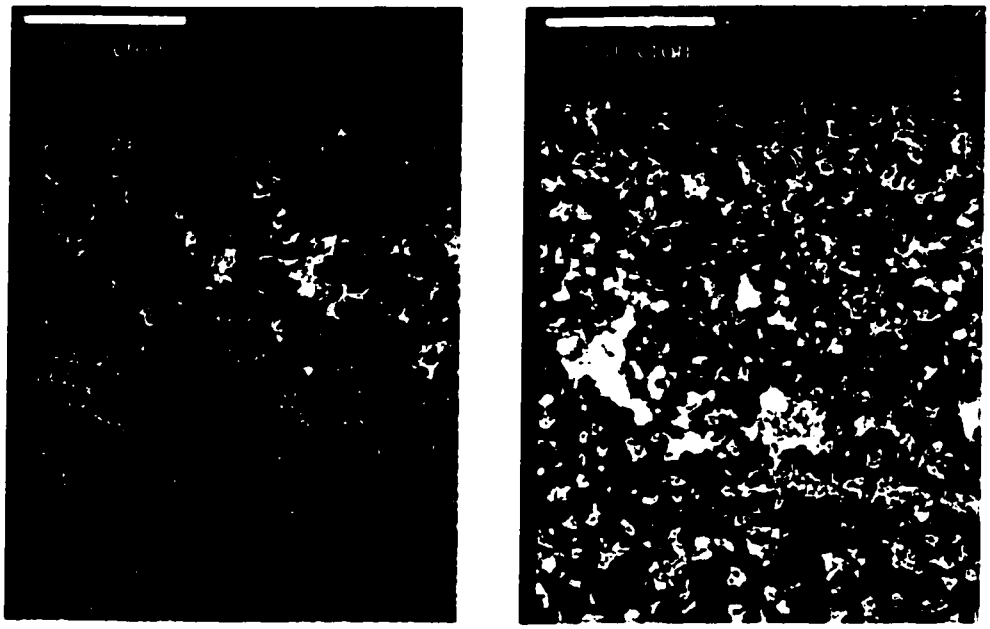

e. -1200mV f. -1500mV

Fig.4-13 Surface morphologies after hydrogen charging at various potentials in NS4 (Specimen surface: 240-grit finish)

The particles on the surface were analyzed by EDX (Fig.4-14) and it was shown that all the deposits at different potentials had similar compositions and were likely to be calcium carbonate as they were composed of Ca, C and O. In addition, minor Mg was also detected in the particles. This analysis is consistent with ionic compositions of the treated NS4 solution (Table 3-2). In this table, the concentration of Ca^{2+}, Mg^{2+} and HCO_3^- were reduced due to the deposition of $Ca(HCO_3)_2/CaCO_3$ in comparison with the NS4 solution.

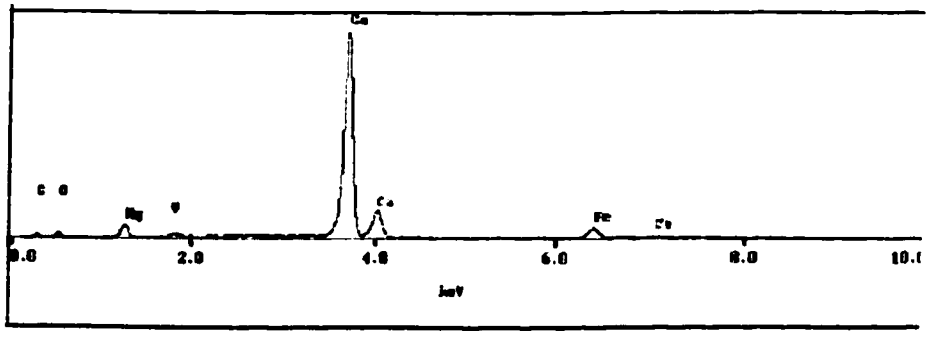

a. Deposits after charging at -1000mV (SCE)

Fig.4-15 Calcium carbonate deposits after charging at −1200mV(SCE) in NS4 solution for various length of time

a. 5 hours | b. 15 hours
c. 67 hours

As a summary, the observation above simply indicates that the influence of cathodic potential on hydrogen contents in the steel charged in NS4 solution coincides with its influence on the formation of calcium carbonate film on the surface.

4.3.3 Influence of surface roughness

The effect of surface roughness on hydrogen content in the steel was investigated at constant potential condition. In general, the mirror-polished specimen had the lowest hydrogen content detected. The difference in hydrogen content between the specimen with 600-grit and 240-grit finish is not quite significant and does not appear consistent at different charging potentials and time.

The surface morphologies of specimens with different surface roughness after hydrogen charging were also examined. As shown in Fig.4-16, the less rough surface was covered with finer and denser particles. This may be responsible for the low hydrogen content detected in the coupon with a mirror finish surface.

to the effect of surface roughness on OCP. Further discussion on these factors is provided in the Discussion.

To further define the effect of surface roughness on hydrogen generation, the specimens were charged under constant current density rather than constant potential. The former is expected to produce the same rate of hydrogen reduction at the charging surface. Fig.4-17 shows the hydrogen content as a function of hydrogen-charging time under constant charging current density. It is seen that the hydrogen content in the steel increases with increasing roughness on the surface. The difference also appears larger at longer charging time. This suggests that the increased hydrogen content in the specimen with rougher surface may be due to the enhanced efficiency of atomic hydrogen absorption to the surface.

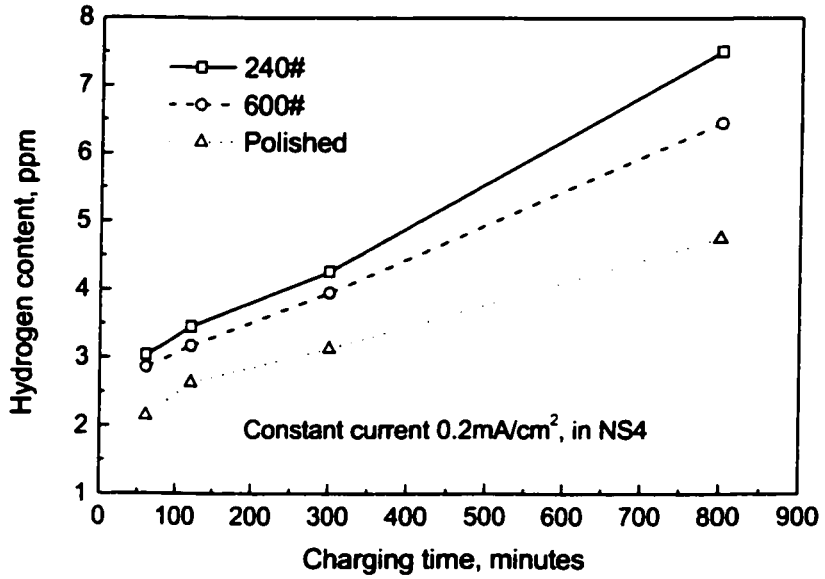

Fig.4-17 The influence of charging time on hydrogen content in steels under constant current density charging in NS4 solution

4.3.4 Effect of surface deposits on hydrogen charging

To confirm the effect of calcium carbonate film on hydrogen charging, some comparative hydrogen charging experiments were conducted in the treated NS4 solution where

calcium content was reduced. Fig.4-18 shows the hydrogen content in steels as a function of potentials in both the standard and the treated NS4 solution. Hydrogen content charged in the treated NS4 solution is less sensitive to the change in cathodic potential up to –900mV, beyond which hydrogen content in the steel increases with decreasing cathodic potential.

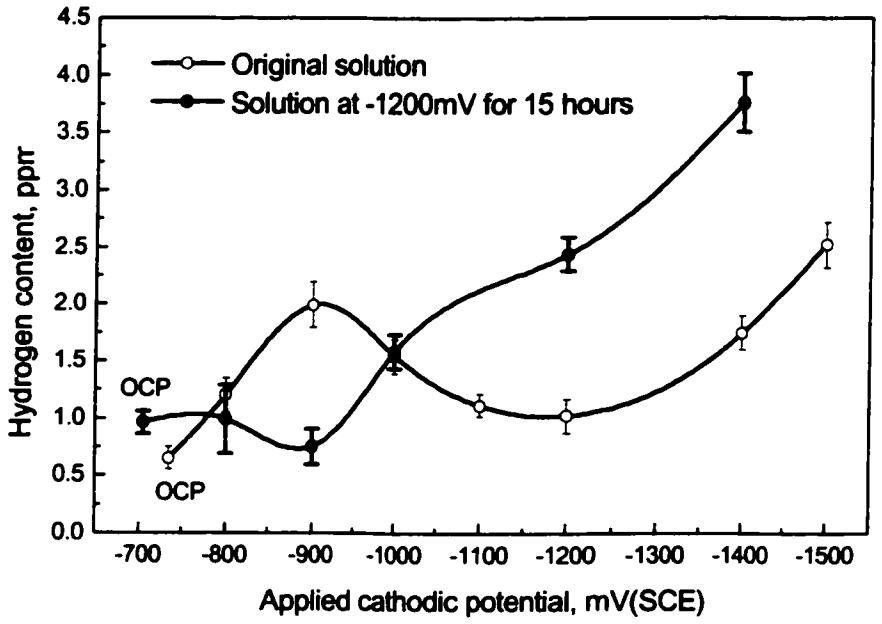

Fig.4-18 Hydrogen generation capability of original and treated NS4 solution

4.4 HYDROGEN PERMEATION BEHAVIOR

The results presented in section 4.3 indicate that the hydrogen content in steel after charging in NS4 under cathodic potentials is probably influenced by the presence of calcium carbonate deposits on the surface of test coupons. This section describes hydrogen permeation behavior of the steel in an attempt to further understand how surface conditions influence the hydrogen ingress to the steel in near-neutral pH environments.

4.4.1 Influence of surface deposits

As described in section 4.3, coupons with calcium carbonate film were prepared by cathodically polarizing the surface of the steel in an NS4 solution at −1200 mV (SCE) for 15 hours. This, as shown in Fig.4-15, produced a dense cover of calcium carbonate film on the surface of the steel coupons. Coupons with the calcium carbonate film were re-used for permeation testing to study how the calcium carbonate film influences the hydrogen permeation of the steel in soil solution. For comparison purposes, hydrogen permeation was also done on coupons on which the calcium carbonate film was stripped off completely after deposition. These two types of coupons were kept in the lab environment for 24 hours before being re-used for hydrogen permeation testing.

Fig.4-19a to 4-19c shows the hydrogen permeation curves of the coupons tested at open circuit potential, -900 mV and −1200 mV, respectively. At all the test conditions, the coupons with calcium carbonate film demonstrated lower hydrogen flux than those free of calcium carbonate film. This difference appears less at OCP, but quite significant at cathodically charged conditions. In addition, the build-up rate of hydrogen flux at the beginning of permeation is substantially lower for the coupons with calcium carbonate films.

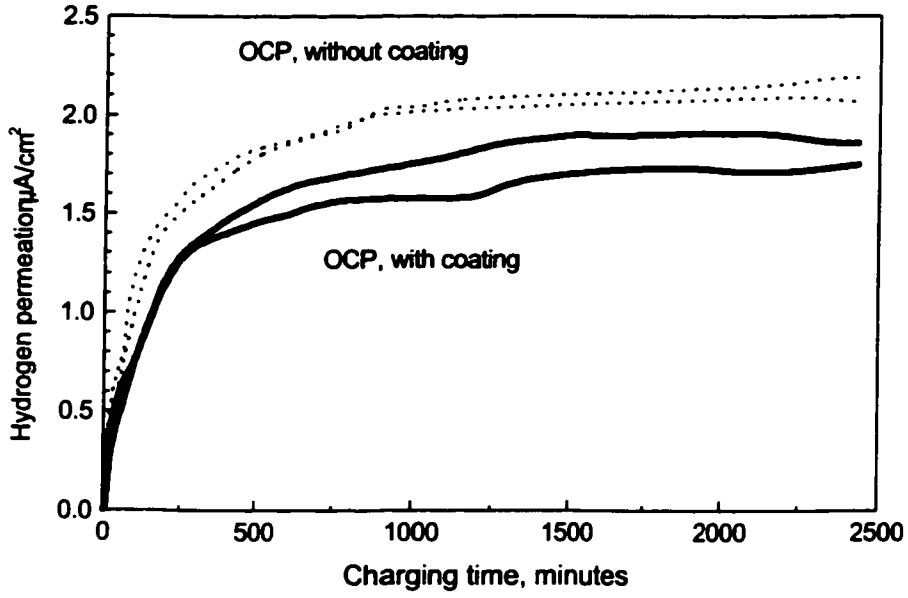

a. OCP

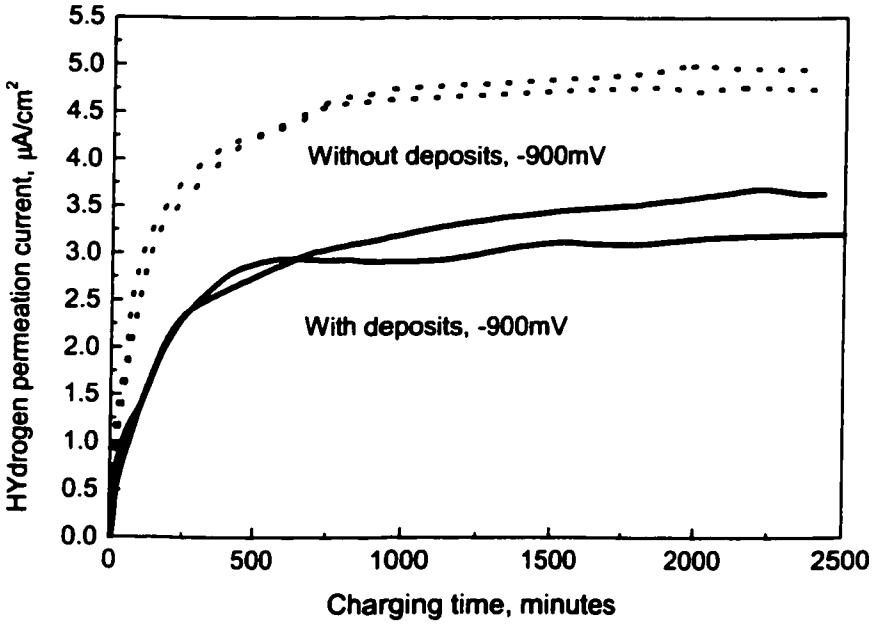

b. –900mV (SCE)

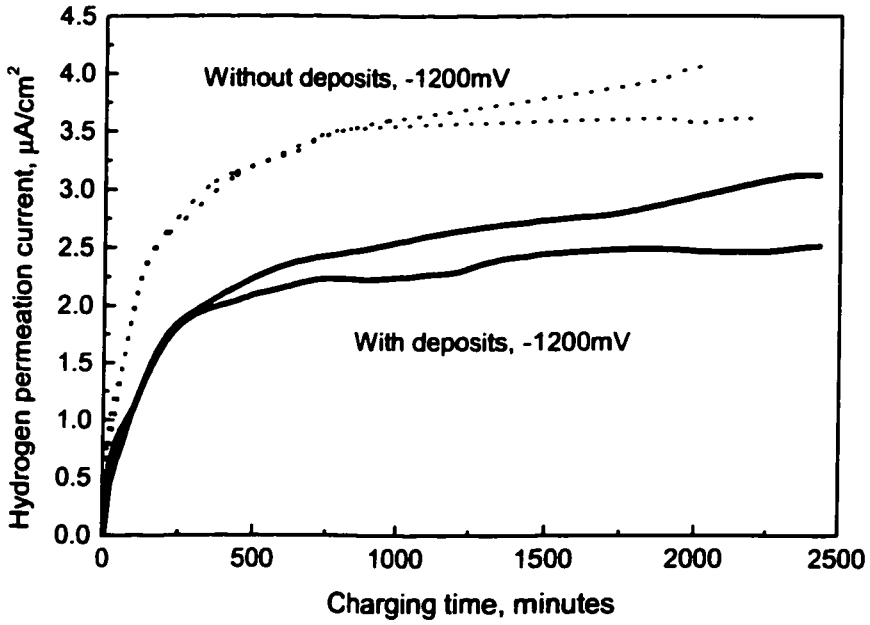

c. −1200mV (SCE)

Fig.4-19 Hydrogen permeation curves of specimens with and without calcium carbonate coatings at OCP, -900mV and −1200mV (SCE), 600-grit finish

The influence of the applied cathodic potentials on the hydrogen flux of the specimens with and without calcium carbonate film is summarized in Fig.4-20. The dependence of hydrogen flux on cathodic potential is significantly stronger for the coupons without calcium carbonate films than for those with deposits. In addition, hydrogen flux is lower at −1200 mV than at −900 mV for both the coupons with and without calcium carbonate film. For the coupons without calcium carbonate film, this should be due to the formation of calcium carbonate film as described in the previous section. For the specimen with calcium carbonate film prior to the permeation test in NS4, it may be attributed to the increased coverage of calcium carbonate on the surface.

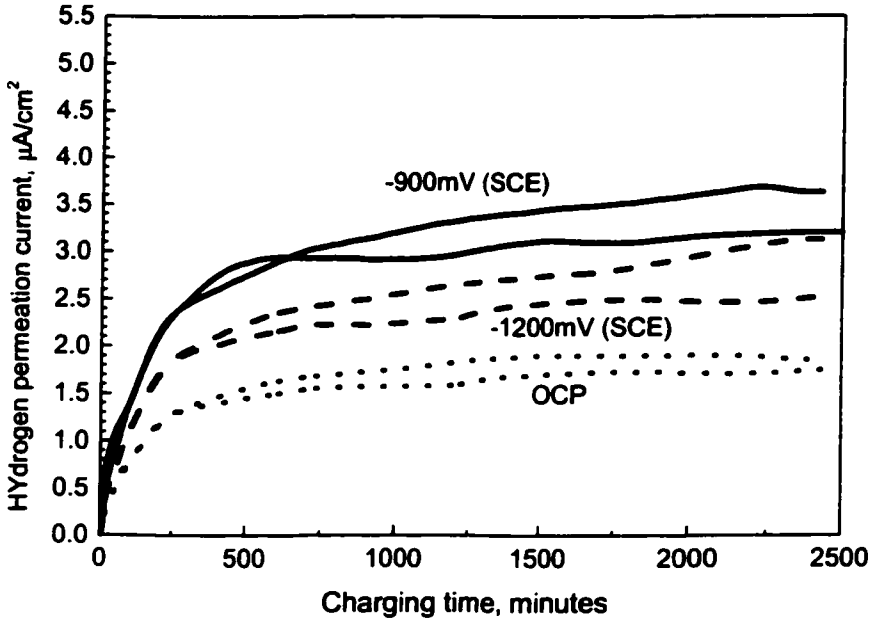

a. Coupons with calcium carbonate film

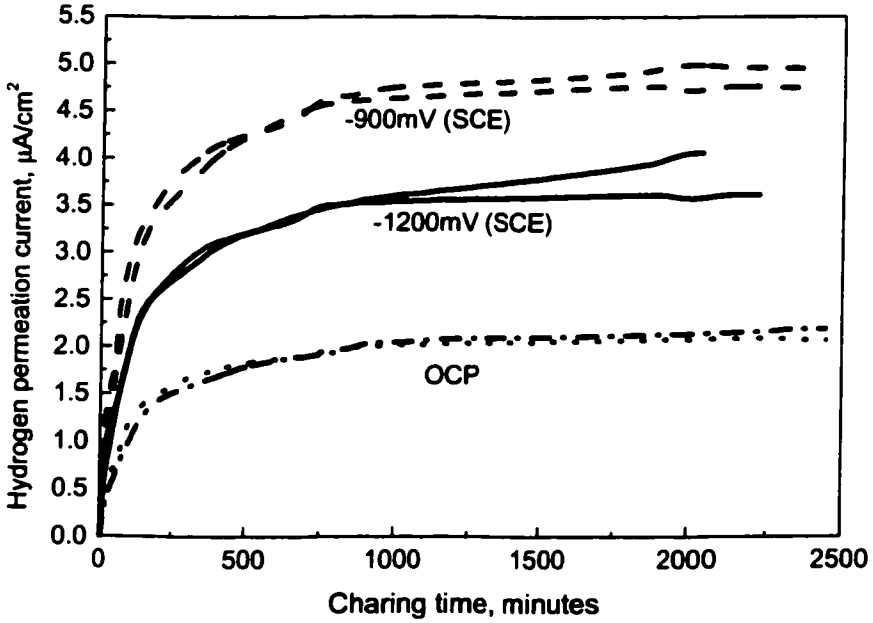

b. Coupons without calcium carbonate film

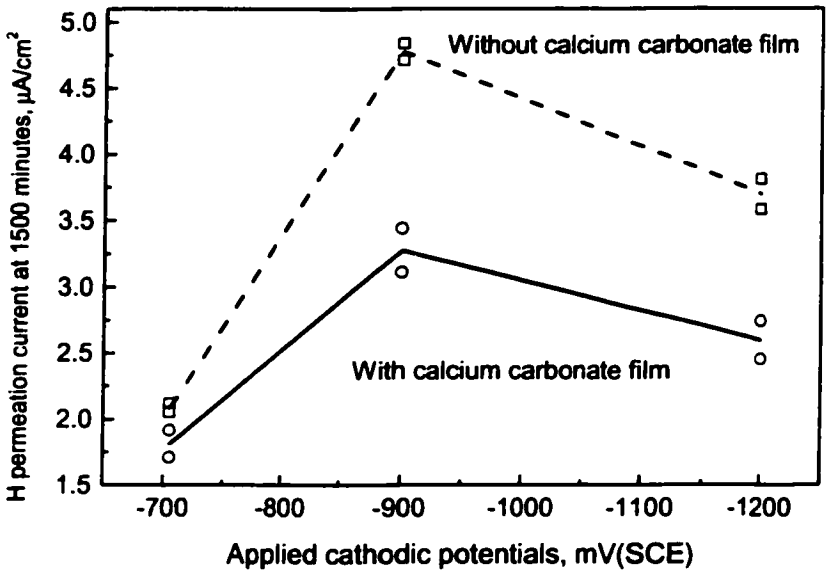

c. Hydrogen flux at 1500 minutes as a function of the applied cathodic potentials

Fig.4-20 The influence of applied cathodic potentials on the hydrogen permeation behavior of the specimens with and without calcium carbonate coatings 600-grit finish

4.4.2. Hydrogen permeation in treated NS4

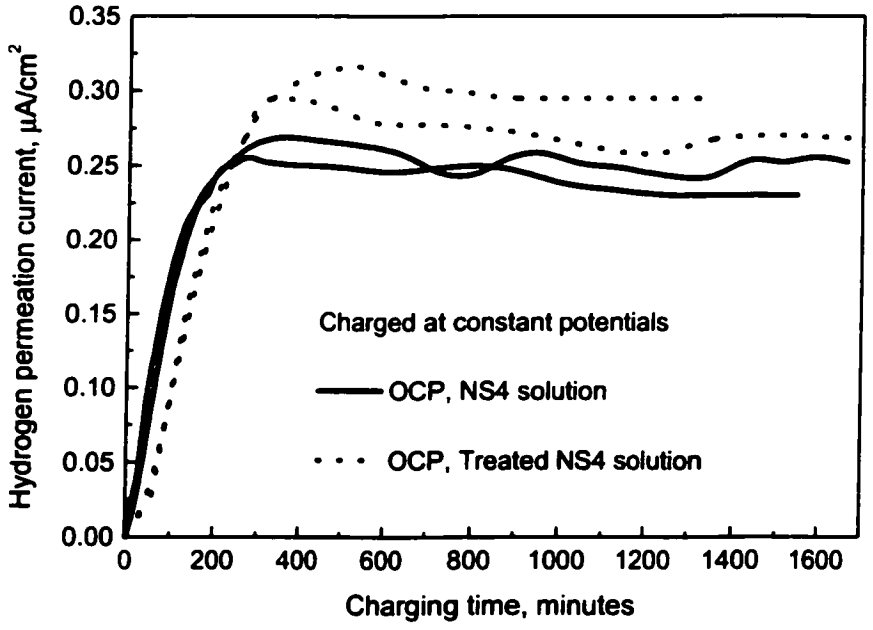

a. OCP

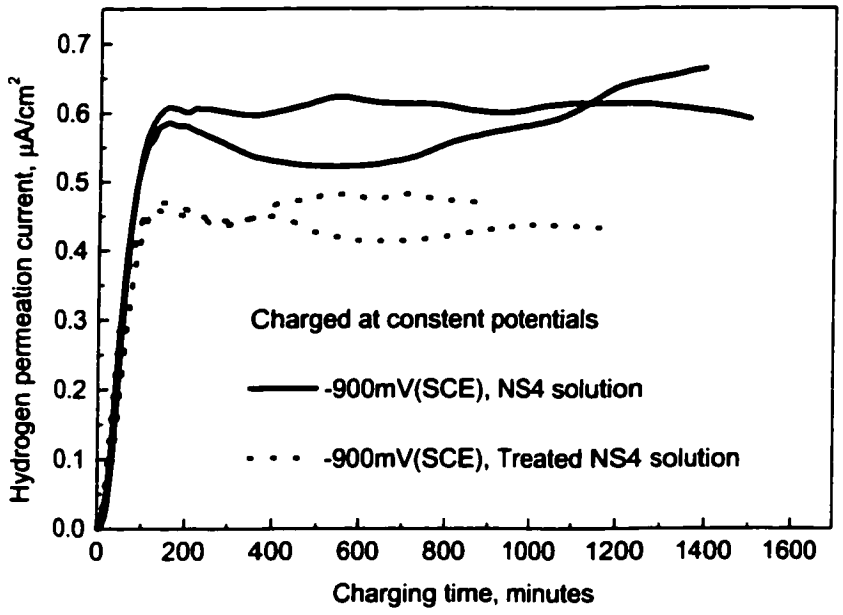

b. –900mV(SCE)

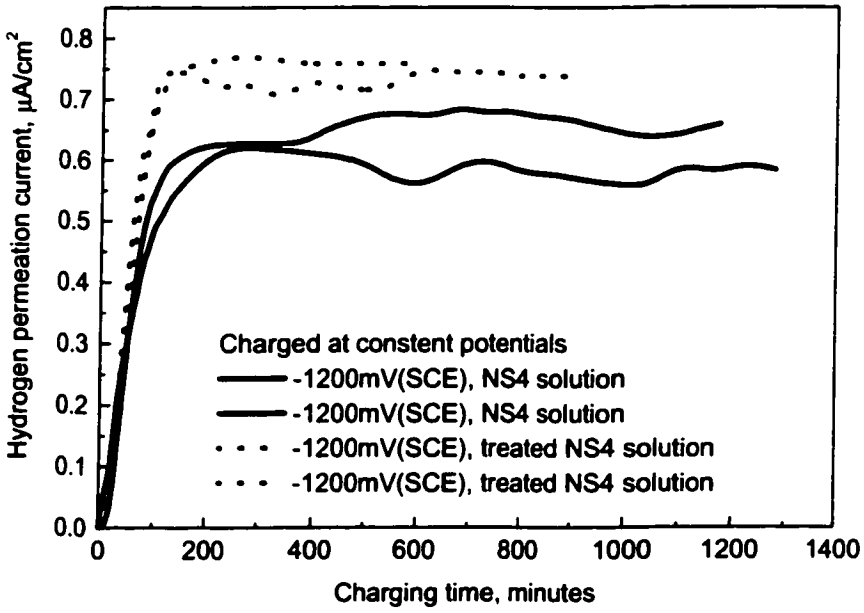

c. –1200mV(SCE)

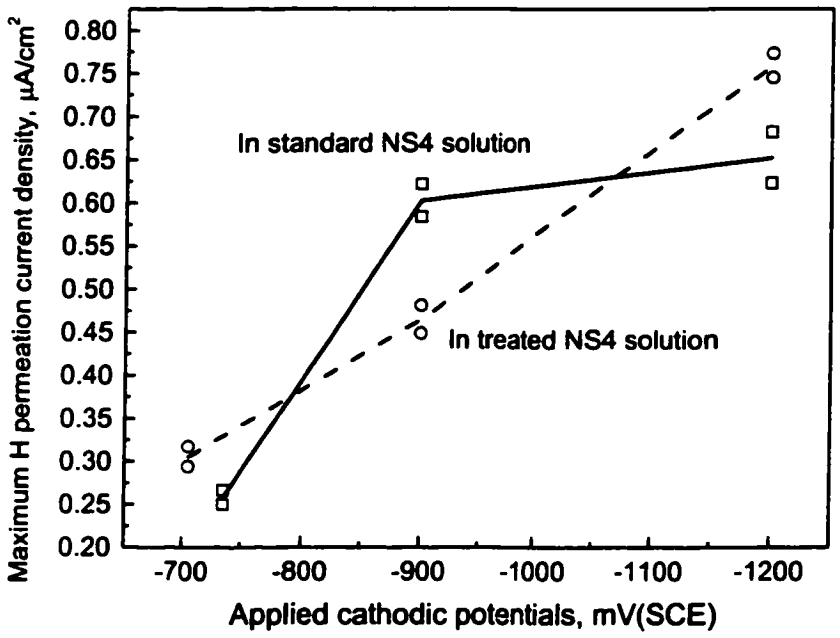

d. Peak hydrogen flux

Fig.4-21 Effect of the solution chemistry on the hydrogen permeation of the steel, 600-grit finish

Fig.4-21a to 4-21c compare the hydrogen permeation curves obtained in the NS4 and the treated NS4. The hydrogen flux is higher in the treated solution than in the NS4 solution at OCP and −1200 mV, but lower at −900 mV (Fig.4-21d). This is consistent with the results shown in Fig.4-18. In addition, there is significant difference in the permeation rate between NS4 and the treated NS4 at OCP. However, this difference appears less profound at more cathodic conditions.

4.4.3 Effect of surface roughness

Fig.4-22 shows the hydrogen permeation curves of specimens with different roughness charged at OCP and -900 mV(SCE). At both OCP and -900 mV, the specimens with rougher surfaces have higher steady state hydrogen flux. In addition, the permeation rate (the slope of the permeation curve) is lower at OCP than at −900 mV. The increased

hydrogen flux at OCP for the specimen with rougher surface may be due to the increased corrosion rate of the material; at cathodic condition, however, the high hydrogen flux for rough surface may also be related to the increased surface area for hydrogen absorption.

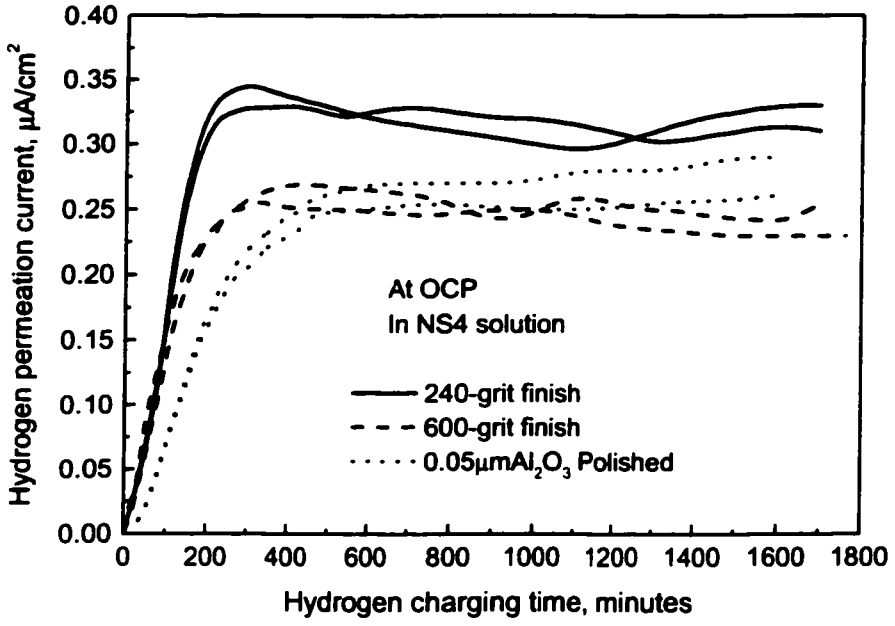

a. at OCP

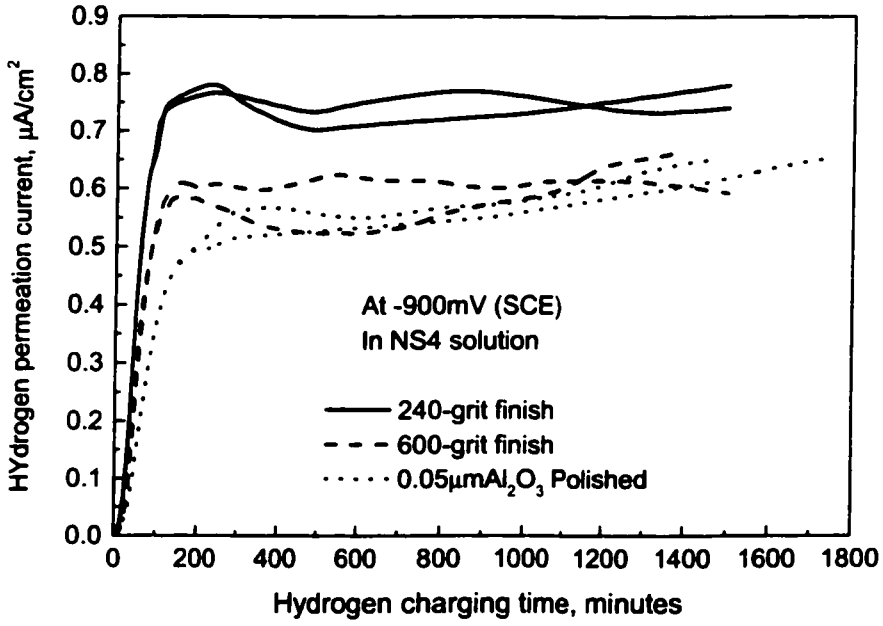

b. At –900mV (SCE)

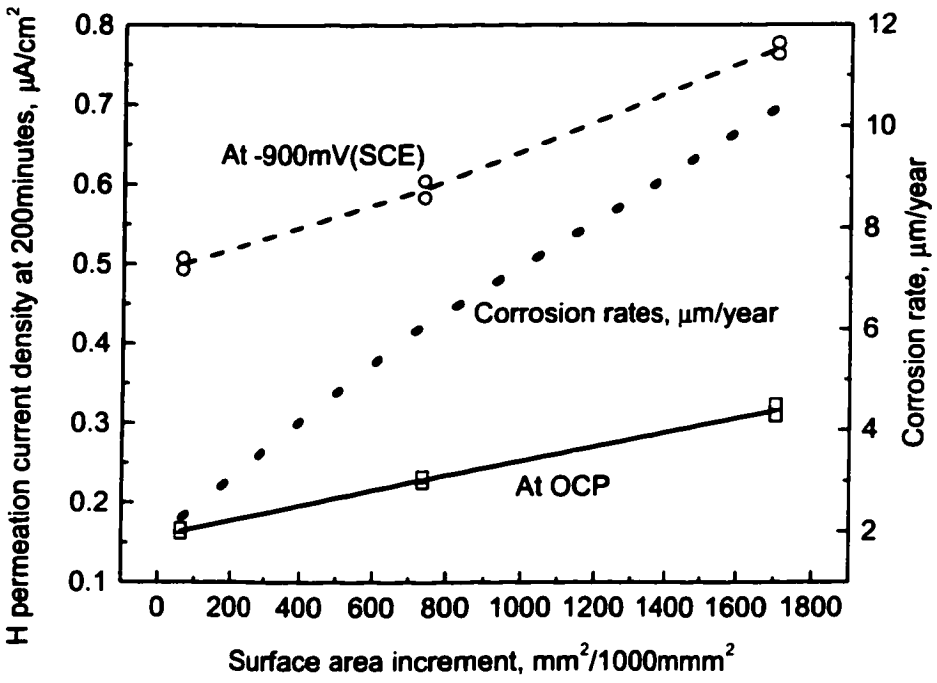

c. Relationship among surface area increment, corrosion rate and the H flux at 200 minutes

Fig.4-22 Hydrogen permeation curves of X65 with various surface roughness tested at OCP and -900mV (SCE)

The effect of surface roughness on hydrogen permeation was also studied under various constant charging current (Fig.4-23). At the same charging current density, the hydrogen reduction rate in the charging cell can be considered to be constant. The hydrogen permeation flux will depend on the rate of H-H recombination at the surface and the efficiency of adsorption of atomic H to the steel surface for diffusion. The large surface area of the rough surface should increase the efficiency of adsorption of H atoms to the surface. This seems consistent with a higher permeation rate observed in the specimen with rougher surface, Fig.4-21a. However, at high charging current density, for example, 0.010 mA/cm^2, the build-up rate of hydrogen flux becomes higher for the specimen with

more flat surface. This might be related to other surface conditions, such as the formation of surface deposits, and the over potentials.

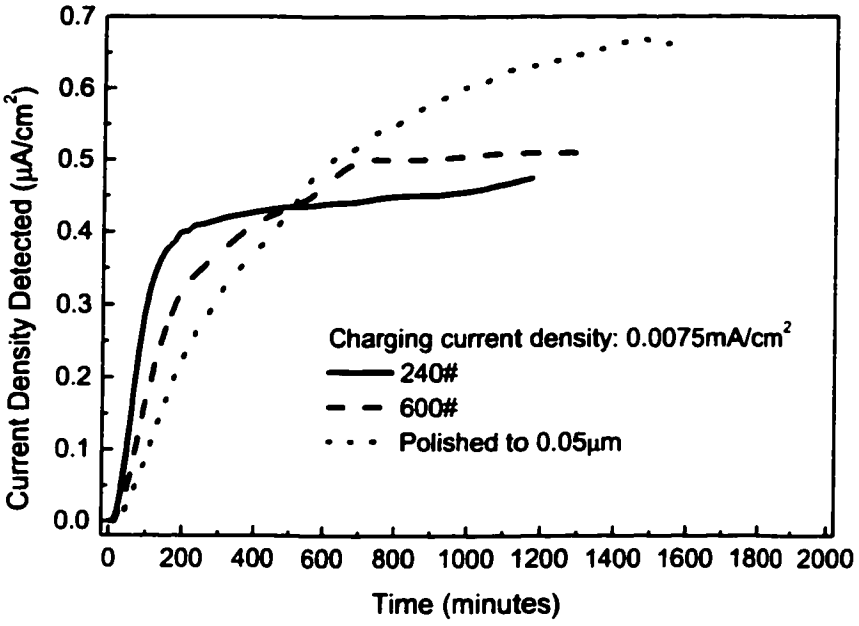

a. Charged at 0.0075mA/cm^2

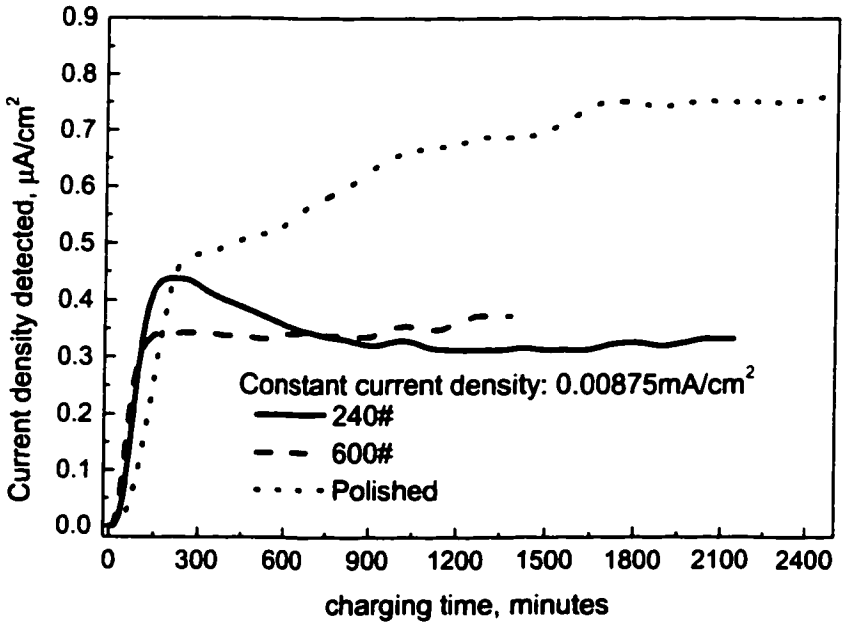

b. Charged at 0.00875mA/cm^2

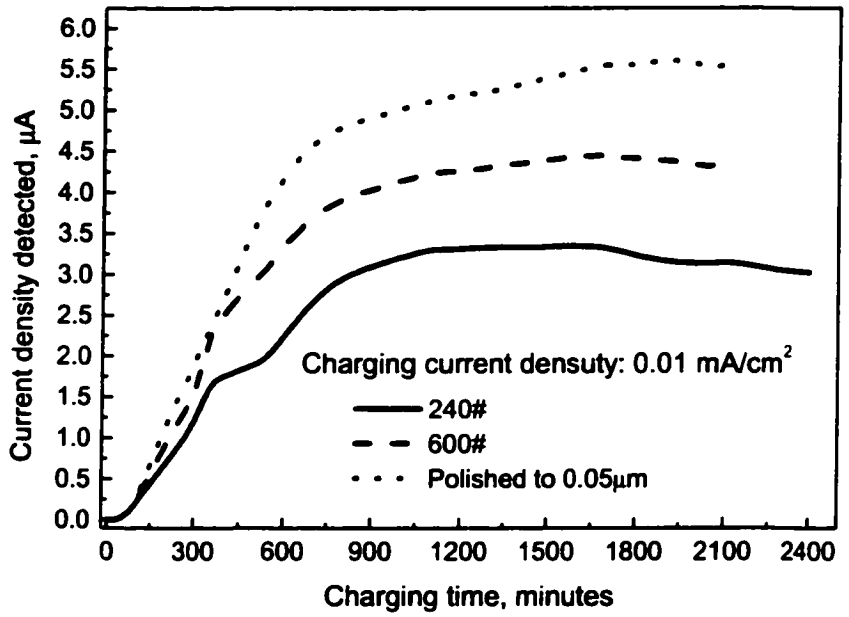

c. Charged at 0.010mA/cm^2

Fig.4-23 Influence of the surface roughness on the hydrogen permeation of steels in NS4 solution

4.5 SSRT BEHAVIORS

Slow strain rate tensile testing is one of the viable techniques often used for a quick evaluation of the susceptibility of a material to stress corrosion cracking. In this section, surface variables such as surface roughness, scratch orientation, and surface calcium carbonate deposits were considered in the test program to understand how they influence SCC susceptibility of the line pipe steel exposed to near-neutral pH environments.

4.5.1 Effect of potential and calcium carbonate film

The influence of the applied cathodic potentials on the SSRT properties of the steel in NS4 solution was investigated and the experimental results are presented in Fig.4-24. In the tests, the samples were immersed in the solution for various lengths of time prior to loading. This allows the diffusion of hydrogen into the test specimen, corrosion attack on the surface, and the formation of calcium carbonate film at the lower cathodic potentials.

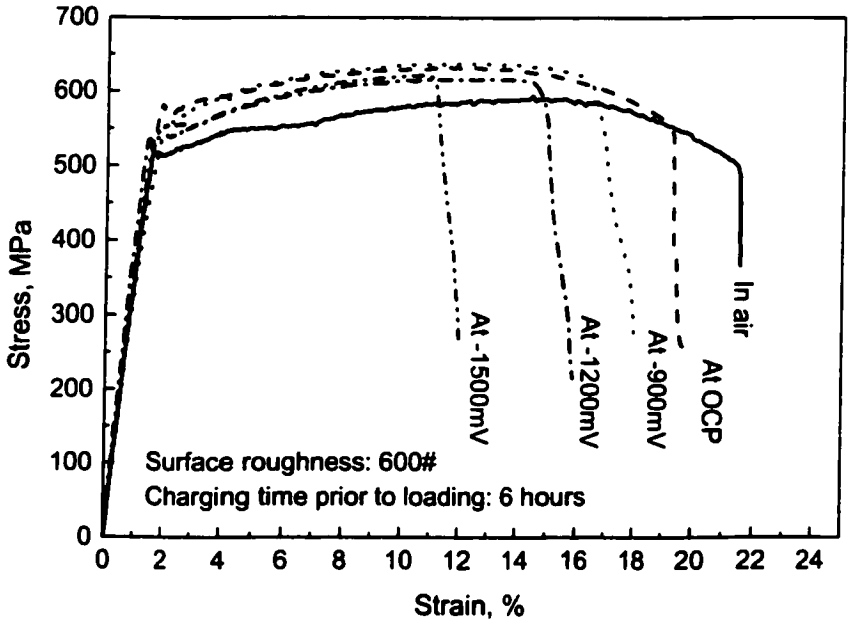

a. 6 hours charging prior to loading

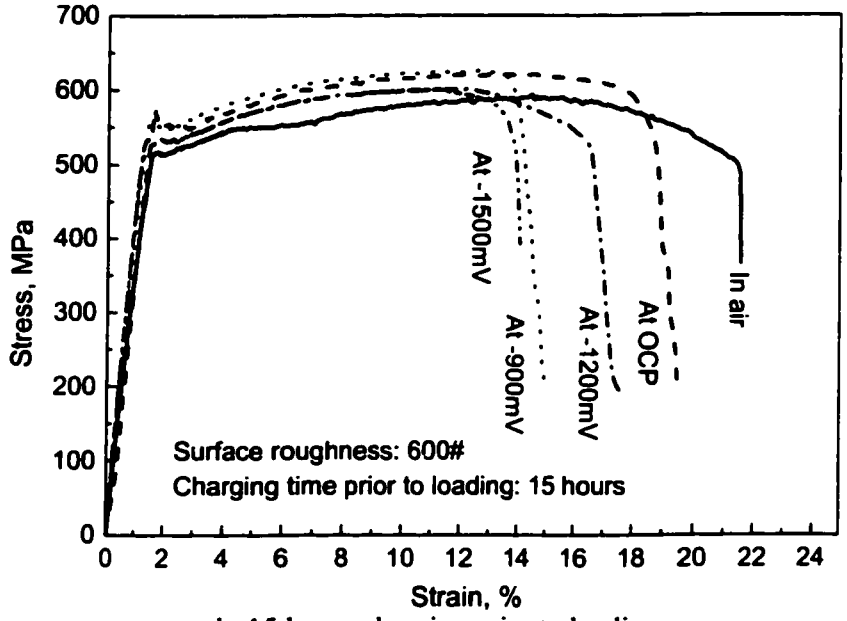

b. 15 hours charging prior to loading

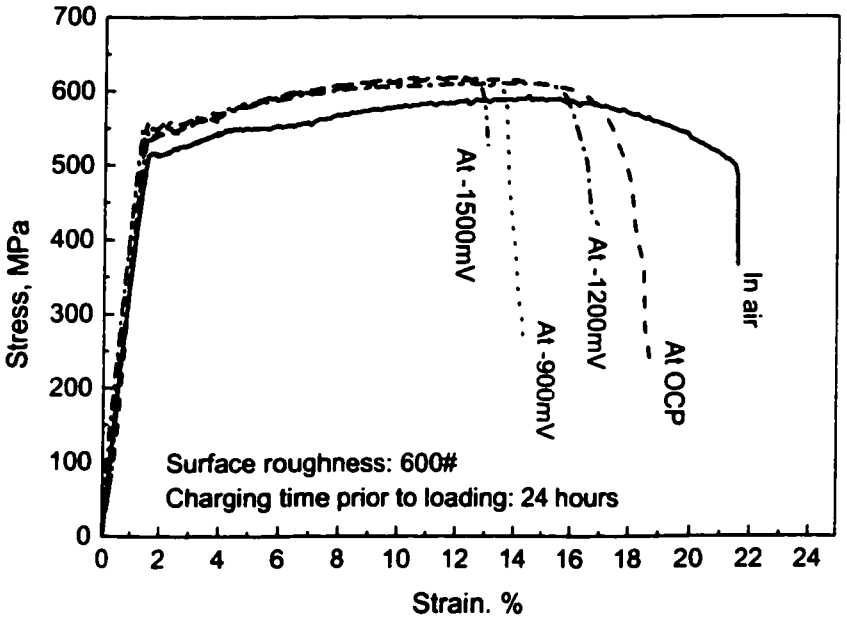

c. 24 hours charging prior to loading

Fig.4-24 Influence of the applied cathodic potentials on the mechanical properties of steels in NS4 solution

Fig.4-25 shows the influence of the hold time prior to loading on the SSRT curves of the steel tested in NS4 solution. The ductility results of the testing are summarized in Fig.4-26. When the specimens were held in NS4 for 6 hours prior to the loading, the ductility was seen to decrease almost linearly with decreasing cathodic potential. For the specimen with an increased hold time prior to the loading, however, an abnormal increase in ductility was observed at −1200 mV. This increased ductility at −1200 mV coincides with the lowest hydrogen content measured at -1200mV, suggesting the dependence of SSRT on the amount of hydrogen in the steel.

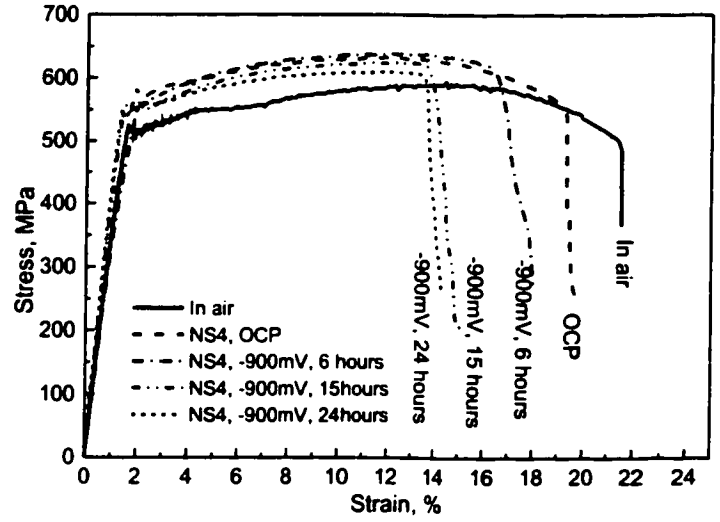

a. NS4, -900mV (SCE)

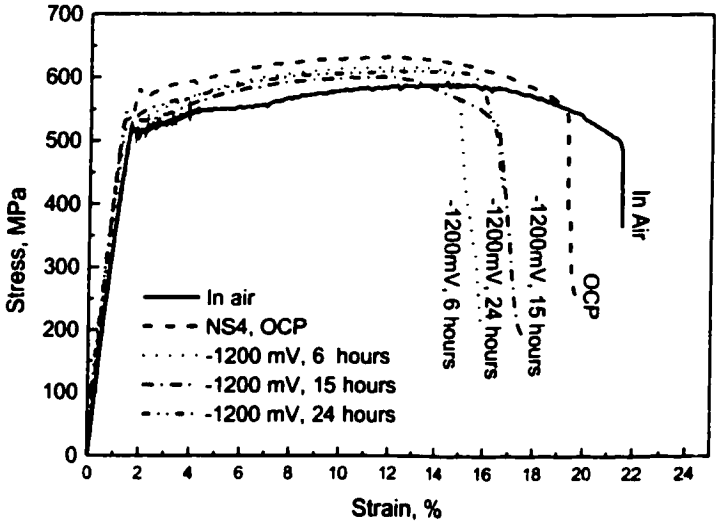

b. NS4, -1200mV (SCE)

Fig.4-25 Effect of the pre-loading charging time on the SSRT properties of steels

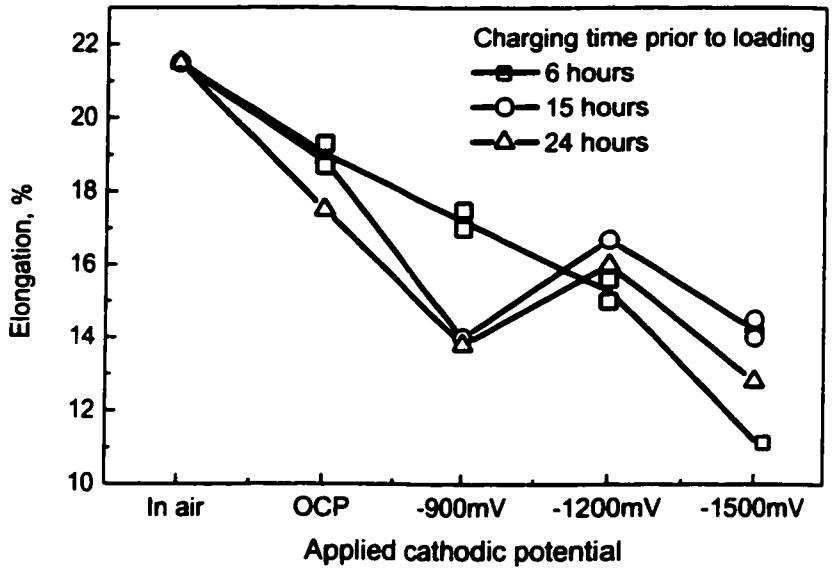

Fig.4-26 Effect of applied cathodic potentials on the ductility of the steel tested in NS4 solution at a strain rate of $10^{-6}s^{-1}$

4.5.2 SSRT in the treated NS4

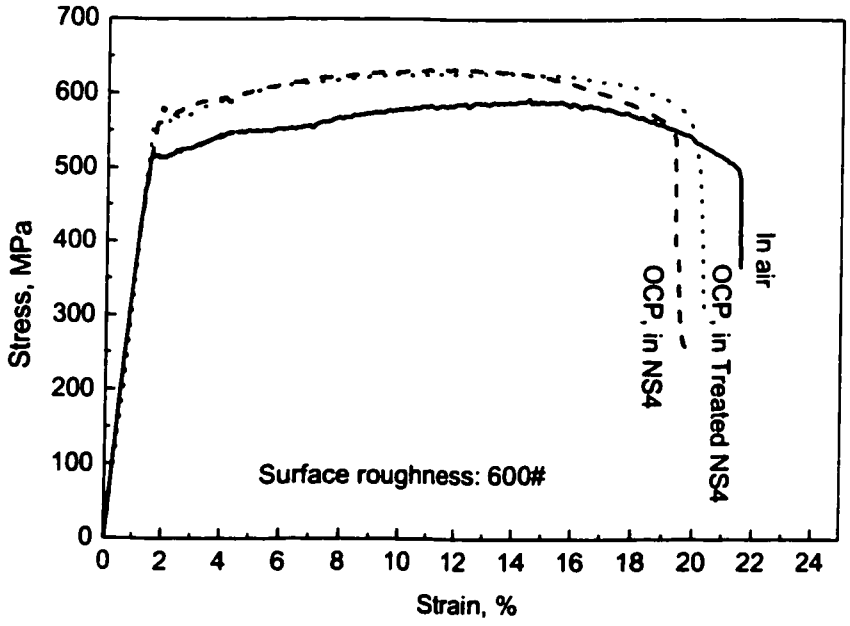

a. OCP, 6 hours prior to loading

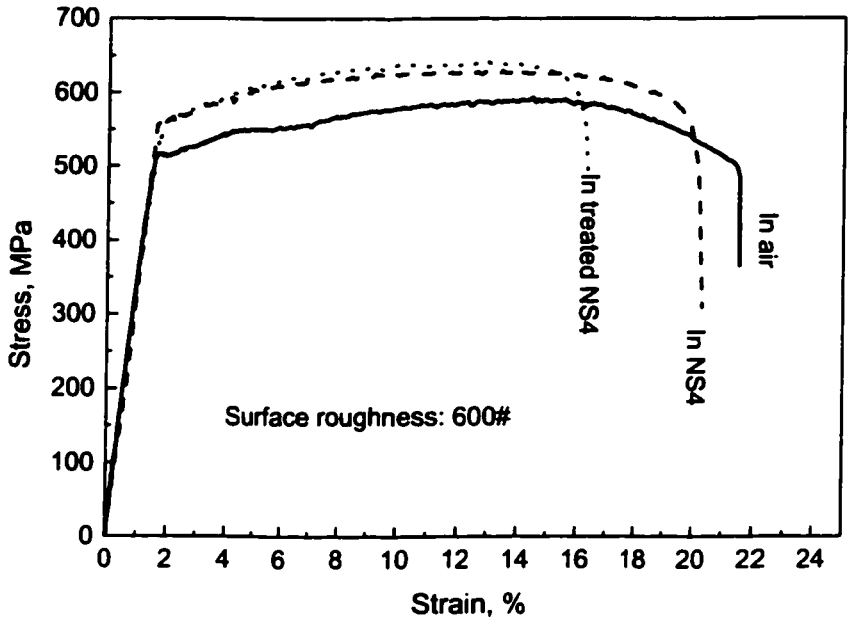

b. -900mV, 6 hours charging prior to loading

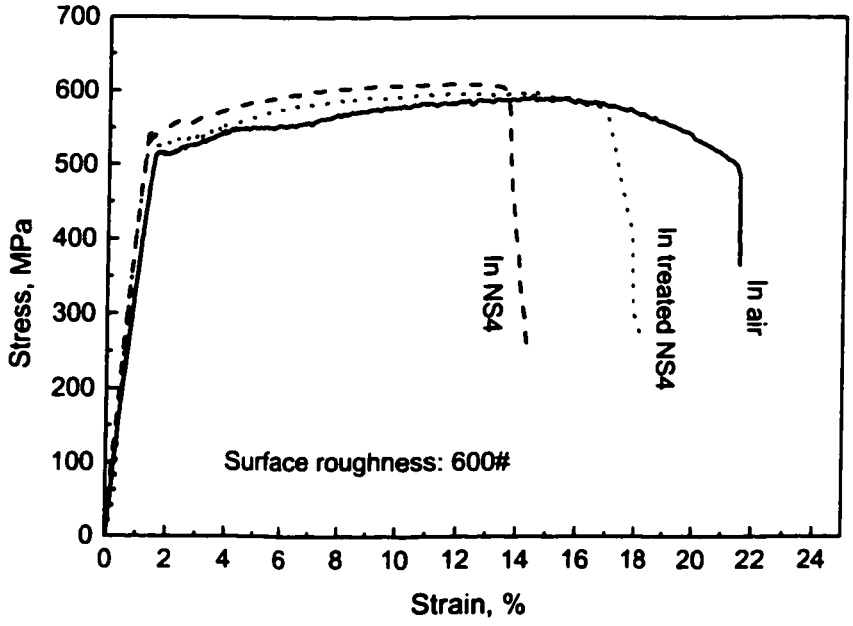

c. -900mV, 24 hours charging prior to loading

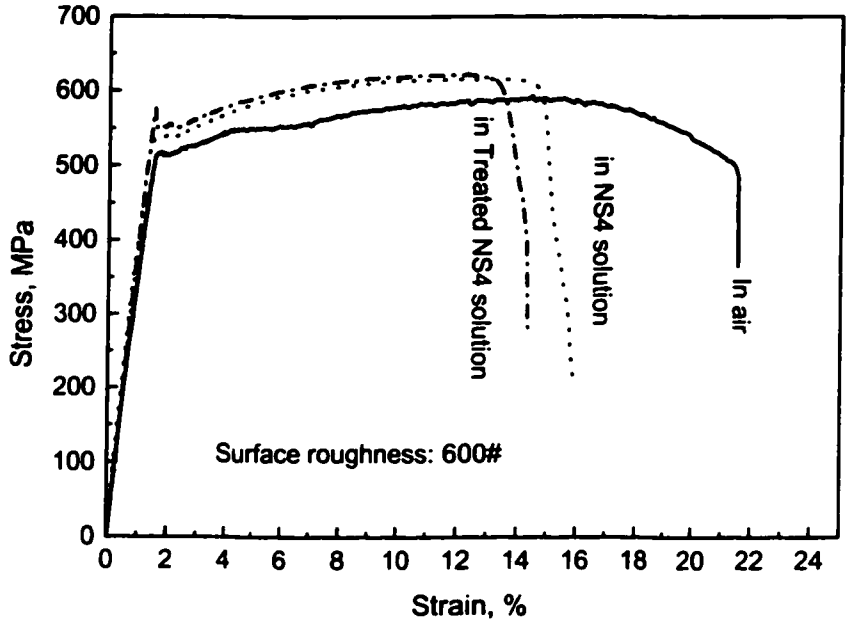

d. -1200mV, 6 hours charging prior to loading

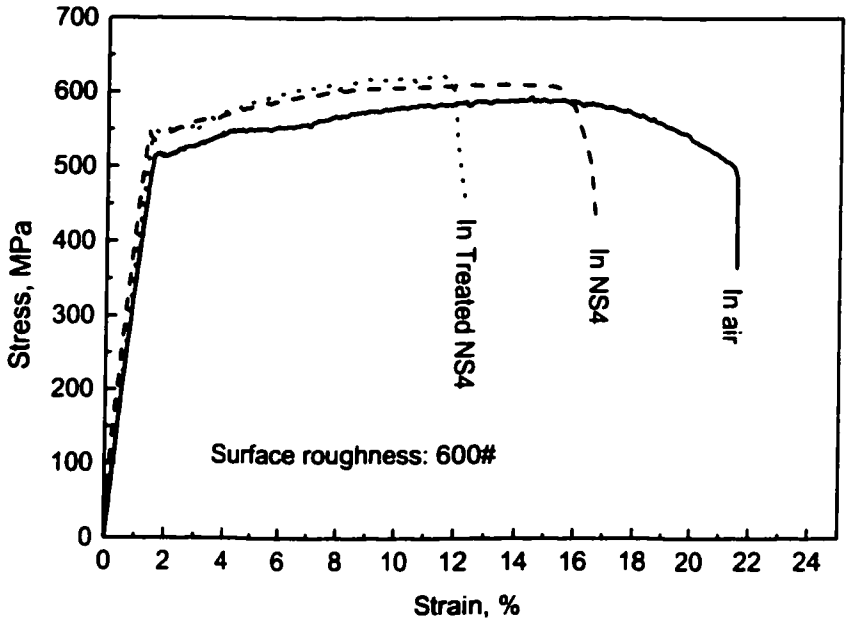

e. -1200mV, 24 hours charging prior to loading

Fig.4-27 SSRT results of steels in NS4 and the treated-NS4 solution

It was found previously that the hydrogen content in the steels charged in the treated NS4 solution was quite different from that in NS4. The effect of the two solutions on SSRT behavior of the steel was evaluated at various cathodic potentials and hold times prior to SSRT loading. Fig.4-27 shows the SSRT curves obtained from each test, and a summary of the SSRT properties is presented in Fig.4-28.

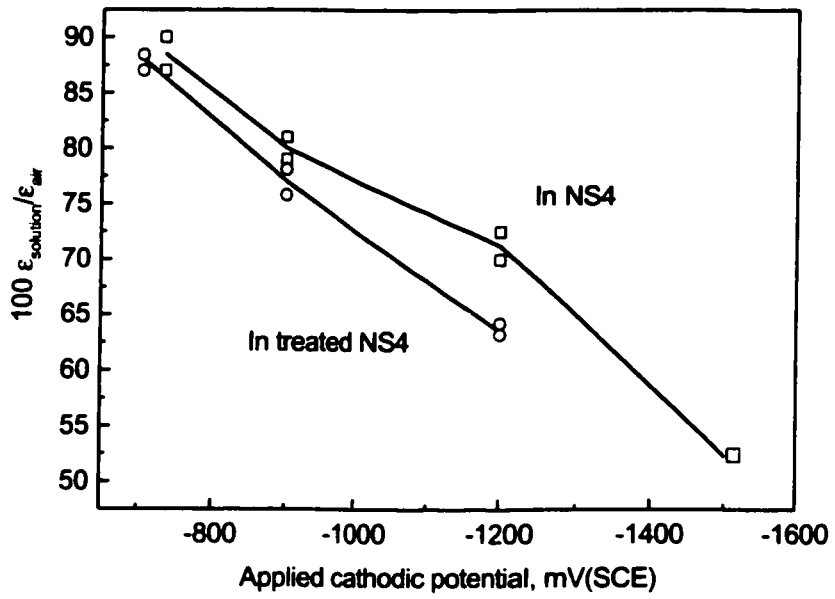

a. Charged for 6 hours prior to loading

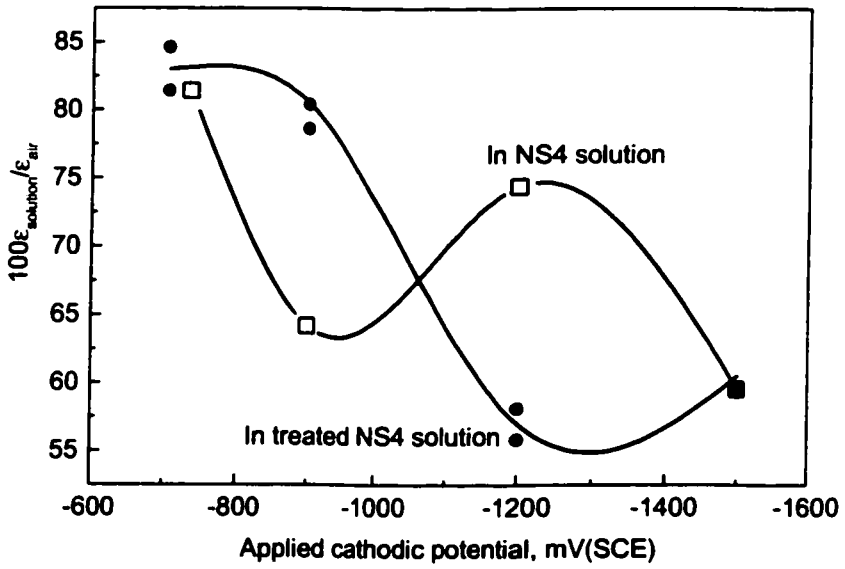

b. Charged for 24 hours prior to loading

Fig.4-28 summary of the SSRT properties in both solutions

As shown in Fig.4-27 to Fig.29, the effect of solution chemistry on SSRT properties of specimens depends on both the hold time prior to loading and the cathodic potential. Fig.4-28 compares the SSRT results obtained in the treated NS4 with those in NS4. With a short hold time prior to loading, the SSRT properties in the treated NS4 are generally lower than those in NS4 (Fig.4-28a). With an increased hold time, the large difference in SSRT properties is observed at −900 mV and −1200 mV (Fig.4-28b). This difference is in fact consistent with the hydrogen data presented in Fig.4-10. In contrast, the difference in hydrogen content between the treated NS4 and NS4 at −1500 mV is almost the same as that at −1200 mV. However, the SSRT properties tested in both solutions at −1500 mV is almost the same. This indicates that hydrogen may not be the only factor affecting SSRT properties.

Fig.4-29 summarizes the influence of charging time prior to loading on SSRT properties of the steel in the treated NS4 solution, which is different from the result in standard NS4 solution indicated in Fig.4-26. In general, the ductility of the specimens in the treated NS4 solution decreases with the decreasing of cathodic potential, especially from OCP to -1200 mV (SCE), regardless of the pre-loading charging time. A slight increase in ductility was observed at −1500 mV with a hold time of 24 hours in the treated NS4 solution. This might be due to the fact that the treated NS4 solution was treated at −1200 mV before being used for SSRT testing. At −1500 mV, deposition of calcium carbonate becomes possible again, which should reduce hydrogen ingress as indicated before.

At −900 mV(SCE), the longer hold time in the treated NS4 solution caused an increased ductility in the treated NS4 solution. This is consistent with the results presented in Fig.4-18a, in which lower hydrogen content was detected in the steel exposed to the treated NS4 solution. In contrast, the lower ductility obtained in the test with 24 hour hold time at OCP in the treated NS4 contradicts the belief that hydrogen is responsible for SSRT properties. However, the effect of hold time on SSRT properties at OCP is consistent between the tests in NS4 and in the treated NS4. In both cases, ductility decreases with increased hold time. This might be caused by increased corrosion at OCP, which shortens the time for crack initiation.

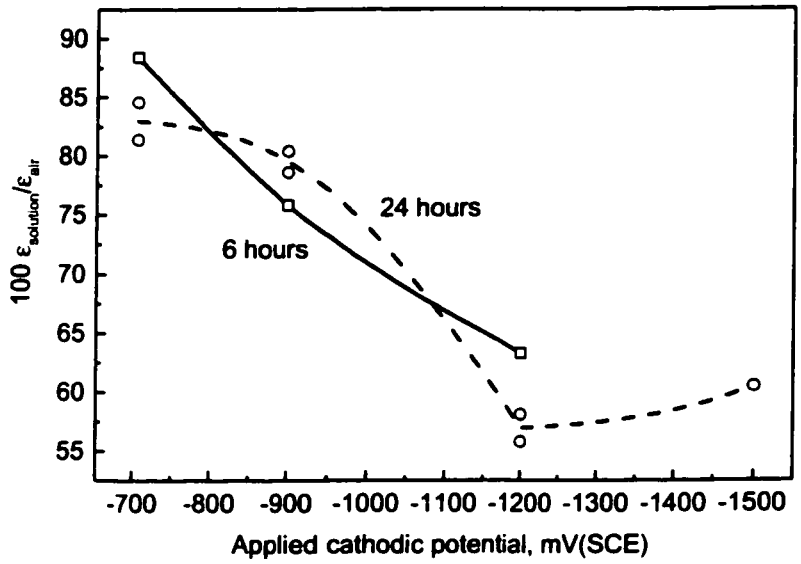

Fig.4-29 The influence of charging time prior to loading on SSRT properties of the steel in the treated NS4 solution

4.5.3 Effect of surface roughness and orientation

The solution extracted from a water-saturated soil was used in the study below. Tensile specimens were prepared with different scratch orientation and roughness.

4.5.3.1 Effect of Scratch Orientation

A comparison of stress-strain curves for different scratch orientations is shown in Fig.4-30a to 4-30c. The ratio of the ductility between the test in solution and in air, $\varepsilon_E/\varepsilon_A$, is listed in Table 4-1 for all the test conditions. In general, all the tests in the soil electrolyte caused a reduction in ductility of the steel compared to tests in air. The reduction was the highest in the test using samples with the scratch orientation perpendicular to the tensile stress axis. The least reduction occurred in the test of the specimen with the surface scratch orientation parallel to the loading direction. The difference in $\varepsilon_E/\varepsilon_A$ ratio between the tests with parallel and perpendicular scratches is in a range from 0.12 at OCP to about 0.15 at –800 mV (SCE). The reduction in ductility due to the effect of scratch

orientation appeared to increase when the test was conducted under a more cathodic condition.

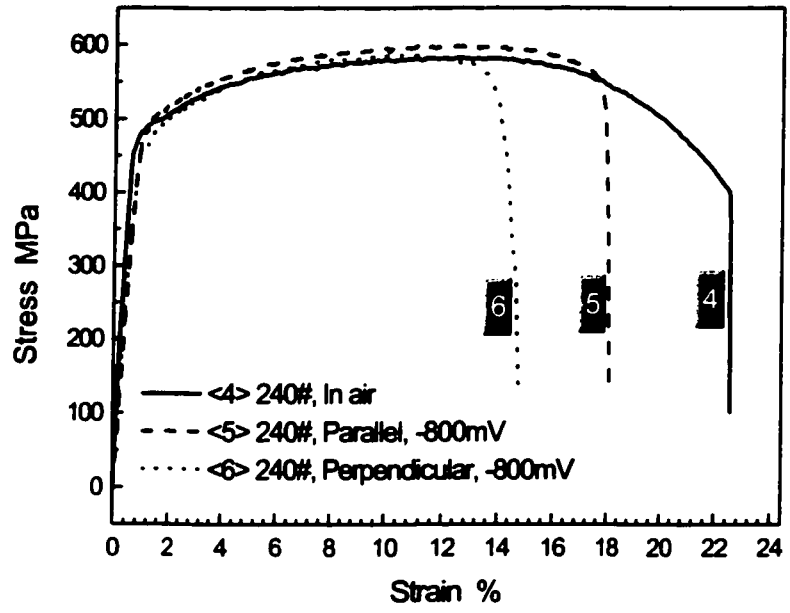

a. 240#, -800mV

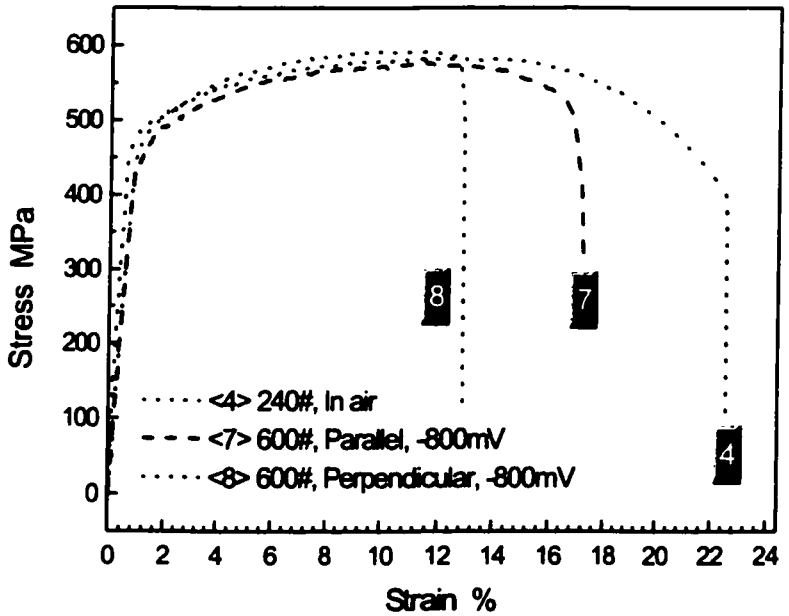

b. 600#, -800mV

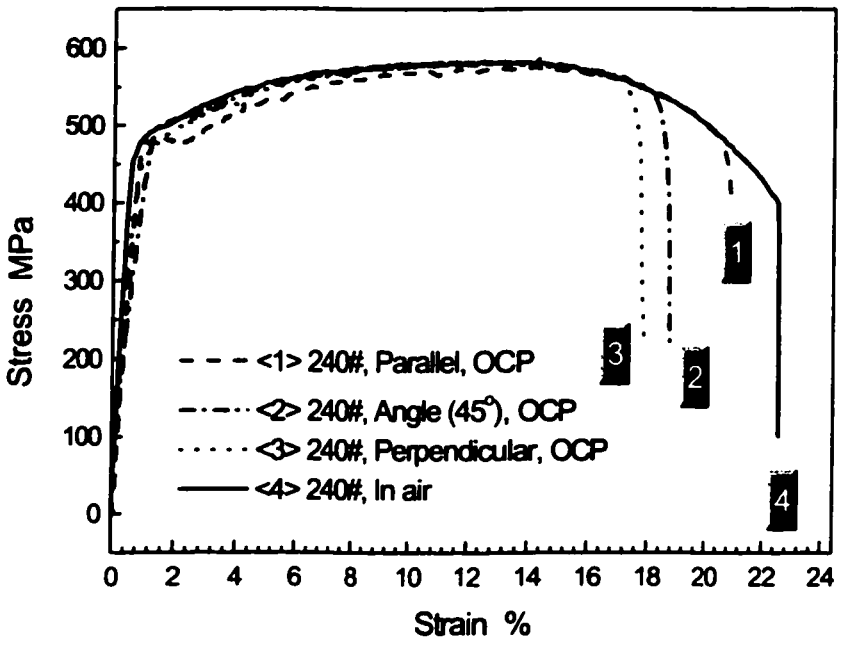

c. 240#, OCP

Fig.4-30 Effects of scratch orientation on the ductility of pipeline steel

Table 4-1 Summary of slow strain rate test results

Surface Roughness/Potential	$\varepsilon_E/\varepsilon_A$ *		
	Parallel Scratch	Perpendicular Scratch	Average difference between parallel and perpendicular scratch
240# / OCP	0.90	0.78	0.12
600# / OCP	0.93	0.79	0.14
240# /-800mV(SCE)	0.80, 0.80	0.65	0.15
600# /-800mV(SCE)	0.74, 0.70	0.56, 0.59	0.15

* $\varepsilon_E/\varepsilon_A$: Ratio of the ductility between the test in soil environment and in air

4.5.3.2 Effect of Scratch Roughness

Stress-strain curves obtained from tests on samples with different roughness are compared in Fig.4-31a to 4-31c. The effect of roughness on ductility can also be seen from the data in Table 4-1. It appears that the effect of roughness at OCP condition is not significant, although more reduction in ductility may be seen for the sample with the rougher surface. Under cathodic conditions, surface roughness does have some effect on the ductility of the steel although its effect is not as significant as the effect of orientation on ductility. As indicated in Fig.4-30 and Table 4-1, finer scratches appear to cause more reduction in ductility under a cathodic condition. For example, for samples either with parallel scratches or perpendicular ones, an average of about 8% more reduction is seen for the sample with scratches produced by 600# grit SiC paper as compared with the sample with scratches produced by 240# grit.

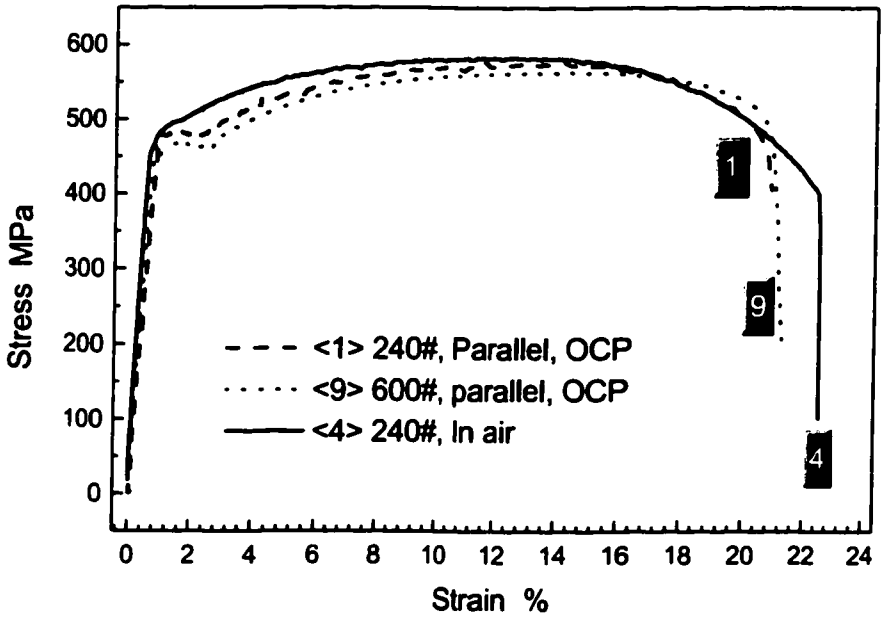

a. Samples with parallel scratch tested at OCP

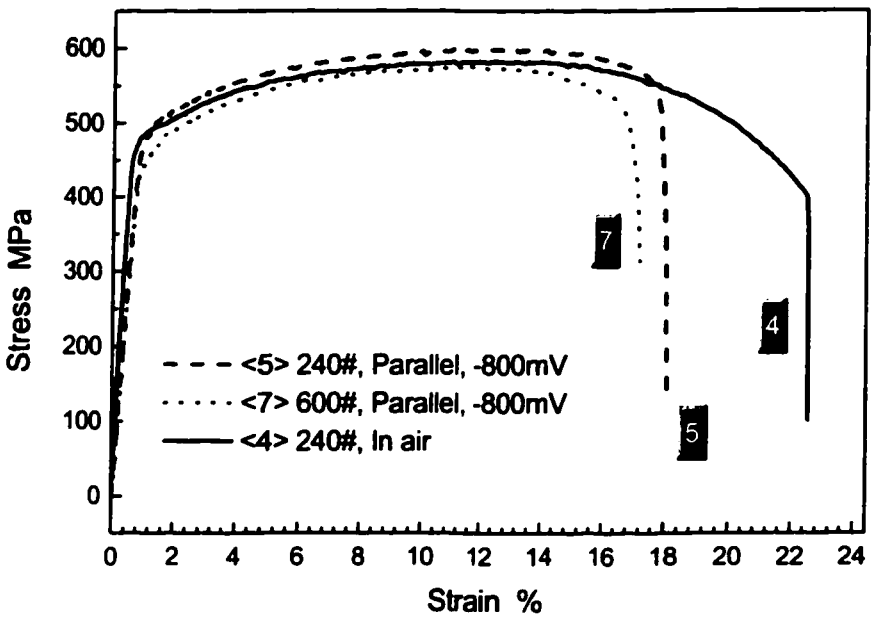

b. Samples with parallel scratch tested at -800mV

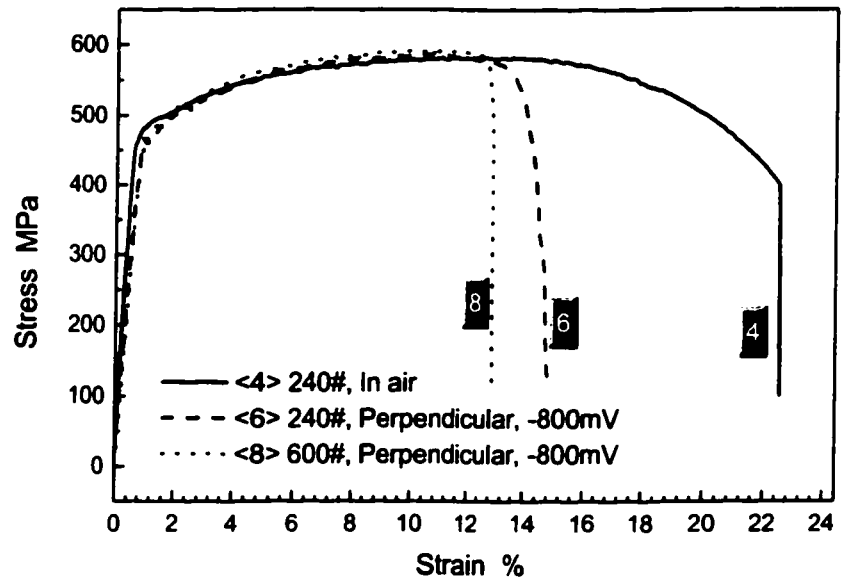

c. Samples with perpendicular scratch tested at -800mV

Fig.4-31 Effects of surface roughness on the ductility of pipeline steel

4.5.3.3 Effect of Cathodic Potentials

The effect of cathodic potential on the $\varepsilon_E/\varepsilon_A$ ratio appears to depend on the scratch roughness (table 4-2). For example, the difference between the $\varepsilon_E/\varepsilon_A$ ratio at OCP and -800 mV (SCE) is about 10% for the tests with parallel scratches produced by 240-grit sandpaper. However, this difference is increased to about 20% for the tests with the same scratch orientation but produced by 600-grit sandpaper.

Table 4-2 Effect of applied potential on $^{\bullet}\varepsilon_E/\varepsilon_A$ ratio

Scratch Orientation	Parallel		Perpendicular
Surface Roughness	240#	600#	240#
OCP	0.90	0.93	0.78
-800mV(SCE)	0.80, 0.80	0.74, 0.70	0.65
Difference Between OCP and -800mV	0.10	0.21	0.13

$^{\bullet}\varepsilon_E/\varepsilon_A$: Ratio of the ductility between the test in soil environment and in air

4.5.3.4 Morphology Examination

In order to understand the effect of scratch orientation and roughness on crack initiation and propagation, the failed specimens were examined in the SEM. Fig. 4-32a to 4-32c compare the cracks developed on the surface with respect to the initial scratch orientation and loading axis. For the tensile specimen with scratches perpendicular to the gauge length and loading axis, cracks have developed along scratches. For those with scratches parallel to the loading direction, no cracks developed in the direction perpendicular to the stress axis. For these specimens, only short cracks developed, orientated at about 45° to the stress axis. This suggests that scratches parallel to the loading direction did not facilitate crack initiation. For the sample with 45° scratches, cracks also developed along the scratches but orientated approximately 45° to the stress axis.

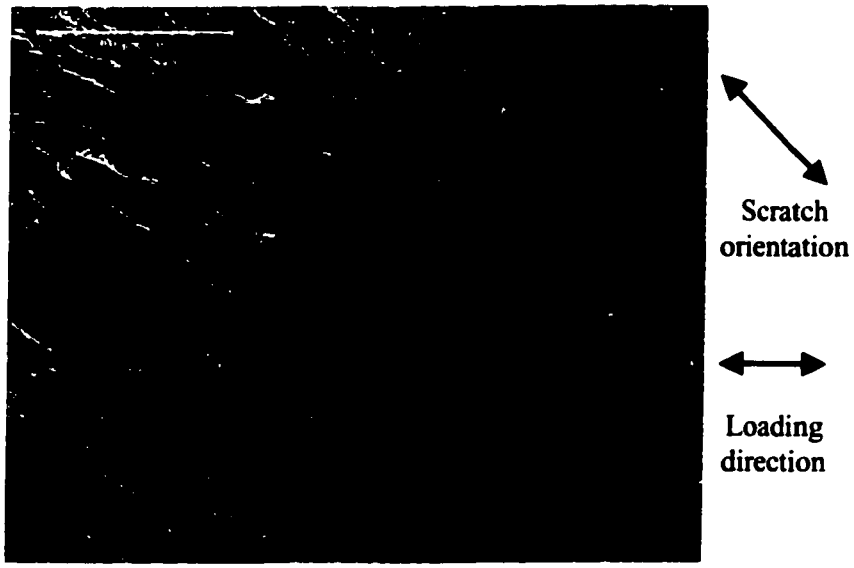

c. Scratch orientation is 45° inclined to loading

Fig.4-32 Effects of scratch orientation on crack initiation

The above surface observations are also consistent with the fracture morphologies after failure. In Fig. 4-33a, the fracture developed from a crack at site A. The crack surface at this site is orientated in a direction perpendicular to the stress direction. The cracks on the sample surface next to the fracture site were slightly tilted because of necking deformation. For samples with scratches parallel to the loading direction, only very short cracks were observed near the fracture site, Fig.4-32b. The reduction in cross sectional area is also clearly larger than in Fig.4-33a for the sample with scratches perpendicular to the stress axis. The failed tensile sample with the 45° scratch orientation shows a large portion of surface cracks parallel to the scratch orientation, Fig.4-33c.

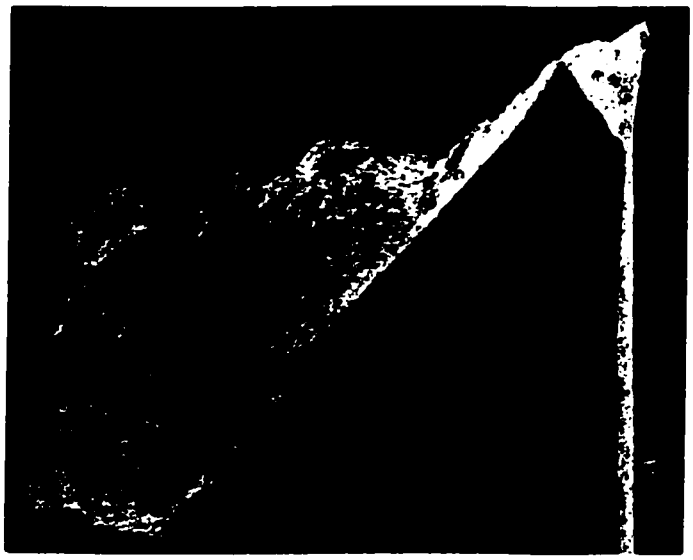

c. 45° inclined scratch

Fig.4-33 Fracture morphologies of the failed specimens

5 Discussion

5.1 HYDROGEN GENERATION IN NEAR-NEUTRAL pH SOIL ENVIRONMENTS

Ingress of hydrogen into the steel exposed to near-neutral pH environments is apparently influenced by the surface roughness, cathodic potential and electrochemical reactions at the surface. All these factors are mutually connected and influence the hydrogen ingress in a synergistic way.

The surface scratches produced by grinding with SiC paper is characterized by scratch depth, scratch density and probably deformation layers on the surface. The combination of scratch depth and scratch density is represented by surface area increment. Regardless of the ease of dissolution due to the deformation at the surface, a surface with a large area increment increases the area of corrosion exposure at the surface. This might be the most important reason that the specimen with rougher surface has a higher corrosion rate and more negative open circuit potential in both NS4 and the treated NS4 solution.

At open circuit potential, the generation of hydrogen is related to the dissolution of iron, which supplies the electrons for hydrogen reduction reaction. As a result, the rate of iron dissolution should be proportionally related to the hydrogen generation. This is quite consistent with the observation that hydrogen flux at the exit side of permeation cell increases with the increasing of corrosion rates shown in Fig.4-21c.

At cathodic protection conditions, the dissolution of iron is prohibited, and consequently, the hydrogen reduction is realized by the externally imposed cathodic current. Under these circumstances, hydrogen generation and permeation are further complicated by the formation of calcium carbonate deposits at low cathodic potentials.

At cathodic condition where the calcium carbonate deposits are not formed, hydrogen content in the steel also increases with an increase in the surface area increment. Two factors might be relevant to this observation. The first of these is the overpotential, which is the potential difference between the charging potential and the open circuit potential. High overpotential may produce higher cathodic current for the hydrogen reduction

reaction. This assumption is actually contrary to the experimental observation presented in Fig.4-21 and Fig.4-5.

The second factor to be considered is the effective surface area. It was characterized that the cathodic current under constant potential varied significantly with permeation time (Fig.5-1). The cathodic current was observed to be significantly high in the first few hours of permeation, but reduced to a quite low level afterwards. This suggests that hydrogen reduction under constant cathodic potential might be quite intense initially. As a large number of hydrogen atoms is produced in a short time, the efficiency of hydrogen absorption to steel surface might be the controlling factor for the rate of hydrogen permeation. Under the circumstances, it is certain that the larger the surface area, the more hydrogen atoms could be adsorbed to the steel surface for permeation. This is also quite consistent with the permeation curve shown in Fig.4-21. In that figure, a large difference in hydrogen flux is observed in the built-up stage of hydrogen permeation between the specimens with different surface area increment / scratch roughness.

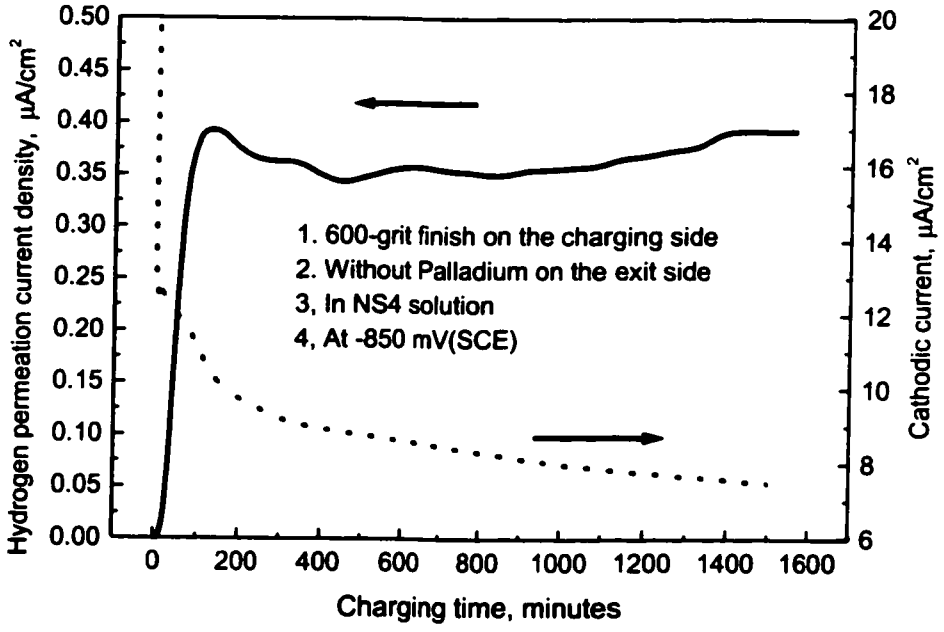

Fig.5-1 the cathodic and hydrogen-permeation current densities as a function of the charging time

Under more negative cathodic potential, calcium carbonate was deposited on the steel surface. In this case, the hydrogen permeation depends also on the effective area for atomic hydrogen absorption on the steel surface. In addition, part of the atomic hydrogen produced may stay with the calcium carbonate and will be recombined to form hydrogen gas that will not contribute to atomic hydrogen permeation through the steel. Under the circumstances, the surface with smaller effective surface area was seen to be covered with more calcium carbonate particles, and therefore should be less effective in hydrogen absorption for permeation. This is consistent with the experimental results (Fig.4-16).

The hydrogen content in the steel also depends on the chemistry of the electrolyte it is exposed to. In the treated NS4 solution, the concentration of Ca^{++} and HCO_3^- are reduced. Much lower hydrogen content was detected in the steel in the treated NS4 when the cathodic potential was higher than −1000 mV (SCE), implying that both the ions enhance the hydrogen permeation in the high cathodic potential region. This may be due to the fact that hydrogen reduction is usually accompanied by the production of OH^-, which may react with CO_2 to form HCO_3^-. The increase in HCO_3^- at surface requires the migration of positive ions such as Ca^{++} to the surface to achieve balance in electrical charge. The lack of Ca^{++} in the solution may therefore suppress the reaction of OH^- with CO_2 and therefore the hydrogen reduction reaction.

On the other hand, the solution with dilute Ca^{++} may either reduce the amount of calcium carbonate deposition or delay its formation to a lower cathodic potential. This would make more atomic hydrogen available for hydrogen permeation by a mechanism, as proposed before.

5.2 FACTORS INFLUENCING SSRT PROPERTIES IN NEAR NEUTRAL PH SOIL ENVIRONMENTS

The failure of the specimen under SSRT is a consequence of crack initiation and propagation. It is well documented that micro-cracks, when tensile testing is conducted in air, are usually initiated at the center of the necked region of the tensile specimen. These micro-cracks propagate towards the surface in a direction perpendicular to the stress axis. As the remaining cross section becomes smaller, slant shearing will take place at the

surface of the sample. The failed end is generally characterized with so-called cup-cone morphologies. When tested in a near-neutral pH solution, the crack was initiated at the surface of the specimen as a result of corrosion attack. The initiation of micro-cracks at the surface in a corrosive environment is usually faster than the initiation of microvoid in the necked region of the specimen tested in air. Crack propagates from the surface to the center and shearing may also take place at the end as a result of the reduced cross sectional area. To discuss the factors influencing SSRT properties is therefore to understand the factors influencing crack initiation and propagation in near-neutral pH environments. These factors may include scratch roughness and orientation, corrosion rate, hydrogen content, cathodic potential, and solution chemistries.

5.2.1 Effect of Scratch roughness and orientation

During SSRT in the soil solution environment, surface scratch orientation and roughness should have a direct influence on crack initiation. For example, a perpendicular scratch facilitates the development of cracks in a direction perpendicular to loading direction, while scratches parallel to the loading direction appear to have little influence on the initiation of cracks, since cracks appearing on the surface have no correlation with the scratch orientation (Fig.4-32). The effect of roughness on ductility appears to be minor at OCP, but significant under cathodic polarization.

Scratch roughness and orientation should not have any direct effect on the crack propagation rate. Its indirect effect on crack propagation may come from the following two aspects: 1) the crack propagation path, because the scratch orientation can influence the direction of crack initiation and subsequently propagation; 2) coalescence of neighboring cracks during propagation. However, the surface condition should not have any direct effect on crack propagation in the depth direction.

The roughness appears to have less effect on the ductility at OCP for the specimen with parallel scratches. A slight increase in ductility was seen for the specimen with finer scratches. However, under cathodic polarization, the scratch roughness has a stronger effect on ductility. In addition, a reverse dependence of ductility on the scratch roughness is seen under cathodic polarization as compared to that seen at OCP, that is, the finer grit

size causes more reduction in ductility (about 8%) for samples with either perpendicular or parallel scratches.

The effect of roughness on ductility at a cathodic potential may be attributed to the dependence of crack initiation on scratch roughness. For example, the rougher surface has deeper physical discontinuities, and may cause an earlier crack initiation than the less rough surface. This suggestion appears consistent with the effect of roughness on the ductility at OCP; however, it is contrary to the roughness effect on the ductility seen at a cathodic potential. Alternative factors have to be considered in order to understand the effect of the surface condition on the susceptibility of pipeline steel to stress corrosion cracking in near-neutral pH environments.

One of the alternative factors to be considered might be the difference in hydrogen content arising from different roughness. It is believed that the presence of hydrogen enhances crack propagation. At cathodic potential, the rougher surface has consistently shown higher hydrogen content in the steel. This again appears contrary to the observation that the ductility is higher in the specimen with finer scratches.

Although hydrogen content in the specimen is important, the hydrogen content at crack tip might be more relevant to the crack propagation. As shown in Fig.4-2, the rougher surface is characterized not only with deeper scratches but also with more deep scratches. It would be expected that fewer microcracks might be developed on the specimen on the less rough surface. Since the hydrogen content at crack tip is usually several times higher than that in the matrix, the hydrogen content per crack may not necessarily be smaller in the specimen that is less rough. In addition, on the surface with dense micro-cracks, stress shielding might be in effect, which may cause some dormant cracks. This may also contribute to a reduced propagation rate in the specimen with rougher surface.

5.2.2 Effect of Cathodic potential

The effect of cathodic potential on SSRT is through its effect on hydrogen generation and prohibition of corrosion. With a decrease in cathodic protection, corrosion attack at the surface is enhanced, but the hydrogen content in the steel is reduced. The former is responsible for crack initiation at the surface, while the latter is responsible for crack

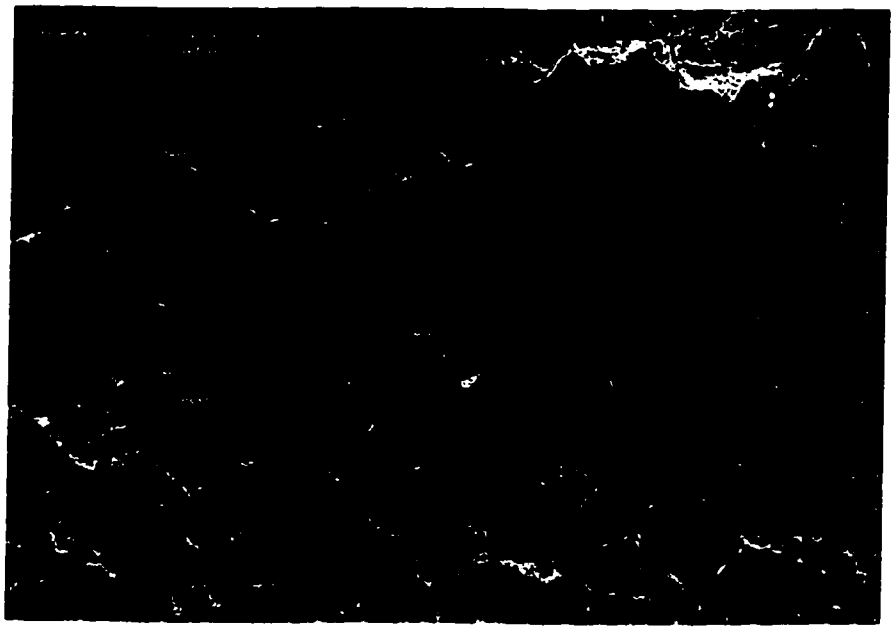

b. 24 hours

Fig.5-3 Surface morphologies of specimens after SSRT in NS4 solution at OCP with different corrosion time prior to loading

In contrast, corrosion at the surface under cathodic condition becomes very different, and fewer cracks are developed at the surface. Crack initiation by hydrogen mechanisms will prevail over that by corrosion mechanisms at the surface at very low cathodic condition. As a result, the increased ductility at −1200 mV in Fig.4-25 should be caused by the reduction in hydrogen content in the steel due to the formation of calcium carbonate film at the surface, as is shown in Fig.4-11. The dependence of ductility on the exposure time prior to SSRT should be attributed to the effect of calcium carbonate particles at the surface on hydrogen permeation. In this case, short exposure time may result in an incomplete coverage of calcium carbonate particles on the surface, and an extended exposure time may yield a fragile calcium carbonate film that can be easily spalled off the surface during loading.

5.2.3 Effect of Solution chemistry

The solution chemistries were altered in this study through cathodic reactions at −1200 mV, which caused the deposition of calcium carbonate on the steel surface. As a result, the ionic concentration of Ca^{++}, and CO_3^{2-}/HCO_3^- in the so-treated NS4 solution was reduced.

The effect of solution chemistry on SSRT properties should be related to its effect on crack initiation and propagation. The former is related to the corrosion attack at the surface, while the latter is mainly attributed to the hydrogen content in the steel.

Based on the electrochemical measurements, the corrosion rate of steels in the standard NS4 solution at OCP is a little higher than that in the treated NS4 solution, while hydrogen content is a little higher in the treated solution than the standard NS4 solution. The resulting SSRT properties at OCP in both the solutions were not very different regardless of the hold time prior to mechanical loading. This indicates that the difference in solution chemistry might not be large enough to cause a substantial effect on SSRT properties.

The greatest effect of solution chemistry on SSRT properties occurs at cathodically protected conditions, particularly at prolonged hold time prior to mechanical loading. As is shown in Fig. 4-28, the $\varepsilon_{solution}/\varepsilon_{air}$ at −900 mV is higher in the treated NS4 than in the standard NS4. However, the opposite was observed at −1200 mV.

By examining the surface after the SSRT test, crack density and size at −900 mV were observed to be substantially greater on the surface exposed to standard NS4 solution than that exposed to the treated NS4 solution (Fig.5-4). In addition, the hydrogen content in the former case was also higher than in the latter. Both of these should make the standard NS4 solution much more susceptible to cracking. However it is not known from this comparison whether their significant effect on SSRT properties is related to the effect of solution chemistry on crack initiation or to the effect of hydrogen on crack propagation. In addition, it is not clear if hydrogen makes any contribution to the crack initiation.

a. In NS4 solution

b. In the treated NS4 solution

Fig.5-6 Fracture of the specimens in both NS4 and the treated NS4 solution at -1200mV (SCE), charged for 24 hours prior to loading

6 Summaries and suggestions

6.1 MAIN CONCLUSIONS

This research has focused on the effect of surface conditions on electrochemical and mechanical properties of pipeline steels exposed to near-neutral pH environment. These conditions included surface roughness, surface scratch orientation, and surface deposits. The effect of these surface conditions was evaluated at various cathodic potentials. Special attention was placed on hydrogen generation and hydrogen permeation of the pipeline steel in the corrosion system. The behavior of the steel under slow strain rate tensile testing in the environment was further studied in an attempt to understand the mechanisms governing the SCC of pipeline steels exposed to near-neutral pH environments. The following is a summary of major findings from this investigation.

1) The OCP and the corrosion rate of the steel in both NS4 and the treated NS4 solution appeared quite sensitive to the surface roughness/surface area increment. The specimen with rougher surface or more surface area increment had lower open circuit potential, but a higher corrosion rate. The OCP and the corrosion rate were lower in the treated solution than in the standard NS4 solution.

2) Hydrogen content in the steel charged in near-neutral pH solution depended on the charging time and cathodic potentials. Hydrogen content appeared less sensitive to cathodic potential at short charging time. For an elongated charging time, hydrogen content in the steel increased almost linearly with the potential from OCP up to −900 mV. At the potential lower than -900mV, the hydrogen content in the steel decreased first with decreasing potential, and then increased again with a minimum hydrogen content at around −1200 mV.

3) The influence of cathodic potential on the hydrogen content in the steel can be correlated to the development of calcium carbonate film on the specimen surface that builds up with increasing charging time. This calcium carbonate film started to form at a cathodic potential lower than −900 mV. Its coverage on the surface appeared to

be maximized at −1200 mV. At a potential lower than this, calcium carbonate particles were observed to be very coarse and fragile.

4) In the treated solution, when the applied potential was above −950 mV, the hydrogen content in the steel was less sensitive to cathodic potential and was lower than that in the standard NS4 solution. At the potential lower than −950 mV, hydrogen content in the steel increased linearly with a decrease in cathodic potential and was significantly higher than that in standard NS4.

5) In the hydrogen permeation testing, the coupons with calcium carbonate films demonstrated lower hydrogen flux than those free of calcium carbonate films. This difference appeared less at OCP, but quite significant at cathodically charged conditions. In addition, the build-up rate of hydrogen flux at the beginning of permeation was substantially lower for all the coupons with calcium carbonate films.

6) At both OCP and -900mV, the specimens with rougher surfaces had higher steady state hydrogen flux. In addition, the permeation rate was lower at OCP than at −900 mV.

7) When the specimens were held in NS4 for 6 hours prior to SSR testing, the ductility was seen to decrease almost linearly with decreasing cathodic potential. For the specimen with an increased hold time prior to the loading, however, an abnormal increase in ductility was observed at −1200 mV. This was due to the fact that, at this potential, the steel had the lowest hydrogen content.

8) In the treated NS4 solution, the SSRT properties under a short hold time before loading were generally lower than those in NS4. With an increased hold time, larger difference in SSRT properties was observed between the standard and the treated NS4, which is believed to result from the significant difference in hydrogen content in the steel between the two solutions.

9) Scratches produced in a direction perpendicular to the loading direction facilitated the development of SCC cracks, while those produced in a direction parallel to the loading direction appear to have little effect on crack initiation.

10) Roughness appeared to have little effect on the ductility of the specimen with parallel scratches. For the specimen with scratches perpendicular to the load direction, the effect of scratch roughness on ductility depends on the electrochemical potential. Its effect appeared to be minor at OCP, but became significant at cathodic potentials. This is attributed to the difference in the density of surface cracks and the hydrogen content at crack tip on the specimen with different roughnesses.

11) The difference in ductility arising from scratch roughness and orientation was consistent with the observation of surface conditions after the test. For samples with perpendicular and angle scratches, cracks were seen to coincide with scratch lines. For those with parallel scratches, only short cracks were developed in a direction approximately 45° to stress axis.

6.2 SUGGESTIONS FOR FUTURE WORK

SOLUTION CHEMISTRY Solution chemistry from this study appears to have significant effect on crack initiation and propagation through its effect on surface corrosion attack and the generation of hydrogen. A systematic study should be conducted to understand the role of individual ion species in corrosion attack at the steel surface and in the generation of hydrogen. Along with more studies on solution chemistry, attention may have to be paid to the idea of inhibition of corrosion attack at the surface and of generation of excessive hydrogen in the system. Application of this idea to the field operation should also be explored. Although it is hard to alter the chemistry in the soil solution, the chemistry at the pipe surface upon the access of ground water may be changed by using specially designed coatings and by pre-chemically treating pipe surface that could reduce the susceptibility to crack initiation and inhibit the adsorption and absorption of hydrogen.

HYDROGEN Experimental results shown in this study indicated that samples with different surface roughness have resulted in different ductility in SSR testing. Further

work should be conducted to differentiate the roles of roughness and hydrogen in crack initiation and propagation.

STRESS Loading conditions in the slow strain rate testing are considered to be too aggressive in comparison with actual loading conditions in the field. More realistic loading conditions should be applied to evaluate the SCC susceptibility of line pipe steel exposed to near-neutral pH environments.

INCLUSION During the hydrogen permeation testing, it was observed that inclusions (surface or exposed inclusion) might contribute to hydrogen generation due to microelectrode effect. Researches on this effect are not available, although considerable researches were conducted on the effect of inclusions on hydrogen trapping in the steel.

OXIDE FILM The surface of steel line pipe is often heavily oxidized during fabrication. The effect of surface oxides on corrosion attack and hydrogen adsorption should be explored in order to understand how SCC is developed on the steel surface in the field.

References

Abramov E.and Eliezer D., Minerals, Metals and Materials Society/AIME, (1996)293

Arkid R., H transport and cracking in metals, Teddington, UK, April 13-14, 1994

Asano S., Hara K., Nakai Y. and Ohtani N., J. Jap. Inst. Met., 38(1974)626

Asaoko T., Dagbert C., Aucouturier M. and Galland J., Scripta Met. 11(1977)467

Beavers J. A., Durr C. L.and Shademan S. S., "Mechanistic studies of near-neutral pH SCC on underground pipelines", Materials for Resource Recovery and Transport, eds. L. Collins, 1998, p31.

Beck W., Bockris J. O'M., McBreen J. and Nais L., Proc. Roy. Soc., A290(1966)220

Belash I., Antonov V. and Pnyatovskii. Fiz E.. Metal. Metallov., 47(1979)357

Benson J. and Edyvean R. G. J., Corrosion Engineering Section, 54(1998)732

Boes and Zuchner H., J. Less-Common Metals, 49(1976)223

Boes N andZuchner H., J. Less-common metals, 49, (1976)223

Boes N. andZuchner H., J. Less-common metals, 49(1976)223 J.G.Early, Acta Metall., 26(1978)1215

Bolton K.and Shreir L.L, corrosion Science, 3(1963)17 S. Wach, Br. Corrosion . J., 6(1971)114

Bowker P. and Hardie D., Met. Sci., 9(1975)432]

Brass A.M. and Chene J., Materials Science and Engineering A, 242(1998)210-221

Brass A.M., Chene J. and Gonzalez J., Metallurgy. Transaction., 25A(1994)1159

Brass A.M., Chene J. andBoutry-Forveille A., Corrosion Science, 37(1996)569

Brass A.M., Garet M. and Etter A.L., DECHEMA, EUROCORR '99 Proceedings (Germany), Sept. 1999,105

Brown B. F., Stress corrosion cracking control measures Washington: U.S. Dept. of Commerce, National Bureau of Standards: for sale by the Supt. of Docs, U.S. Govt. Print. Off, 1977

Bruzzoni P. and Garavaglia R., Corrosion Science, 33(1992)1797

Budin C., Lucasson A. and Lucasson P., Etudes isochrones du cuivre trempe en athmosphere d'hydrogine, J Physique, 25(1964)751

Burke Delanty, John O'Beirne; Oil & Gas Journal, 15(1992)39-44

Cailletet L., Compt. Rend., 58(1864)327

Carlos *et al.*, Corrosion 2000, paper00469

Casanova T. andCrousier J., Corrosion Science, 38(1996)1535

Chan S. L. I., Journal of the Chinese Institute of Engineers (Taiwan), 22(1999)43-53

Charitidou E., Papapolymerou G., Haidenmenopoulos G. N., Hasiotis N. and Bontozoglou V., Scripta Materialia (USA), 41(1999)1327

Charles E. A. and Parkins R. N.; Corrosion, 1995, vol. 51, pp518-527

Chaudhari B S and Radhakrishban T P, Corrosion Science, 25(1985)1077

Flitt H. J and Bockris J. O'M, International Journal of Hydrogen Energy, 7(1982)411

Chaudhari B. S. and Radhakrishan T. P., Surface Technology, 22(1984)353

Chaudhari B. S. and Radhakrishnan T. P., Corrosion Science, 30(1990)1219

Chaudhari B. S. and Radhakrishnan T. P., Materials Transactions, JIM, 5(1993)443

Chaudhari S. and Radhakrishnan T P, Corrosion Science, 25(1985)1077

Chaudhari S. andTadhakrishnan T. P., Corrosion Science, 30(1990)1219

Chen W., Wilmott M. and Jack T., "Effect of Cathodic Protection on Neutral pH SCC Crack Initiation of X-70 Pipeline Steel", NACE Western Conference, Calgary, Mar. 8-11, 1999, paper 3A.

Chen W., Wilmott M. L. and Jack T. R., "Evaluation of Soil Susceptibility to Neutral pH SCC Using X-70 Pipeline Steel", Nova Research and Technology Corporation, Internal report # 01285, January 1999.

Chen W.,. Wilmott M. L, Jack T. R. and King F., "H Permeation and Surface Deterioration of Line pipe Steel in Neutral pH SCC Environment" GRI report, Contract No. 5094-260-3049, Jan.1999.

Chen W.; Wilmott M.; Jack T.; NOVA Research Report, 1999, No. 01311, GRI 99/0059

Chew B., Metal Science Journal, 5(1971)195

Courant R.and Hilbert D., Methods of mathematical physics, vol. II, pp512-515, interscience publications, New York(1962)

Crank J., Mathematics of diffusion, p33, Oxford University Press, Fair Lawn, NJ, 1956

Dautovich D. P. andFloreen S., Met. Trans., 4(1973)2627

Delanty B. S., Marr J. E.; CANMET int. conference pipeline relaibiliby, Calgary, Canada, 1992, (Ottawa, Canada; CANMET, 1992)

DeLuccia J. J. and Berman D. A., An electrochemical technique to measure diffusible hydrogen in metals (Barnacle Electrode), Electrochemical corrosion testing, ASTM STP 727, 1981, 256

Deluccia J. J. And Berman D. A., Electrochemical corrosion testing, ASTM STP 727, Florian Mansfeld and Ugo Bertocci, eds., American Society for testing and materials, 1981, pp256

Devanathan A. and Stachurski Z., Proc. of the Royal Society, A270(1962)90

Devanathan M A V and Stachurski Z. O. J., Journal of the electrochemical society, 111 (1964)619

Devanathan M A V and Stachurski Z. O. J., Proc. Roy. Soc., A270(1962)90

Devanathan M A V, Stachurski Z. O. J. and Beckm W. ibid., 110(1963)886

Early J G, Acta Metall., 26(1978)1215

El-Sherik A. M. and Shirkhanzadeh M., Corrosion, 48(1992)1001

Fessler R R; Proc. 6th Symposium on Line Pipe Research, American Gas Association, Arlington, Catalogue No. L30175 R-1, 1979

Flis J. and Zakroczymaki T., Corrosion, 7(1992)530

Flitt H. J and Bockris J. O'M, Int. J. Hydrogen Energy, 7(1982)411

Frank R C, J. Appl. Phys., 29(1958)1263

Fullenwider M. A., J. Electrochem. Soc., 122(1975)649 J.G.Early, Acta Met., 26(1978)1215

Galaktionowa N. A., Hydrogen-metal systems databook, Ordentlich publishers, 1981

Galaktionowa N. A., Metallurgiya Stali, ONTI, 1935

Garet M., Brass A.M., Haut C., Guttierez-Solana F., Corrosion Science, 40(1998)1073

Gerberich W. W., Chen Y. T. and John C. St., Met. Trans. 6A(1975)1485

Gibala R., Stress corrosion cracking and hydrogen embrittlement of iron base alloys, R. W. Staehle et al., eds., NACE, Houston, 197

Gu B., Luo J., Mao X.; Corrosion, 55(1999)96-106

Hardy J. A.; British Corrosion Journal; 18(1983)190-193

Hay M. G. and Rider D. W., Corrosion 99, paper395

Hay M. G., CIM conference of metallurgists, Hydrogen sulphide symposium, Edmonton, Canada, 1983

Hirth J. P., Met. Trans. A, 11A(1980)861

Hsiao C. M.; Chu W. Y.; Hydrogen Effect in Materials; eds. Bernstein I. M.; Thompson A. W. (Warrendale, PA: AIME, 1981)

HU R.P., Manolatos P., Jerome M., Meyer M. and Galland J., Corrosion science, 40(1998)619

Hutchings R. B., Ferriss D. H. and Turnbull A., British Corrosion Journal, 28(1993)309

Jack T. R, Wilmott M. L., Chen W., "SCC Susceptibility of X-70 Steel in Contact with Various Neutral pH Soil Solutions", EPRG/PRCI 12th Biennial Joint Tech Mtg. Netherlands, paper 10, 1999.

Jack T. R., Boven G. Van, et al; NACE International, Canada Region Western Conference, February 7-10, 1994, Calgary, Alberta, p 504-526

Jack T. R.; Ban Boven G. et al; Materials Performance, 33(1994)17

Jerkiewicz G., P. Marcus, Electrochemical surface science of hydrogen adsorption and absorption, Montreal, Canada, May 1997

Jimei XIAO, Metal corrosion under stress, Chemical industrial publishing company 1990, in Chinese

Johnson D. L. and WU J. K., J. Materials for energy systems, 8(1987)402

Johnson H. H. and Lin R. W., Hydrogen in metals, 3rd International conference on effect of hydrogen in behavior of metals, Wyoming, 1980, 3-25

Johnson H. H. and Lin R. Y., Third Int Conf. On Effect of hydrogen on behavior of Materials, ed. I. M Bernstein and A. W. Thompson. The Metallurgical Society of AIME, Warrendale, PA, 1981, p3

Johnson H.H., Metallurgical Transaction, 19A(1988)2371

Jung C.B., and Lee K.S., Scripta Materialia, 35(1996)267-271

Kato C., Grabke H. J., Egert B. and Panzner G., Corrosion Science, 24(1984)591

Kazinczy F.de, Jernkont. Ann., 140(1956)347

Kim, K B; Park, K; Lee, J S, Metals and Materials [Metals and Mater.], 4(1998)1013

King Fraser, Jack Tom, Weixing Chen et al; Corrosion 2000, paper No. 00361, pp00361/1-00361/19

Kiuchi K and Mclelan R. B., Acta Metall., 31(1983)961

Krasnikov A. I., Izvestiya OTN AN SSSR, no.1, 1946

Kumkum A. A., Banerjee and Chatterjee U. K., Scripta mater. 44(2001)213-216

Kumnick A.J.and Johnson H.H., Metallurgical Transactions, 5(1974)1199

Kushida T., Netsu Shori (J. of the Japan Society for Heat Treatment), 37(1997)69-73

L. S. Darken and R.W. Gurry, Physical chemistry of metals, McGraw-Hill, New York, 1953

Lacombe P., *et al.*, Stress corrosion cracking and hydrogen embrittlement of iron base alloys, NACE publishing, Unieux, France, (1977)423

Lambert S. B. and Plumtree A.; NACE International, Canada Region Western Conference, February 7-10, 1994, Calgary, Alberta, p 456-462

Le Yuyen D., Wilde B. E., Corrosion, 39(1983)258

Leblond J B and D Dubois, Acta Met., 31(1983)1471

Leblond J B and Dubois D, Acta Met., 31(1983)1459

Leis B. N. and Colwell J. A., "Effects of the Environment on Initiation of Crack Growth", ASTM STP 1298, Eds. W. A. Van Der Sluys, R. S. Piascik and R. Zawierucha, 1997, p34.

Linnet N.; Radiometer A/S, Copenhagen, 1970

Liu. X.; Mao X.; Reviw R. W.; Proc. 12th International Corrosion Congress, September 19-24, 1993, Vol. 4 (Houston TX: NACE, 1993), p 2831

Lukito H., Szklarska-Smialowska Z., Corrosion Science, 39(1997)2151-2169

Luppo M.I. and Ovejero-Garcia J., Materials Characterization, 40(1998)189-196

Luppo M.I. andOvejero-Garcia J., Corrosion Science, 32(1991)1125

Lyer R N, Pickering H W and Zamanzadeh M, J. Electrochem Soc., 137(1990)1464

Lyer R N, Pickering H W and Zamanzadeh M, J. Electrochem. Soc., 136(1989)2463

Lyer R N, Pickering H W and Zamanzadeh M, Scripta Metall., 22(1988)911

MacBreen J., Nanis L. and Beck W., J. Electrochem. Soc., 113(1966)1218

Mailer H. J., Schettler A. and Kaesche H., Werkstoffe und Korrosion, 42(1991)212

Manohar M., and Wilde B.E., Corrosion Science, 37(1995)607

Mcbreen J., Beck W. and Nanis L, A method for determination of the permeation rate of hydrogen through metal membrane, Journal of the electrochemical society,

113(11), (1966)1218

McBreen J., Nanis L. and Beek W., J. Electrochem. Soc., 113(1966)1218

McNabb A. and.Foster P.K, Trans. Am. Inst. Min. Engrs., 227(1963)618

Miyazawa K. and Mori M., Journal of the Japan Institute of Metals (Japan), 62(1998)215-223

Moro L; Obiol E; Roviglione A; Hermida D; and Juan A, Journal of Physics D, Applied Physics (UK), 31(1998)893-899

Nagumo M., Takai K., andOkuda N., Journal of alloys and compounds, 293-295(1999)310

Nakagawa I., Obinata T., Kudo J., Kawabata F., Kimura M. and Amano K., Metallurgy of Vacuum-degassed steel products, edited by R. Pradhan, The minerals, metals & materials society, 1990

Nanis L and Namboodhiri T K G, J. Electrochem. Soc., 119(1972)691

Nanis L. and NamBoodhiri T. K. D., J Electrochem. Soc., 119(1972)691

Oriani, R. A. Acta Met., 18(1970)147

Parker D. H. and Jenkins N., The welding institute research bulletin, 28(1987)11

Parkins R N; NACE International, Canada Region Western Conference, February 7-10, 1994, Calgary, Alberta, p 423-455

Parkins R. N, Progess Report 4, September-October , 1997

Parkins R. N., "Investigations Relating to Environment Sensitive Fracture in the TransCanada Pipeline System" Report to TCPL, 1988.

Parkins R. N., Blanchard W. K., Delanty B. S.; Corrosion, 50(1994)394

Parkins R. N., Eelhimer E., Blanchard W. K.; Corrosion, 49(1993)951

Parkins R. N., Singh P. M.; Corrosion, 46(1990)485

Parkins R. N., W. K. Blanchard Jr., and B. S. Delanty, Corrosion, 50(1993)395.

Parkins R. N.; 5th Symp. Line Pipe Research L30174, paper No. U1 (Arlington, VA: AGA, 1974)

Parkins R. N.; Blanchard W. K.; Fr. B. S. Delanty; Corrosion, 50(1994)394

Parkins R. N.; Progess Report 5, November-December, 1997

Pickering H W, A review of the mechanism and kinetics of electrochemical hydrogen

entry degradation of metallic systems, Annual report to office of naval research, Contract USN00014-84-K-0201 (January 1990)

Pickering H W, Hydrogen sulfide effect of hydrogen entry into iron-A mechanistic study, report, contract No.N000014-84-K-0201 (December 1989)

Pilkey A. K., Lambert S. B., Plumtree A, Corrosion, 51(1995)91

Popov B N; Zheng G. and White R.E., Corrosion, 51(1995) 429

Pound B. G., Acta Materialia, 46(1998)5733

Pound B. G., Corrosion, 54(1998)988

Pound B. G., National Association of Corrosion Engineers, Corrosion 99, Apr. 1999, 8

Pound B. G., Naval Surface Warfare Center-Carderock Division, 5(1997)17

Pressouyre G. M. and Bernstein I. M., Met. Trans. A, 9A(1978)1571

Pressouyre G. M. and Bernstein I. M., Acta Met. 27(1979)89

Pressouyre G. M., Acta Met. 28(1980)895

Pressouyre G. M., Met. Trans. A, 10A(1979)1571

Pumphrey P. H., Scripta met.,14(1980)695

Pumphrey P. H., The effect of sulfide inclusions on the diffusion of hydrogen in steels

Pyun S. I. and Oriani R A, The permeation of hydrogen through the passivating films on iron and nickel, Corrosion Science, 29(1989)485

Rak-hyun song, Su-il pyun and R. A. Oriani, J. Electrochem. Soc., 137(1990)1703

Razzini G., M. Cabrini, Maffi S., G. Mussati and L. P. Bicelli, Corrosion Science, 41(1999)203

Razzini G., Maffi S., Mussati S., Bicelli P. and Mitsi G., Corrosion Science, 39(1997) 613

Razzini G., Peraldo Bicelle L. andScrosati B., Electrochemistry. Acta, 38(1993)89

Rebak R. B., Safruddin R., Szklarska-Smialowska Z.; Corrosion, 52(1996)396-405

Revie R. W., Sastri V. S., Elboujadini M., Ramsingh R. R. and Lafreniere Y., Hydrogen-induced cracking of linepipe steels part II-laboratory studies on the determination of hydrogen flux in linepipe steel used in sour service, Metals technology laboratories report 91-61(J)

Rhoades J. D., "Soluble Salts." Pages 167 to 197 in Methods of Soil Analysis Part 2, Chemical and Microbiological Properties, Second Edition. A.L. Page, R.H.

Mller and D.R. Keeney (editors), Number 9(2) in the Series, Agronomy, American Society of Agronomy, Inc., Soil Science Society of America, Inc., Madison, Wisconsin (1982).

Ross D. K., Stefanopoulos K. and Kemali M., Journal of Alloys and Compounds, 293-295(1999)346

Ryun Su-iL andOrian R. A. i, Corrosion Science., 29(1989)485

Saito H. and Kasuya T., Welding International, 13(1998)5-8

Saito H., Mori M. and Ishida Y., J. of the Japan Institute of Metals, 60(1996)914-920

Saito H., Mori M. and Ishida Y., J. of the Japan Institute of Metals, 59(1995)910-916

Saito H., Nogawa N., Mori M. and Ishida Y., Seisan-Kenkyu (Journal of Institute of Industrial Science, University of Tokyo) (Japan), 48(1996)23-26

Sakamoto Y. andMantani T., Trans. Jap. Inst. Metals, 17(1976)743

Schmitt G., Sadlowsky B. andNoga J., Corrosion 2000, paper 00466

Shaw W J D; Bizon A; and LeBlanc T, Corrosion 98; NACE (1998)392/1-392/13

Smith S. M. and Scully J. R., Metallurgical and Materials Transactions A, 31A(2000)179

Smith S. M. and Scully J. R., Minerals, Metals and Materials Society/AIME, 1996,131

Stephens M. F. and M.Berstein I., Metallurgical Transactions A, 20A(1989)909

Szklarska-Smialowska Z. and Xia Z., Corrosion Science, 39(1997)2171-2180

Takai K., Yamauchi G., Nakamura M. and Nagumo M., Journal of the Japan Institute of Metals (Japan), 62(1998)267-275

Tomlison L.; Hurdus M. H.; Sliver P. B.; Jr. Corrosion Science, Vol. 21, 1981, pp 36

Turnbull, Corros. Sci., 34(1993)1751

Turnbull, M. Saenz de Santa Maria and N. D. Thomas, Corros. Sci., 29(1989)89

Valentini R., Solina A., Matera S., Gregorio P. de, Metallurgical and Materials Transactions A, 27A(1996)3773-3780

Valentini R., Solina A., Tonelli L., Lanza S., Benamati G. and Donato A., Journal of Nuclear Materials (Netherlands), 233-237(1996)1123-1127

Victor Baez Baez, Concepcion Mendez and Jose R. Vera, Corrosion 2000, paper 00465

Wang Y. Z., Revie R. W.and Shehata M. T., in "Materials for Resoruce Recovery and Transport", Ed. L. Collins, The Metallurgical Society of CIM, 1998, p71.

Wang Y-Z., Revie R. W., Parkins R. N., Corrosion 99, paper No. 143.

Wilde B. E. and Kim C. D., Corrosion, 37(1981)449

Williams D. P. and Nelson H. G., Met. Trans., 1(1970)63

Willis E. R.; Walsh D. W.; Corrosion 96, 1996, Paper 251, NACE International

Wilmott Martyn J., Diakow David A.; International Pipeline Conference-Vol. 1, ASME 1996, p507-524; 573-585

Yahalom J., Aladjem A., editors. Stress corrosion cracking / Tel-Aviv: Freund Pub. House; Aedermannsdorf, Switzerland: Distributed by Trans Tech Publication, c1980

Yen S. K., Materials Chemistry and Physics [Mater. Chem. Phys.], vol. 59(1999)210

Yu W. Z., Luo J. L., Mao X.; Corrosion, 55(1999)312-318

Zakcroczymaki T. and Szklarska-Smialowska Z., J. Electrochem. Soc. 132(1985)2548

Zakroczymski T; Lukomsk N and Flis J, Metallurgy and Foundry Engineering [Metall. Foundry Eng.], 23(1997)147

Zapffe C., Trans. Am. Soc. Metals, 39(1947)191